Oleocanthal ameliorates metabolic and behavioral phenotypes, and pathology in a mouse model of Alzheimer's disease

by

Euitaek Yang

A dissertation submitted to the Graduate Faculty of
Auburn University
in partial fulfillment of the
requirements for the Degree of
Doctor of Philosophy

Auburn, Alabama
December 10, 2022

Keywords; Alzheimer's disease, TRPA1, Blood-brain barrier, Brain endothelial cells, 5xFAD, Metabolic phenotype.

Approved by

Amal Kaddoumi, Chair, Professor, Department of Drug Discovery and Development
Jay Ramapuram, Professor, Department of Drug Discovery and Development
Murali Dhanasekaran, Professor, Department of Drug Discovery and Development
Vishnu Suppiramaniam, Professor, Department of Drug Discovery and Development
Michael Greene, Associate Professor, Department of Nutrition, Dietetics, and Hospitality Management.

Abstract

The blood-brain barrier (BBB) healthiness is important to maintain brain homeostasis. The deposition of amyloid-β (Aβ) is one of Alzheimer's disease's (AD) causative pathways to induce brain neuronal loss. In addition, AD patients experience BBB dysfunction, and several studies reported correlations between Aβ and BBB dysfunction. The first project aimed to investigate the correlation between BBB healthiness and metabolic and behavioral changes in five AD characteristic-carried (5xFAD) mice as a model for AD as a function of age and pathology. Therefore, in this project, we assessed the mice at 4 and 9 months to represent early and advanced stages of AD for changes in their metabolic and behavioral phenotypes compared with wild-type mice at the same ages. While the pathological characteristics of AD are well established, our understanding of the metabolic and behavioral phenotypes changes, which could be important for early AD diagnosis and staging, continues to be limited. First, we evaluated the metabolic and behavioral alterations by monitoring changes in several parameters, including activity rate, anxiety-like behavior, and sleeping pattern, which are relevant to alterations observed in AD patients. Our findings demonstrated that aging and pathology alter body metabolism and behavior, such as activity rate and sleeping pattern. However, the effect of the pathology on monitored parameters was significantly higher than normal aging, an effect associated with increased Aβ deposition and BBB disruption. In addition, we found a positive correlation between BBB breakdown and increased brain Aβ levels, while a negative correlation was observed between BBB breakdown and sleeping time. In the second project, we aimed to evaluate the effect of repairing the BBB function by targeting the receptor TRPA1 on Aβ pathology and metabolic and behavior phenotypes by the compound oleocanthal (OC) in 5xFAD mice. Previous studies from our laboratory demonstrated the protective and treatment effects of OC against Aβ pathology in AD

mice models, an effect that is mediated by enhancing the BBB function. Our studies also showed that OC downregulated the receptor transient receptor potential ankyrin 1 (TRPA1) expression, which upregulated AD. 5xFAD mice (6 months old) were treated with OC at two different doses (1 and 10 mg/kg) for three months by oral gavage. At the end of treatment, mice were assessed for changes in metabolic and behavioral phenotypes, BBB function, BBB endothelium-TRPA1 levels, and Aβ pathology. Our findings demonstrated that 10 mg/kg OC restored the activity rate and sleep pattern to that of the wild-type mice. In addition, our findings demonstrated that OC significantly reduced total and endothelium-TRPA1 and enhanced BBB function. To better clarify the effect of OC on endothelium-TRPA1 expression and function, we performed in vitro studies using the mice brain endothelial cell line bEnd3. Results confirmed TRPA1 expression in bEnd3 cells and that OC treatment reduced Aβ-induced TRPA1 expression and the effect that was associated with reduced intracellular calcium levels. In addition, this effect was associated with enhanced cell-based BBB model integrity and function. Collectively, these findings suggest that OC rectifies the BBB function, at least in part, by reducing endothelium-TRPA1 expression. In conclusion, our findings show that aging and Aβ-related pathology increase activity rate and reduce sleep time, which is associated with BBB dysfunction. Furthermore, restoring the BBB function by OC alters metabolic and behavioral phenotypes to levels similar to wild-type mice.

Acknowledgments

I can stand here because God is holding me tight and ruling my life. All this glory belongs to him, the holy spirit, and his son Jesus Christ; I appreciate his love for me.

It is my honor to fill a knowledge gap that might be useful in Alzheimer's disease research. I hope my work may be helpful and useful to design and develop medicines for patients with dementia in the future.

I appreciate my advisor Dr. Amal Kaddoumi, who inspires me to get passionate about Alzheimer's disease research. Joining Dr. Kaddoumi's lab was the best decision and luckiest opportunity for me. I can stand here as a mature scientist thanks to her supervision. In addition, I could continue earning a Ph.D. with her patience with me. I appreciate her for taking care of me as much as my parents. Dr. Kaddoumi has transformed me into a more firm and responsible person. I appreciate again for her efforts for me.

I appreciate my committee member, Dr.Jayachandra Ramapuram, Dr. Muralikrishnan Dhanasekaran, and Dr. Vishnu Suppiramaniam, for being supportive, advising, and supervising my dissertation. Especially, I thank Dr. Michael Greene for reviewing and guiding me in building metabolic phenotyping experiments for my dissertation work.

I appreciate my friends on and out of the campus and church while earning my Ph.D. degree. Especially, I thank my friend Dr. Youssef Mousa, who helped me settle everything when I moved to Auburn. I could start my life at Auburn smoothly thanks to his help and support. In addition, I thank my friend Dr. Andrew Brannen, who helped me to develop my imaging skills in the microscope and other imaging tools, which has become one of my strengths in the research field. In addition, I want to mention my friend at the church, Sangmin Park and Eunmi Kim, who helped my wife and me to settle down in Auburn for everything. I appreciate their kindness to us.

I also appreciate my parents, Kyungjin Yang (father), Sichang Kim (mother), and my younger brother Jiho Yang, who gave unlimited financial and emotional support and helped me to study in the U.S. I can establish my life in the U.S. thanks to my family, so I can continue to seek what I like to research and develop. Especially, I thank my father, who devoted himself to keeping his business to support my studying.

I want to thank my relatives, especially my parents-in-law, Geon Sagong (father-in-law), and Jaehee Koo (mother-in-law). I appreciate their support and belief in me to accomplish my Ph.D. degree. I could maintain my life full of joy and happiness with the most beautiful woman, Hae Sagong, thanks to their permission and blessing for our marriage. In addition, I want to mention my brother-in-law Byungil Sagong for being a good friend and brother to my wife and me.

Finally, I would like to send my heartfelt thanks and love to my wife, Dr. Hae Sagong. I cannot even start and accomplish my Ph.D. degree without her help and support. I remember every moment we have been together everywhere and every meal we cooked and ate together since she moved from South Korea to Auburn with me. I appreciate her love for me; she brightens my life and is always there whenever I want to see her. Thanks to her guidance, I experienced many different things that I never did before and became a grow-up person thanks to her help. I appreciate her continuous support, love, and belief in me.

Table of Contents

List of Tables

List of Figures

List of Abbreviations

A9	A 967079 (TRPA1 antagonist)
AD	Alzheimer's disease
AICD	APP intracellular domain
AITC	Allyl isothiocyanate (TRPA1 agonist)
AMPAR	α-amino-3-hydroxy-5-methyl-4-isoxazole propionic acid receptors
AMPK	Adenosine monophosphate -activated protein kinase
ATP	Adenosine triphosphate
Aβ	Amyloid β
BBB	Blood-brain barrier
BCA	Bicinchoninic acid
BCRP	Breast cancer resistant protein
C99	Transmembrane carboxyl-terminal domain of the amyloid precursor protein
CaM	Calmodulin
CNS	Central nervous system
CO2	Carbon dioxide
CSF	Cerebrospinal fluid
CTFα	C-terminal fragments-α
CTFβ	C-terminal fragments-β
DMSO	Dimethyl sulfoxide
ECs	Endothelial cells
EE	Energy expenditure
ELISA	Enzyme-linked immunoassay

FEPS	familial episodic pain syndrome
HEK293	Human embryonic kidney 293 cells
hTRPA1	Human- Transient receptor potential ankyrin 1
IF	Immunofluorescence
IgG	Immunoglobulin G
IL-1α	Interleukin-1α
IL-6	Interleukin-6
JAMs	Junctional adhesion molecules
LRR	A leucine-rich repeat
LTP	long-term potentiation
MAP	Microtubule-associated proteins
MCI	Mild cognitive impairment
MRI	Magnetic resonance imaging
NACHT	NAIP (neuronal apoptosis inhibitor protein), C2TA (MHC (major histocompatibility complex) class 2 transcription activator), HET-E (incompatibility locus protein from Podospora anserina) and TP1 (telomerase-associated protein)
NFT	Neural fibrillary tangles
NLRP3	NOD-like receptor Family Pyrin Domain Containing 3
NMDA	N-methyl-D-aspartate
O.C.T	Optimal cutting temperature
O2	Oxygen
OC	Oleocanthal

P3	Amyloid β- peptide (Aβ)17–40/42
PBS	Phosphate buffer saline
PBST	Phosphate buffer saline and tween-20
P-gp	P-glycoprotein
PSEN1	Presenilin 1
PSEN2	Presenilin 2
PVDF	Polyvinylidene difluoride
RNS	Reactive nitrogen species
ROS	Reactive oxygen species
sAPPα	Soluble amyloid precursor protein- α
sAPPβ	Soluble amyloid precursor protein- β
SDS-PAGE	Sodium dodecyl sulfate – Polyacrylamide Gel Electrophoresis
TEMED	Tetramethylethylenediamine
ThioS	Thioflavin-S
TNF-α	Tumor necrosis factor-α
TRP	Transient receptor potential
TRPA	Transient receptor potential ankyrin
TRPA1	Transient receptor potential ankyrin 1
TRPC	Transient receptor potential canonical
TRPM	Transient receptor potential melastatin
TRPML	Transient receptor potential mucolipin
TRPN	Transient receptor potential NOMPC (no mechanoreceptor potential C)-like
TRPP	Transient receptor potential polycystin

TRPV	Transient receptor potential vanilloid
ULK1	Unc-51 like autophagy activating kinase 1
ZO-1	Zonulae occludens-1

CHAPTERS

1. Review and literature

1. Alzheimer's disease

1.1 Alzheimer's disease

Alzheimer's disease (AD) patients have neuronal synaptic injury that causes neurodegeneration (1) followed by neuronal loss (2). Neurodegeneration also induces volume loss (or shrinkage) of the brain accompanied by dementia, which is the most characteristic shown in AD patients (3). Recently, several AD pathological hallmarks were investigated that are involved in neurodegeneration. Mild cognitive impairment (MCI) is a transitional stage between the cognition of normal aging and mild dementia. Depending on the level of cognitive impairment, the stage of memory dysfunction is divided into preclinical, MCI, and dementia. Clinically, the stage of the MCI is an important state because when patients are diagnosed with Alzheimer's disease (AD) with a high risk for dementia; however, many do not show progression and may even revert to normal cognition (4, 5). Patients with MCI can be grouped into two groups amnestic with impaired episodic memory or non-amnestic with impairment in cognitive domains other than memory, such as executive function, language, or visuospatial abilities (6). In AD, patients with amnestic MCI are showed at high risk for AD (7, 8). AD is a specific brain disease that accounts for up to 80 percent of dementia patients. In AD, patients are experiencing neurodegeneration induced by the deposition of beta-amyloid (Aβ) in the brain, tau-phosphorylation (neurofibrillary tangles), oxidative stress, Ca2+homeostatiss failure, and neuroinflammation. In addition, AD decreases the volume of the brain with the structural changes that are believed to be induced by

neurodegeneration to change the behavior of AD patients. All the AD pathological markers are shown to induce dementia with neurodegeneration, and currently, AD is totally fatal; therefore, preventing or delaying the disease stage is the best treatment strategy today. In humans, AD patients show some behavioral changes, including emotional unstable, language ability, imagining things that are not there, acting depressed or not interested in things, wandering away from home, or misunderstanding what they see or hear. AD patients cannot control or maintain their life by themselves without caregivers' support because AD is an unstoppable progressive memory dysfunction disease. Therefore, alternative animal models, such as mice models with genetic modification that induces AD-like pathological hallmarks, are spotlighted to investigate and understand AD pathologies.

1.2 Type of AD

1.2.1 Early-onset

AD most commonly affects older adults 60s, but it can also affect people in their 30s or 40s. When AD occurs in patients under age 65, it is known as early-onset (or younger-onset) AD. Currently, a family history of AD is the only known risk factor for early-onset AD. For most patients with early-onset AD, the symptoms similarly mirror those of other forms of AD, such as forgetting important things, mainly newly obtained information or some special dates, repeating asking for the same information, troubling to solve fundamental problems, such as keeping follow of bills or following a favorite recipe, staying in a depressed mood, behavior changes, deepening confusion about time, place, and life events. Currently, AD transgenic mice are available to investigate early-onset AD by mutating the gens of APP, PSEN-1, and PSEN-2.

1.2.2 Late-onset (Sporadic)

Late-onset AD is the most common type of AD, which normally occurs in people aged 60 years and older. It may or may not be related to family AD. Prospective population-based studies provide strong evidence that the risk of late-life cognitive impairment and dementia is modified by medical comorbidities, lifestyle choices, and other environmental factors (9). The risk rate of dementia is increased in patients with vascular risk factors, and growing evidence suggests that aggressive treatment of these risk factors as early as midlife can attenuate the risk of developing cognitive impairment in older age (10, 11).

1.3 Pathological hallmarks

1.3.1 β-Amyloid (Aβ) plaques

β-Amyloid (Aβ) peptide accumulation in the brain is the main component of senile plaques and is produced from the proteolytic cleavage of amyloid precursor protein (APP) (12). APP is an important type 1 membrane glycoprotein that plays a role in neuronal homeostases, such as neuronal development, signaling, and intracellular transport. The cleavage process of APP is divided into two pathways non-amyloidogenic and amyloidogenic. In the non-amyloidogenic process, α-secretase cleave the APP into membrane-tethered α-C terminal fragment CTFα (C83) and the N-terminal fragment sAPPα. Then γ-secretases cleave the CTFα to produce extracellular P3 and the APP intracellular domain (AICD) (Chen, 2017). In the amyloidogenic process, APP is cleaved by β-secretase into N-terminal sAPPβ and the membrane-tethered C-terminal fragments β (CTFβ or C99). Then the γ-secretases cleave the CTFβ into Aβ and APP intracellular domain (AICD) (12). In AD, deposits of Aβ peptides are mainly observed in the region of the hippocampus, the cortex, and the cerebrovasculature (12). The main isoform of Aβ found in

amyloid deposits in the brain is 40 and 42 amino acids long. A study shows that familial forms of early-onset AD are associated with an increase in the Aβ42/Aβ40 concentration ratio (13, 14).

1.3.2 Neural fibrillary tangles

Neural fibrillary tangles (NFT) or tau tangles belong to the microtubule-associated proteins (MAP) family (15). In humans, tau tangles are found in the neurons and non-neuronal cells (16). For neurons, tau is an important component of the internal skeleton of neurons that helps nutrients and other essential substances travel to reach different parts of the neuron. For instance, tau proteins are expressed in glial cells in pathological conditions (17). Tau exists in the brain in six different isoforms ranging from 352 to 441 amino acids (15), and it is called tangles. Each different form of tangles is likely to have particular physiological roles that isoforms are differentially expressed during expression (15). In AD, these abnormal six forms of tau protein aggregate with other tau proteins inside the neuron and form tangles. Same as with Aβ plaques, tau tangles are largely accumulated in the brain of AD patients, slowing a person's ability to think and remember. Therefore, tau tangle accumulation in the brain is the hallmark of Alzheimer's disease.

1.3.3 Oxidative stress

Oxidative phosphorylation in the mitochondria is a process to produce ATP. As the by-product of oxidative phosphorylation, it produces free radicals or reactive oxygen species (ROS), reactive nitrogen species (RNS), and carbon- and sulfur-centered radicals to induce oxidative stress. Oxidative stress is often defined and described as a self-propagating process based on observations. This means oxidative stress is caused by excessive ROS release that triggers cellular damage, and damaged macromolecules themselves may behave as and/or become ROS (18). The brain contains high levels of lipid contents, requires high energy to maintain brain homeostasis,

and has a low level of antioxidant capacity (19). Therefore, it might be harmful to the brain if excessive oxidative stress-induced (19). In AD, for example, protein carbonyls (oxidative stress marker) are elevated in AD brain regions rich in Aβ but show at normal levels in brain regions devoid of Aβ plaques (20). The other study shows significantly elevated protein carbonyl levels in AD brains and cerebrospinal fluid (CSF) (21, 22). This increased oxidative damage results in glucose dysmetabolism and loss of ion gradients resulting in impaired action potentials and Ca2+ dyshomeostasis (23).

1.3.4 Neuroinflammation

Neuroinflammation is a complicated response to brain injury. It involves the activation of glial cells like astrocytes and microglia, the release of cytokines and chemokines, and the generation of ROS. Also, neuroinflammation is defined as the activation of the brain's innate immune system in response to an inflammatory response. In AD, neuroinflammation contributes much or more to the pathogenesis than the Aβ plaques and tau tangles. For example, increasing levels of Aβ in aging AD transgenic mice show increased pro-inflammatory cytokines, including TNF-α, IL-6, and IL-1α (24). In AD patients, plasma and CNS macrophage colony-stimulating factor levels of AD patients are significantly increased in AD patients when compared to age-matched healthy controls or patients with mild cognitive impairment (25, 26).

1.3.5 Ca^{2+} dyshomeostasis

It has been reported that intracellular calcium signaling has an important role in synaptic transmission and neuronal intra- and paracellular signal sending. A large amount of neuronal ATP is required to modulate ion exchange at the plasma membrane and ER to control intracellular calcium levels (27). Therefore, many studies show clear evidence of calcium dysregulation in AD

neurons with elevated intracellular calcium levels. Increased intracellular calcium levels are linked to excessive ROS generation, metabolic derangement, and mitochondrial dysfunction, all prominent features of AD pathogenesis (28).

Mitochondria are important intracellular organelles of cells that produce ATP for the cell's viability. Mitochondrial dysfunction is known to induce pathogenesis in AD (29). Also, mitochondria control the intracellular Ca^{2+} homeostasis where proper Ca^{2+} levels in the mitochondrial matrix are tightly regulated in oxidative phosphorylation activity, maintaining the rate of ATP production (30). However, mitochondrial respiration can be impaired if mitochondria receive excessive cytosolic Ca^{2+} or excessive Ca^{2+} transfer from the endoplasmic retuculum (31). Failing of mitochondrial Ca^{2+} homeostasis induces an increases the production of reactive oxygen species (ROS) (32). High levels of ROS in the mitochondria impairs mitochondrial membrane permeabilization that might results in cell death.

In addition, excessive synaptic-glutamate release can result to the Ca^{2+}homeostasis failure and thus excitotoxicity (33, 34). Glutamate is the neurotransmitter, which most commonly engaged in the mammalian central nervous system (CNS) to induce excitatory neurotransmission (34). Glutamate binds to calcium-permeable ionotropic receptors N-methyl-D-aspartate receptors (NMDAR) and α-amino-3-hydroxy-5-methyl-4-isoxazole propionic acid receptors (AMPAR) (35). In excitotoxicity, brain ischemic injury results in impaired glutamate transporter function. The resulting elevation in extracellular glutamate induces a massive calcium influx into neurons via NMDAR that elevated calcium influx contributes ultimately to irreversible excitotoxic injury(36, 37).

2. BBB

2.1 Function

The blood-brain barrier (BBB) is used to describe the unique functions of the CNS microvasculature. CNS vessels are continuously nonfenestrated, in addition, contain a series of additional functions that tightly regulate the movement of molecules, ions, and cells between the blood and the CNS. Therefore, BBB is the physical barrier between blood and the brain. This heavily restricting barrier function allows BBB endothelial cells to regulate CNS homeostasis, which is important to maintain neuronal function and protect the CNS from neuro-toxicants, pathogens, inflammation, injury, and disease. The restrictive function of the BBB is the challenge for drug delivery to the CNS, and, thus, most major efforts have been conducted to find the best methods to let the drug pass the BBB for delivery of therapeutics. In AD, loosening BBB tightness or losing its function is a major problem. BBB dysfunction can result in failures such as ion dysregulation, altered signaling homeostasis, and entry of immune cells and molecules into the CNS. Therefore, BBB disruption might lead to neuronal dysfunction and degeneration. The functional components of the BBB alterations and dysfunction can occur naturally with aging without cognitive decline and dementia (38, 39). BBB disruption in healthy aging may become more detrimental when exposed to inflammation like a second hit (39). For example, in aged mice with BBB disruption may not result in cognitive decline until there is an inflammation challenge (40). Therefore, the morphological (physical) and molecular (proteomic) alterations of the BBB happen in without disease (39). A study defined that healthy aging is the accumulation of time-dependent cellular damage resulting from oxidative stress, epigenetic changes, genomic instability, telomere attrition, and dysregulation of cell signaling and inflammatory responses, upon further hit, this natural disruption may become detrimental (41).

2.2 Structure

2.2.1 Brain Endothelial Cells

BBB Endothelial cells (ECs) are extremely thin cells that are 39% less thick than muscle ECs (42). BBB ECs form a monolayer, which is the first line of defense against circulating factors. The monolayer of the ECs is connected to one another by tight junctions and adherens junctions (43). Different from peripheral ECs, BBB ECs express tight junction proteins such as claudin5, occluding, and zona occludin-1. In addition, ECs are creating a physical barrier to BBB and have decreased pinocytosis, restricting vesicle-mediated transcellular transport and transporters (44). ECs have largely yielded most of the BBB surface that the transportation of the proteins and molecules can efficiently move into and out of the brain with the large surface area. This tight paracellular and transcellular physical barrier creates a polarized cell with distinct luminal and abluminal membrane compartments, therefore, transporting of the components is tightly regulated (45). ECs express efflux transporters, which polarized to the lumenal surface and transport a wide variety of lipophilic molecules that could otherwise diffuse across the cell membrane, toward the blood (46, 47). The other transporters facilitate the transport of specific nutrients across the BBB into the brain, as well as the removal of specific waste products from the brain to the blood (48). In addition, BBB ECs are known to contain a higher amount of mitochondria than the other type ECs that require a higher amount of ATP to drive the ion gradients critical for transport functions. Immune cells pass the BBB ECs and their transportation is regulated by less expression of leukocyte adhesion molecules as compared with the other type of ECs (49-51). Therefore, the physical barrier properties such as tight junctions, molecular barrier properties, as well as specific transporters to deliver required nutrients, allow the ECs to tightly regulate brain homeostasis (46). Tight junctions are the gap between the BBB monolayer of ECS, and it is required to separate tissue spaces and regulate the selective movement of solutes across the epithelium (52). Tight

junctions create the border between the apical and basolateral cell surface domains in polarized ECs, and maintenance of cell ECs polarity by restricting intermixing of apical and basolateral transmembrane components (53). Tight junctions create bidirectional signaling pathways that receive signals from the interior cell that regulate their assembly and function (53). Also, tight junction transduces signals to the cell interior to control cell proliferation, migration, differentiation, and survival (53). Tight Junction proteins are major components of ECs–ECs adhesion complexes that separate apical from the basolateral side of the BBB membrane domains (54). Tight junction proteins also maintain ECs polarity by forming an intramembrane to control the transportation of certain molecules (54). The main tight junction transmembrane proteins are the claudin (26 members in humans), occludin, the junctional adhesion molecules (JAMs) cytosolic scaffold proteins, and the intracellular zonulae occludens (ZO) like ZO-1 (55-58).

2.2.2 Astrocytes

In the brain, astrocytes regulate all different types of neuronal functions such as neuronal survival, development, metabolism, and neurotransmission (59). The brain's metabolic responses are regulated by astrocytes responding to changes in the CNS environment (60-62). In the BBB, astrocytes affect the BBB ECs by regulating the permeability of ECs by secreting several molecules (63-65). The end-feet of astrocyte ensheath the BBB and it helps to regulate the water and ion homeostasis (66). Thanks to fluid homeostasis, the brain can regulate CNS fluid flow and clearance of neurotoxins (67).

2.2.3 Pericytes

Pericytes are located on the abluminal side of the ECs and are embedded in the vascular basement membrane (67). Pericytes maintain and stabilize the BBB ECs and tight junction by regulating

angiogenesis and depositing the extracellular matrix (67). Based on neuronal activity, pericytes regulate blood flow in response (46, 68). Blood flow regulation by pericytes is important to control vascular tone and help the neural communication necessary for this particular function (67).

3. BBB and Alzheimer's disease

3.1 BBB dysfunction in humans and mouse models

Recent MRI studies to determine BBB permeability to the contrast agent Gadolinium, in patients with MCI and early AD have showed BBB dysfunction and breakdown in the hippocampus (69, 70). In addition, several gray and white matter regions were also observed (71). Increased CNS cerebral microbleeds (small chronic brain hemorrhages reflecting loss of cerebrovascular integrity) have also been showed by MRI studies in 25% of individuals with MCI and 45–78% of individuals with early AD before dementia (72-77). The BBB disruption in AD has been observed by more than 20 independent postmortem human research showing brain microvessels leakages and perivascular accumulation of blood-derived fibrinogen, thrombin, albumin, immunoglobulin G (IgG), and hemosiderin deposits, pericyte and endothelial degeneration, loss of BBB tight junctions, and RBC extravasation, as recently reviewed (78). The other studies show that an early cerebral disorder, vascular dysregulation, ischemic vascular damage from comorbidities and vascular risk factors, and small vessel disease of the brain may introduce additional vascular components contributing to BBB breakdown in AD (78-86). In the mice model, the AD mice model showed a breakdown in tight junction morphology from 5XFAD mice brains and this result supports the possibility of BBB breakdown in AD brains (87). In addition, the other mice model study showed BBB disruption by inhibiting P-glycoprotein (P-gp) and breast cancer resistant

protein (BCRP) that induced AD pathology in a mice model of AD, and indicate that therapeutic drugs that inhibit P-gp and BCRP could increase the risk for AD (88).

4. TRPA1

4.1 TRP family receptors

The transient receptor potential (TRP) multigene superfamily encodes integral membrane proteins that function as ion channels (89). The TRP family consists of seven different subfamilies, which included TRPC (canonical), TRPV (vanilloid), TRPM (melastatin), TRPP (polycystin), TRPML (mucolipin), TRPA (ankyrin), and TRPN (NOMPC-like), the latter is found only in invertebrates and fish (89). TRP family receptors are widely expressed in many different types of organs (brain, heart, small intestine, lung, bladder, joints and skeletal muscles) and cell types (89). TRP receptors are charged in many different physiological responses, such as the sensation of different stimuli or ion homeostasis (89). Most TRP receptors are non-selective cation channels that only a few of the receptors are highly Ca2+ selective and the others are permeable for highly hydrated Mg2+ ions (89). Many different of gating mechanisms are showed for these TRP channels by ligand binding, voltage, and changes in temperature to covalent modifications of nucleophilic residues (89). TRP channels activation results in the depolarization of the cellular membrane by voltage-dependent ion channels that increase intracellular Ca2+ concentration for the function of endosomes and lysosomes (89). Not only takes the ions to the intracellular, but it also releases the ions from the intracellular to maintain the cellular organelles (89). Some of the TRP receptors are expressed in a wide range of diseases in humans (90, 91).

4.2 TRPA1 Function

Transient receptor potential ankyrin 1 (TRPA1) is a calcium-permeable non-selective cation channel that is also widely expressed in sensory neurons and in non-neuronal cells (92). TRPA1 is involved in calcium ion homeostatic functions in the different types of endothelial cells (93). TRPA1 is activated by cold (mostly) and heat senses, such as pain response (94). For the first time, TRPA1 is known to be activated by spices and herbs (capsaicin and mustard oil) involving the chemically induced opening of these channels indirectly interacting with the gustatory system (95). Chemesthetic and taste systems serve as co-mediators of aversive responses to acidic and some bitter taste stimuli. Recently, an AD study demonstrated higher levels of (TRPA1) in the whole brain homogenate of the AD mice model (96). Another study demonstrate that rescued AD by blockade astrocyte expressed TRPA1 that the negative effect of amyloid-β on astrocytes induced by TRPA1 channel activation is pivotal to Alzheimer's disease progression. However, the role of TRPA1 in the BBB endothelial cell has not been investigated in AD. In the other disease, TRPA1 is a nociceptive channel expressed in the etiology of an autosomal dominant familial episodic pain syndrome (FEPS) that is demonstrated by episodes of upper body pain, triggered by fasting and physical stress (Nilius, 2011). FEPS patients show an enhanced cutaneous flare response with secondary hyperalgesia to punctuate stimuli in the presence of TRPA1 agonists (97). Calmodulin (CaM) is a Ca2+-binding protein, ubiquitously, and it is an important mediator of Ca2+-dependent regulation of TRP channels (98). A study shows that Ca2+-dependent potentiation and inactivation of TRPA1 were selectively prevented by disrupting the interaction of the carboxy-lobe of calmodulin with a calmodulin-binding domain in the C-terminus of TRPA1 (99). Therefore, TRPA1 is activated by sensing the Ca^{2+} with Calmodulin. In the brain, astrocyte is known to express TRPA1 to induce the TRPA1 channel-mediated transmembrane Ca2+ flux pathway (100). Astrocyte TRPA1 channels contribute to basal Ca^{2+} levels and are required for constitutive D-

serine release into the extracellular space, which contributes to NMDA receptor-dependent hippocampal long-term potentiation (LTP), a form of synaptic plasticity involved in learning and memory (101). Currently, only expression of TRPA was observed in the astroglial cell in AD (101). OC is known as a TRPA1 activator (102), and activation and higher expression of TRPA1 are known as an inflammatory response (103). However, our recent study shows a reduction of brain TRPA1 levels in the long-term OC-treated AD mice model at the same time cognition ability enhancement (96). Therefore, it is required to investigate the association between OC consumption and TRPA1 activation and expression in the BBB endothelial cells.

5. Oleocanthal

5.1 The Mediterranean dietary and EVOO

The Mediterranean diet is associated with beneficial health properties (104). One of the characteristics of the Mediterranean diet is to consumption of extra virgin olive oil (EVOO). Typically in the Mediterranean diet, the consumption of EVOO ranges from 25 to 50 mL per day (105). Therefore, the apparent health benefits have been partially believed to be attributed to the dietary consumption of EVOO by Mediterranean populations (104). Even though the other seed oils contain abundant oleic acid, they do not show the same health benefits as EVOO (106-108). Recently, 36 phenolic compounds have been observed in EVOO, and in vitro and in vivo studies have showed that olive oil phenolics have treatment effects on certain physiological changes such as plasma lipoproteins, oxidative damage, inflammatory markers, platelet, and cellular function, antimicrobial activity, and bone health (109). Oleocanthal (OC), a naturally occurring phenolic secoiridoid isolated from EVOO, has showed anti-inflammatory and antioxidant effects similar to the nonsteroidal anti-inflammatory drug ibuprofen (110). OC is the dialdehydic form of (−)-

deacetoxyligstroside glycoside, which known for the bitter taste of EVOO, and its chemical structure is related to the secoiridoid glycosides ligstroside and oleuropein, which are also common in EVOO (104). Ibuprofen has long been known to exert beneficial effects on markers of neurodegenerative disease (111). Therefore, it was spotlighted to investigate OC's role as a natural pharmacological component that shares similarities with ibuprofen-like compounds in both perceptual and anti-inflammatory properties (112). OC is biochemically transformed to novel marker products oleoglycin and tyrosol acetate (113). These two products are also detected in the mice brain homogenate and *in-vitro* BBB models that suggest permeability of OC cross the BBB (113). There is a study describes low absorption rate of OC in the intestine, however this report doesn't detect the biochemically transformed novel marker products of OC. In addition, OC is amphiphilic that is water soluble, thus, its solubility is not a contributing factor to the reported low intestinal absorption (114). Additional studies are necessary to clarify the pharmacokinetics profile of OC. A study with TgSwDI mice AD model shows that OC-rich EVOO restored the function of BBB and suppressed the AD-associated pathology such as neuroinflammation by inhibition of NACHT, LRR, and PYD domain-containing protein 3 (NLRP3) inflammasome, and promotes autophagy by AMP-activated protein kinase (AMPK)/Unc-51-like autophagy activating kinase 1 (ULK1) pathway (96). Also, feeding mice with an EVOO-enriched diet, beginning at an age before amyloid-β (Aβ) accumulation starts, has significantly reduced total Aβ and tau brain levels with a significant improvement in mice cognitive behavior (115). Collectively, the long-term consumption of EVOO starting at an early age provides a protective effect against AD. Our previous study shows that the clearance function of BBB has been enhanced by receiving OC-rich EVOO treatment that demonstrates less Aβ plaque deposition, increasing levels of tight junction protein, such as claudin5 (96, 116). Therefore. OC-rich EVOO demonstrates treatment effect on

the AD BBB dysfunction that enhances Aβ clearance to prevent AD-linked neurodegenerative pathologies such as neuroinflammation. In the mice behavioral experiment, cognitive impairment of the AD mice model with the OC-rich EVOO treatment was restored in the Morris-water maze behavioral experiment (96). Therefore, enhancing the BBB clearance function might have a positive effect on restoring cognitive impairment.

6. Metabolic phenotyping

6.1 Definition

Metabolic phenotyping is the observation of an alteration in metabolic phenotypes that are the products of interactions among a variety of factors including dietary and other lifestyle and environmental factors (117). Examples of metabolic and behavioral phenotypes include energy expenditure (EE), activity, food intake as well as sleep patterns (118). The pathological phenotype of AD has been well established, but our understanding of metabolic and behavioral phenotypes changes, which necessary to support AD detection and diagnosis, continues to be limited.

6.2 Parameters

Metabolic phenotype is defined by metabolic parameters the reflect subject metabolic function. The energy expenditure is the parameter to measure the consumption of kilocalories of the subject, which related to the consumption of oxygen and CO2 reflecting respiratory quotient to the observer consumption rate of carbohydrate and fat. The other parameters are including, water and food consumption, sleeping time, movement distance and body weight. There are four energy expenditure components, which including sleeping metabolic rate, the required energy for arousal, the food's thermic effect, and the required energy cost for the physical activity or activity-induced

energy expenditure. The energy expenditure is calculated by the basal metabolic rate (BMR) calculator, which estimation of how many calories you burn per day when exercise is taken into account (119). RQ means a proportion of a volume of CO2 generated to the volume of O2 , which consumed at cellular levels. Similarly, RER is the proportion of a volume of CO2 generated to the volume O2, which consumed by using expelled air in the calculation (119). Moreover, RQ value is directly used in measurement in the blood (120); however, RER value indirectly measures from the breath.

6.3 Connection between parameters and AD

In AD, patients experience sleep disturbances that may precede the other clinical signs of this neurodegenerative disease (121). Also, sleep disorders may affect the circadian rhythm, which could lead to fluctuations in the concentrations of amyloid-β in the interstitial brain fluid (ISF) and in the cerebrovascular fluid (CSF) associated with the glymphatic clearance of Aβ (122-125). For example, a preclinical in-vivo study has reported the clearance of Aβ during sleep was two-fold faster than during wakefulness (126). In human, monitoring the sleep-wake cycle in individuals with AD aged 45–75 years has showed decreased sleep efficiency and increased nap frequency in individuals with Aβ deposition compared with those similarly aged without amyloid deposition determined by CSF Aβ42 level (127). Thus, sleep disturbances might contribute to the progression of AD both through impaired glymphatic clearance and disturbances in Aβ production (121). The anxiety is one of the neuropsychiatric symptoms of AD anxiety levels of AD patients are increased with AD biomarkers (128). The anxiety has also been considered a risk factor for AD, especially the anxiety occurring in midlife (129). A human study describes that Human Alzheimer's patients exhibit the anxiety at the mild cognitive impairment stage of AD, which associated with an increased likelihood of developing dementia (130). In addition, transgenic rodent models of

Alzheimer's disease exhibit inconsistent markers of the anxiety in an open field, elevated plus-maze, and light/dark tests (130). Besides sleep disturbances, recently, several studies have reported appetite loss in persons with dementia and mild cognitive impairment (MCI) (131). Decreased meal consumption results in malnutrition, dehydration, failing body homeostasis, weakening immune, and reduced cognitive function. In AD patients, a range of factors, including fastidiousness in eating and the inability to feel hungry as a result of brain atrophy, disturbance of eating behavior, loss of the ability to use eating utensils, and decreased swallowing function can affect appetite (132).

7. Alzheimer's disease mouse model 5xFAD

5XFAD mouse is a genetically modified AD mice model with 3 APP mutations and 2 of presenilin mutations to produce Aβ at an early age (five AD-linked mutations: the Swedish (K670N/M671L), Florida (I716V), and London (V717I) mutations in APP, and the M146L and L286V mutations in PSEN1). 5xFAD is designed to induce many AD-related phenotypes and has a relatively early-age aggressive Aβ accumulation . Amyloid plaques aggregation with gliosis arecommonly found in this mice model at two months of age. At 6 months, neuron loss starts in multiple brain regions in the areas with the most Aβ abundant. Mice show a range of cognitive impairment and motor deficits. These mice produce high levels of intraneuronal Aβ42 from the age 1.5 months (133). In addition, there is a found of intracellular immunoreactivity of cathepsin-D for Aβ, and cathepsin-D is a maker of lysosomes and other acidic organelles (134). Thioflavin S staining shows an intracellular isoluble Aβ42 deposition that may form β-pleated sheet to be aggregated (133). Aβ plaques are found in the hippocampus and the cortex by the age six months. Even older than 6 months, Aβ plaques are present in the olfactory bulb, brainstem, and thalamus, but are absent from

the cerebellum (133). The other study shows an finding of amyloid pathology in the spinal cord, at the age 11 weeks in cervical and lumbar regions and extending along the length of the cord by the age 19 weeks (135). Especially, there is significant Aβ pathology difference in sex that females exhibit more aggressive plaque pathology: higher numbers of plaque in the hippocampus and the cortex are in females than in males, and continue to increase until the age 14 months, while numbers in males plateau at their age 10 months (136).

8. Project-specific aims, hypotheses, and objectives

8.1 Knowledge gap

- No studies are available on changes in metabolic and behavioral phenotypes with aging in AD mouse models.
- No studies are available on whether TRPA1 expression changes with AD pathology in the endothelial cells of the BBB.
- OC effect on the BBB endothelial TRPA1 is unknown.

8.2 Hypothesis and objectives

The objectives of this work are to determine how age and pathology alter metabolic and behavioral parameters in AD mice model, whether these changes are associated with BBB dysfunction, and could OC restore these pathological, metabolic and behavioral phenotypes in 5xFAD mice.

The project hypothesis is that OC-mediated enhanced BBB function improves metabolic and behavioral parameters in 5xFAD mice.

Specific aim 1. To assess the effect of age and pathology on the metabolic and behavioral phenotypes in 5xFAD mice, a model of AD

Specific aim 2. To in vivo examine the effect of OC on metabolic and behavioral phenotypes and BBB function in 5xFAD mice

Sub aim 1.1. Evaluate the effect of OC treatment on metabolic and behavioral parameters

Sub aim 1.2. Determine in vivo effect of OC treatment on BBB function

Specific Aim 3. To in vitro examine the effect of TRPA1 modulation by OC on a cell-based BBB model

2. Metabolic and behavioral phenotype changes with age and amyloid-related pathology in a mouse model of Alzheimer's disease

2.1. Abstract

Alzheimer's disease (AD) is a progressive neurodegenerative disorder that causes cognitive impairment and dementia. Age is considered the major risk factor for AD. Aging induces changes in body metabolism and behavior such as activity rate, body weight, and sleeping pattern to list a few. Currently, there are several examinations to diagnose AD and respond to treatments using surveys and cognition tests; however, besides these tests, additional assessments to monitor changes in metabolic and behavioral phenotypes that might be used as preclinical AD diagnostic tools could be beneficial. In this work, we assessed the effect of aging and pathology on metabolic and behavioral phenotypes in wild-type C57Bl/6 and 5xFAD mice models. Our findings demonstrated both aging and pathology alter body metabolism and behavior, such as activity rate and sleeping pattern. However, the effect of pathology on monitored parameters was significantly higher than with normal aging, an effect that was associated with increased amyloid-β deposition and blood-brain barrier disruption. In conclusion, changes in metabolic and behavioral phenotypes could be used as an assessment for disease severity and treatment efficacy.

2.2. Introduction

Alzheimer's disease (AD) is a neurodegenerative disorder that causes dementia. Neurodegeneration in AD induces cognitive impairment, which cannot be restored to normal once the disease reaches a severe stage. Therefore, early diagnosis, prevention, and treatment of AD could be the best strategy to prevent or hold AD progression.

Aging changes many physiological processes in the human body, including metabolic and behavioral phenotypes (137). The brain is one of the organs that changes its structure constantly from birth throughout its lifetime. Aging induces a reduction in specific cognitive abilities, accompanied by decreased brain volume, synaptic spines, and length of myelinated axons (138). Therefore, aging is considered a major risk factor for developing neurodegenerative diseases, including AD.

Metabolic phenotyping is the observation of an alteration in metabolic and behavioral phenotypes that are the products of interactions among numerous factors, including dietary and other lifestyle and environmental factors (117). Examples of metabolic and behavioral phenotypes that are affected with aging include activity, energy expenditure, food intake, and changes in sleep patterns (118). While the pathological characteristics of AD are well established, our understanding of metabolic and behavioral phenotypes changes, which is necessary for early AD diagnosis and staging, continues to be limited. In AD, patients experience sleep disturbances that may precede the other clinical signs of AD (121). Also, sleep disorders may affect the circadian rhythm that could lead to fluctuations in the concentrations of amyloid-β (Aβ) in the interstitial brain fluid (ISF) and in the cerebrovascular fluid (CSF) associated with the glymphatic clearance of Aβ (122-125). It has been reported that in the adult brain, the clearance of Aβ during sleep is two-fold faster than during wakefulness (126) and that brain Aβ accumulation induces excessive daytime

sleepiness (139). In humans, monitoring the sleep-wake cycle in individuals with AD aged 45–75 years has showed a decreased sleep efficiency and increased nap frequency in individuals with Aβ deposition compared with individuals of the same age group but without Aβ deposition as determined by CSF-$A\beta_{42}$ level (127). Thus, AD could affect the sleep pattern, and at the same time, sleep disturbances might contribute to the progression of AD through impaired glymphatic clearance and disruptions in Aβ production (121).

Besides sleep disturbances, recently, several studies have reported appetite loss in persons with dementia and mild cognitive impairment (MCI) (131). Decreased meal consumption results in malnutrition, dehydration, failing body homeostasis, weakening immunity, and reduced cognitive function (140). In AD patients, a range of factors including fastidiousness in eating and the inability to feel hungry because of brain atrophy, disturbance of eating behavior, loss of the ability to use eating utensils, and decreased swallowing function can affect appetite (132). Loss of appetite means a low energy consumption rate, which results in less energy expenditure. Energy expenditure is analyzed by body size and composition, food intake, and physical activity (141). Body size and composition determine resting energy expenditure (141).

The anxiety is one of the neuropsychiatric symptoms of AD (142). Higher the anxiety levels in AD patients are one of the common behavioral symptoms (128). The anxiety has also been considered a risk factor for AD, especially the anxiety occurring in midlife (129). A human study describes that AD patients exhibit the anxiety at the MCI stage of AD, which is associated with an increased likelihood of developing dementia (130). In addition, transgenic rodent models of AD exhibit inconsistent markers of the anxiety in an open field, elevated plus-maze, and light/dark tests (130).

In AD research, AD mice models are frequently used to understand the pathology and test potential treatments; however, whether these mice models demonstrate similar metabolic and behavior phenotypes changes as those observed in humans is unknown. Thus, this work aimed to compare difference in metabolic and behavioral phenotypes as a function of age (4 vs. 9 months) and pathology in wild-type (WT) and 5xFAD as mice model of AD. Our findings showed that higher levels of sleep disturbances in 4 and 9 months 5xFAD mice group in energy expenditure (EE), higher movement distance, low body weight, and higher O_2 and CO_2 consumption compared to the WT at both ages. Between the age groups, the parameter difference in the 9 months WT and 5xFAD show more distinguishable difference than the 4 months group. There was no significant change in the food intake difference between the two groups at 4 and 9 months. However, water consumption of 5xFAD has decreased. In addition to metabolic and phenotypic assessments, we characterized Aβ levels in the brain and blood tissues, and our findings demonstrated that at 4 months, in 5xFAD blood, mice demonstrated higher $A\beta_{40}$ and $A\beta_{42}$ levels than the WT; however, at 9 months, 5xFAD mice showed lower Aβ levels than the WT. In this work, we also characterized the effect of age and AD pathology on brain Aβ and the blood-brain barrier (BBB) function.

2.3. Methods and materials

2.3. 1. Animal

Male wild-type C57BL/6J and 5xFAD mice models were used in the studies at 4 and 9 months (n=10 mice per group). The transgenic 5xFAD mice expresses human amyloid precursor protein (APP) with the mutations APP KM670/671NL (Swedish), APP I716V (Florida), APP V717I (London), and PSEN1 M146L and PSEN1 L286V, leading to early and aggressive Aβ accumulation associated with inflammatory astrocytes activation, which develops in parallel with plaque deposition, and deficits in spatial learning as the disease progress (Oakley, 2006). In 5xFAD, extracellular Aβ plaque deposition starts at 2 months with gliosis. This early Aβ deposition and gliosis induce synaptic loss, resulting in cognitive impairment at 4 months. Aged C57BL/6J mice are frequently used in studies related to neurodegenerative disorders. C57BL/6 mice demonstrate a decline in physical function as early as 6 months of age, while the cognitive function begins to decline later, with a considerable impairment present at 22 months of age (143).

The WT and 5XFAD mice were purchased from Jackson Laboratory (Bar Harbor, ME) and housed for breeding in plastic containers under 12 h light/dark cycle, 22°C, 35% relative humidity, and *ad libitum* access to water and food. At 4 (n=10 per mice model) and 9 (n=10 per mice model) months of age, mice were transferred to metabolic cages as described below to perform the metabolic and behavior phenotypic assessments. All animal experiments and procedures were approved by the Institutional Animal Care and Use Committee of Auburn University and according to the National Institutes of Health guidelines Principles of laboratory animal care.

2.3. 2. Metabolic and Phenotyping assessments

Promethion metabolic mouse cages (Sable Systems, Las Vegas, NV) were used to house animals for metabolic screening and phenotyping. Animals were transferred from their home cages and singly housed in the metabolic cages at the age of 4 and 9 months. The animals were singly housed in the metabolic cages for 3 consecutive days with the first day stated for the cage environment adaptation and the second and third days for data collection. Animal activity was measured by Promethion XYZ Beambreak Activity Monitor. Food and water intake, body weight, movement distance, sleeping time, mean rate of oxygen consumption (VO_2), and mean rate of carbon dioxide emission (VCO_2) were measured by Promethion precision MM-1 Load Cell sensors. The time for metabolic parameters measurement is defined as 12h:12h light:dark cycle with zeitgeber time (ZT) 0 representing lights on and ZT12 representing lights off. The amount of food and water withdrawn from the container was measured and analyzed. The body weight monitors were plastic tubes that also functioned as in-cage enrichment and nesting devices. The mean rate of water vapor loss (VH_2O), VCO_2, and VO_2 (all measured in ml/min) were analyzed by the Promethion GA-3 gas analyzer to provide detailed respirometry data. Energy expenditure (EE) was calculated in kilocalories (kcal) by utilizing the Weir equation: $60*(0.003941*VO_2\ (n) +0.001106*VCO_2\ (n))$. The respiratory exchange ratio (RER) was determined by measuring gas exchange within the metabolic cages to identify the substrate primarily utilized for energy within the body. Specifically, RER is the ratio of VCO_2 produced to VO_2 ($RER = VCO_2/VO_2$), where an RER ~ 0.7 indicates lipid utilization and an RER ~ 1.0 indicates carbohydrate utilization. All metabolic phenotyping data are analyzed using ExpeData software (version 1.8.2; Sable Systems) with Universal Macro Collection (version 10.1.3; Sable Systems). The parameter All Meters is the sum of all distances traveled within the beam break system in meters (m). This includes fine movement (such as

grooming and scratching) as well as direct locomotion. All assessed parameters are summarized in Table 1.

Table 2.3. 1. Table of the definition of metabolic parameter and its unit

Parameters	Definition
Body weight	Mean Body mass of the animal, in grams (g)
Food intake	Mass of food consumed by animal, in gram (g)
Water intake	Mass of water consumed by animal, in gram (g)
EE	Mean energy expenditure during the 60 mins with the highest EE, in kcal/hr
VCO2	Mean rate of carbon dioxide emission, in ml/min
VO2	Mean rate of oxygen consumption in ml/min
RER	Mean respiratory quotient, VCO2/VO2, unit-less
VH2O	Mean rate of water vapor loss, in ml/min
All Meters	Sum of all distances traveled within 60mins, in meters
Cumulative All meters	Sum of cultivative distance traveled within 60 mins.

2.3. 3. Immunohistochemistry

After the phenotyping assessment, mice were sacrificed to collect the brain and blood tissues. Brain sections of 15 μm were prepared using a ThermoScientific HM525 NX Cryostat (Waltham, MA, USA). Sections were fixed with 4% paraformaldehyde and then blocked for 60 min with the blocking buffer TrueBlack background suppressor (Biotum; Fremont, CA). To assess the blood-brain barrier (BBB) integrity, IgG extravasation from brain microvessels was determined. For this, sections were probed by dual immunohistochemical staining with anti-rabbit collagen-IV as a primary antibody to detect brain microvessels (Millipore Sigma, Burlington, MA), and fluorescein-conjugated goat anti-mouse IgG H&L (Alexa Fluor® 488) (Abcam Cambridge, United Kingdom) to detect IgG extravasation, both at 1:500 dilution. The secondary antibody for collagen

antibody was anti-rabbit (Alexa Fluor® 594) (Abcam Cambridge, United Kingdom). Images were captured and adjusted to the lowest background signal using Nikon Eclipse Ti-S inverted fluorescence microscope (Melville, NY, USA). For quantification of Aβ load and IgG extravasation, sections were normalized to the same background for the hippocampus and the cortex regions. Images were analyzed by Image J software (National Institutes of Health, Bethesda, MD, USA) that was set for mean value, minimum value, maximum value, and limit to the threshold followed by analysis.

2.3. 4. Measurements of brain and plasma Aβ by ELISA

Commercially available ELISA kits were used to determine $A\beta_{40}$ and $A\beta_{42}$ levels in WT and 5xFAD mice brain tissue lysates and plasma according to the manufacturer's instructions (R&D Systems, Minneapolis, MN). All samples were run in duplicate. Brain Aβ levels were corrected to the total protein amount in each sample using the bicinchoninic acid (BCA) assay.

2.3. 5. Statistics

All metabolic phenotype parameters were analyzed in R statistics with Student's *t-test*. Twenty-four-hour circadian data are analyzed by the R program by *t-test* to compare circadian time points of WT animals with 5XFAD. Multiple linear regression analysis (ANCOVA) was applied to assess the impact of aging and AD pathology on metabolic cage parameters. All the tissue sample experiments were analyzed using a one-way ANOVA test with *Tucky post hoc* in the Graphpad Prism (San Diego, California). Significance for all measures was determined at $p < 0.05$ and all data are presented as Mean ± SEM.

2.4. Results

2.4. 1. Effect of age on the phenotypic parameters in WT and 5xFAD mice

The metabolic phenotype parameters were measured from 6 am to the next day at 6 am (24 h). Figure 2.6. 1. and Figure 2.6. 2. show the effect of age (4 vs. 9 months) on assessed parameters in the WT and 5xFAD mice, respectively, over time. As showed in Figure 2.6. 1. and Table 2.3. 2, while a gain in body weight is expected with aging, time points comparison of the parameters demonstrated a significant reduction in EE, VCO_2, VO_2, RER and VH_2O in the WT-9 months mice compared to the WT-4 months mice across multiple time points in the ZT. Interestingly, in 5xFAD mice, except for the significant increase in body weight and VH_2O with age, monitoring changes in assessed parameters over time between 0-24 h, didn't show significant alteration between 4 and 9 months (Figure 2.6. 2. and Table 2.3. 3.).

Figure 2.6. 3. demonstrates the effect of age and pathology on the parameters at day (summation of 0-11 h) and night (12-23 h) times. In the WT and 5xFAD mice, 9 months of age mice have higher body weight than the 4 months mice (Figure 2.6. 3. A.). At 9 months, the body weight increased by 22 and 11% in the WT and 5xFAD mice, respectively, suggesting a lower body weight gain in 5xFAD mice. During the daytime, no significant difference between the 4- and 9-months WT mice was observed in food intake (Figure 2.6.3.B), and all meters (total and accumulative movement distance; Figure 2.6. 3.I&J.). However, the data demonstrated a

significant decrease in EE, CO_2, VCO_2, and RER parameters (Figure 2.6.3.D-G.) in the WT-9 compared to the WT-4 months mice. The older mice demonstrated a shift in the rate of water vapor loss (VH_2O) toward the nighttime with lower rates than the young mice (Figure 2.6. 3. H.). In 5xFAD mice, the age effect was different where a significant increase was observed in food intake, EE, VCO_2, VO_2, VH_2O, and cumulative all meters (Figure 2.6. 3 B, D-F, I, and J.), while no change was observed in other parameters. These results suggest that the aging of the WT mice is associated with less metabolic activity, while 5xFAD demonstrated increased activity in the daytime.

At nighttime, the WT mice demonstrated a similar pattern to the daytime where a significant reduction in metabolic parameters including EE, VCO_2, VO_2, RER, and VH_2O (Figure 2.6. 3. D-H.). Nine months old 5xFAD, on the other hand, demonstrated a significant increase in VH_2O, all meters, and cumulative all meters (Figure 2.6. 3. H-J.), while the RER parameter was significantly reduced (Figure 2.6. 3. G.).

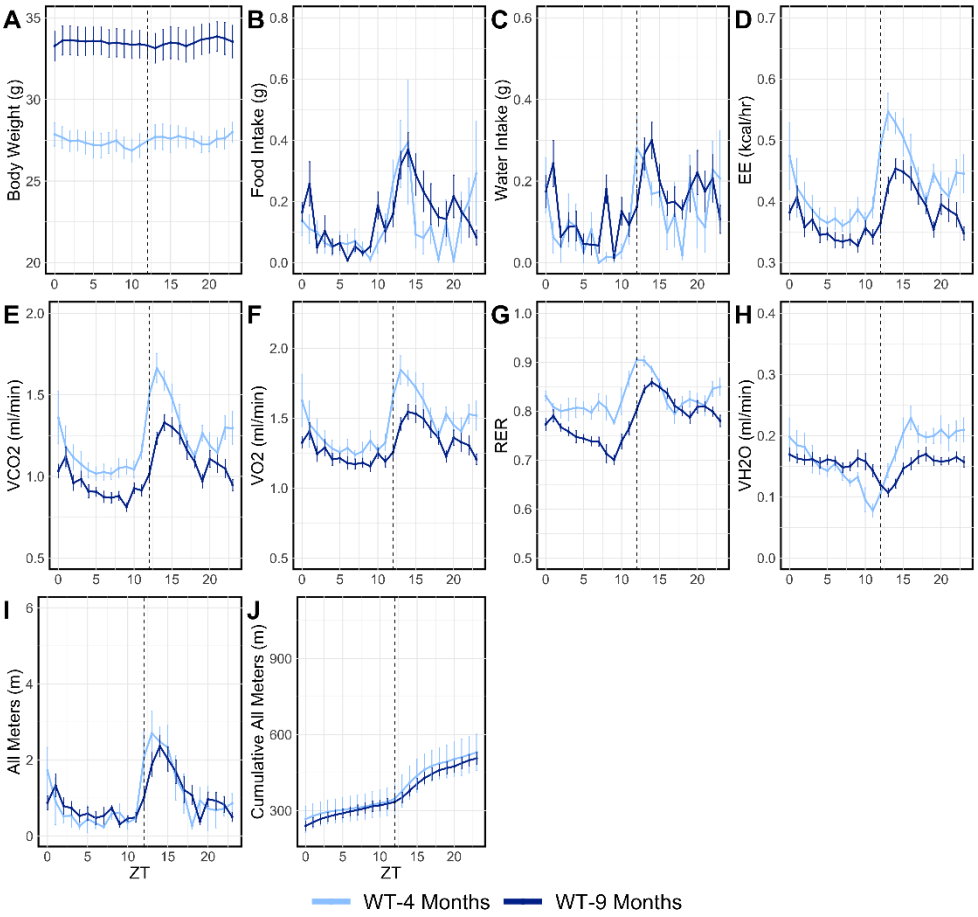

Figure 2.6. 1. Aging effect on metabolic phenotypic parameters in WT mice. A comparison between 4 and 9 months old of the WT. Our data indicate significant changes found in all parameters except in water intake all meters and accumulative all meters. We found that aging relatively reduces respiratory ratio (E, F, and G) and EE (D). However, aging doesn't affect movement distance, the higher movement distance reflect the anxiety levels of the mice. Therefore, our data indicate that aging itself may not induce the anxiety in the mice model.

Table 2.3. 2. Statistical significance of WT-4 vs. WT-9 months shown in Figure 1.

ZT	0	1	2	3	4	5	6	7	8	9	10	11	12	13	14	15	16	17	18	19	20	21	22	23
Body Weight	**	**	***	**	***	***	***	***	**	***	***	***	**	**	**	**	**	**	**	**	***	***	**	**
Food Intake							**												*					
Water Intake									*										*					
EE	*									*			**	***	*					**				**
VCO2	*						*	*	*	***		**	***	***	*					**			*	***
VO2	*									*			**	**	*					**				**
RER	*			*	*	**	**	***	*		*	***	***	***									*	**
VH2O											*	**		*	**	*	**			*	**	*	*	*
All Meters																								
Cumulative All Meters																				*				

$p<0.05$ =*, p<0.01=**, p<0.001=***

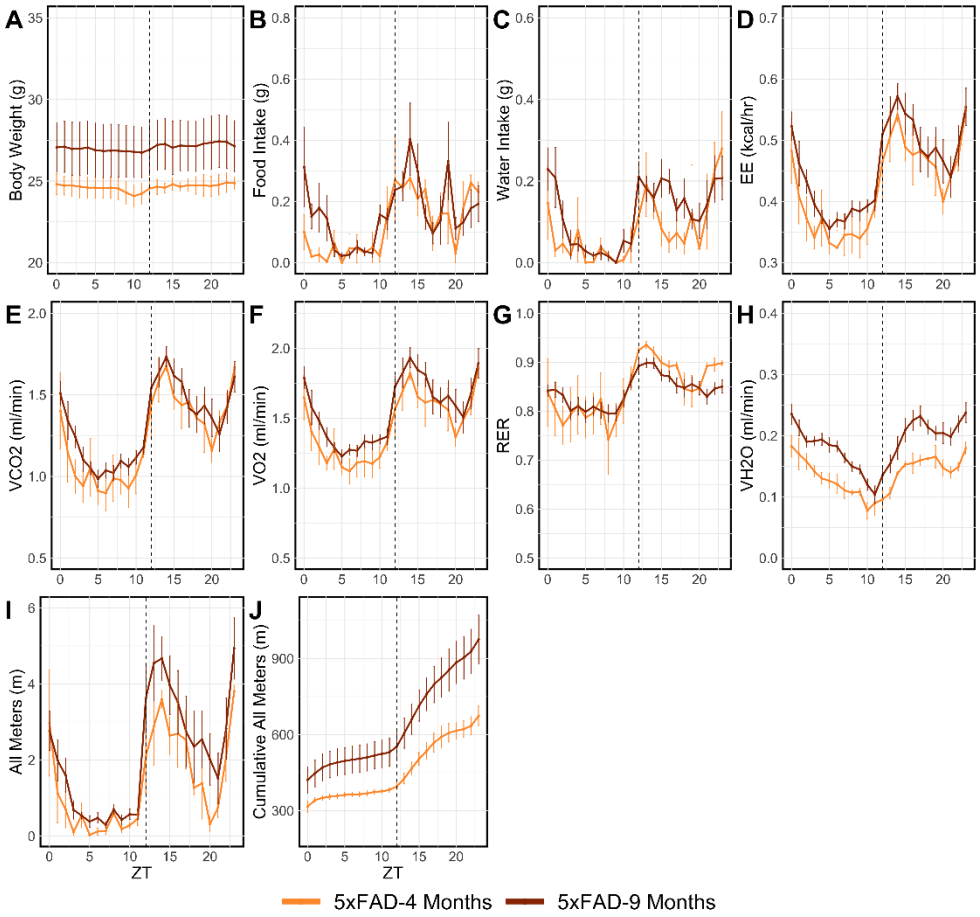

Figure 2.6. 2. Aging effect on metabolic phenotypic parameters in 5xFAD mice. A comparison between 4 and 9 months old of 5xFAD. Our data indicate significant changes found in all parameters except in water intake. Our data indicate an opposite result compared to Fig 2.6. 1. 5xFAD mice model shows a significantly higher movement distance (I and J) that causes significantly higher EE (D) and respiratory index (E, F, and G). Higher movement distance may indicate a level of the anxiety. Therefore, our data indicate that aging in AD may induce the anxiety.

Table 2.3. 3. Statistical significance of 5xFAD-4 vs. 5xFAD-9 months shown in Figure 2.

ZT	0	1	2	3	4	5	6	7	8	9	10	11	12	13	14	15	16	17	18	19	20	21	22	23
Body Weight																								
Food Intake											*													
Water Intake																	*							
EE																								
VCO2																								
VO2																								
RER																						*		
VH2O				**	**	*	**	**	*	*	*						*	*	*				*	
All Meters																								
Cumulative All Meters																								

p<0.05 =*, p<0.01=**, p<0.001=***

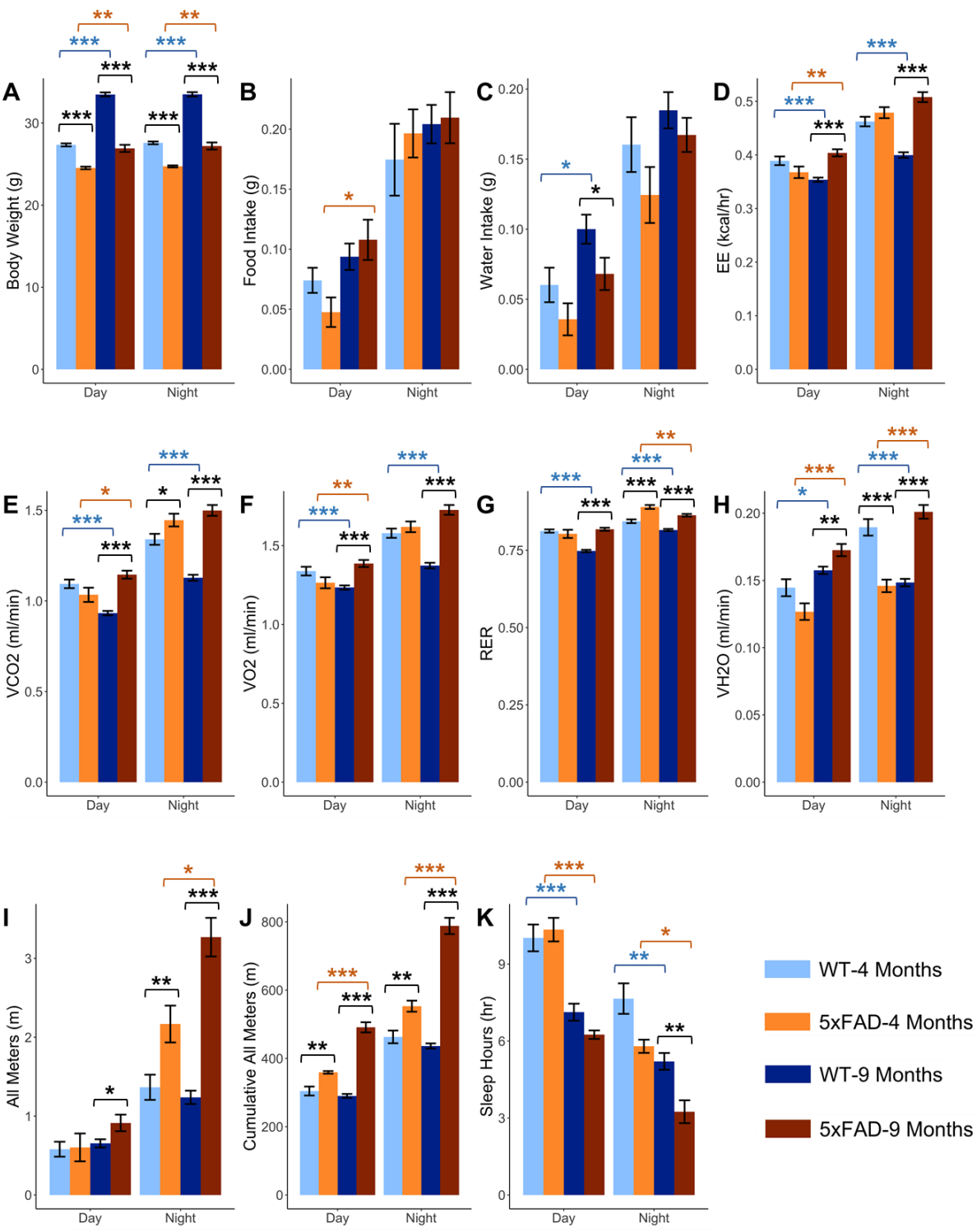
A
Body Weight (g)
B
Food Intake (g)
C
Water Intake (g)
D
EE (kcal/hr)
E
VCO2 (ml/min)
F
VO2 (ml/min)
G
RER
H
VH2O (ml/min)
I
All Meters (m)
J
Cumulative All Meters (m)
K
Sleep Hours (hr)
Day
Night
WT-4 Months
5xFAD-4 Months
WT-9 Months
5xFAD-9 Months

Figure 2.6. 3. Metabolic phenotypic parameters of 4 and 9 months old WT and 5xFAD in day and night separately. This data indicates a measurement comparison between day and night. Our measurement indicates higher metabolic parameters at night that mice are nocturnal (A-L). We found that aging itself induces slight changes in metabolic parameters; however, AD induces significantly increased levels in metabolic parameters day and night. In addition, a sleeping time of 9 months 5xFAD mice show a significantly reduced at night (M and N). Therefore, this data indicates that AD induces sleep disturbance as a neuropsychiatric symptom.

2.4. 2. Effect of pathology on the phenotypic parameters at 4 and 9 months in 5xFAD

Figure 2.6. 4. and Figure 2.6. 5. demonstrate the effect of pathology on assessed parameters over time in the WT and the 5xFAD mice at 4 and 9 months, respectively. At the age of 4 months, the data didn't show a significant difference during the 24 h with the exception of a few time points; however, there was a trend for a difference between 12-23 h (Figure 2.6. 4., Table 2.3. 3), which was better demonstrated in the day and nighttime data showed in Figure 2.6. 3. On the other hand, at the age of 9 months, 5xFAD demonstrated a significant increase in all assessed metabolic parameters almost at all time points between 0-23 h (Figure 2.6. 5.), suggesting a significant pathology effect in older mice.

Compared to the WT mice at 4 and 9 months, 5xFAD demonstrated a significantly lower body weight by 10 and 20%, respectively. Within the daytime (Figure 2.6. 3.), while 5xFAD-4 months mice demonstrated lower food and water intake compared to the WT-4 months mice, this difference was not significant. All other parameters were comparable to the WT mice except for cumulative all meters parameter (Figure 2.6. 3. J.). On the other hand, at 9 months of age, 5xFAD demonstrated a significant reduction in water intake, and a significant increase in the metabolic

parameters EE, VCO_2, VO_2, RER, VH_2O, all meters, and cumulative all meters (Figure 2.6. 3. D-J.). At nighttime; however, 5xFAD-4 months mice showed a significant increase in VCO_2, RER, all meters, and cumulative all meters, which associated with a significant reduction in VH_2O compared to the WT mice. Similar to the 4 months changes, 9 months old 5xFAD mice old 5x-FAD maintained a significant increase in the metabolic parameters EE, VCO_2, VO_2, RER, VH_2O, all meters, and cumulative all meters (Figure 2.6. 4. D-J.).

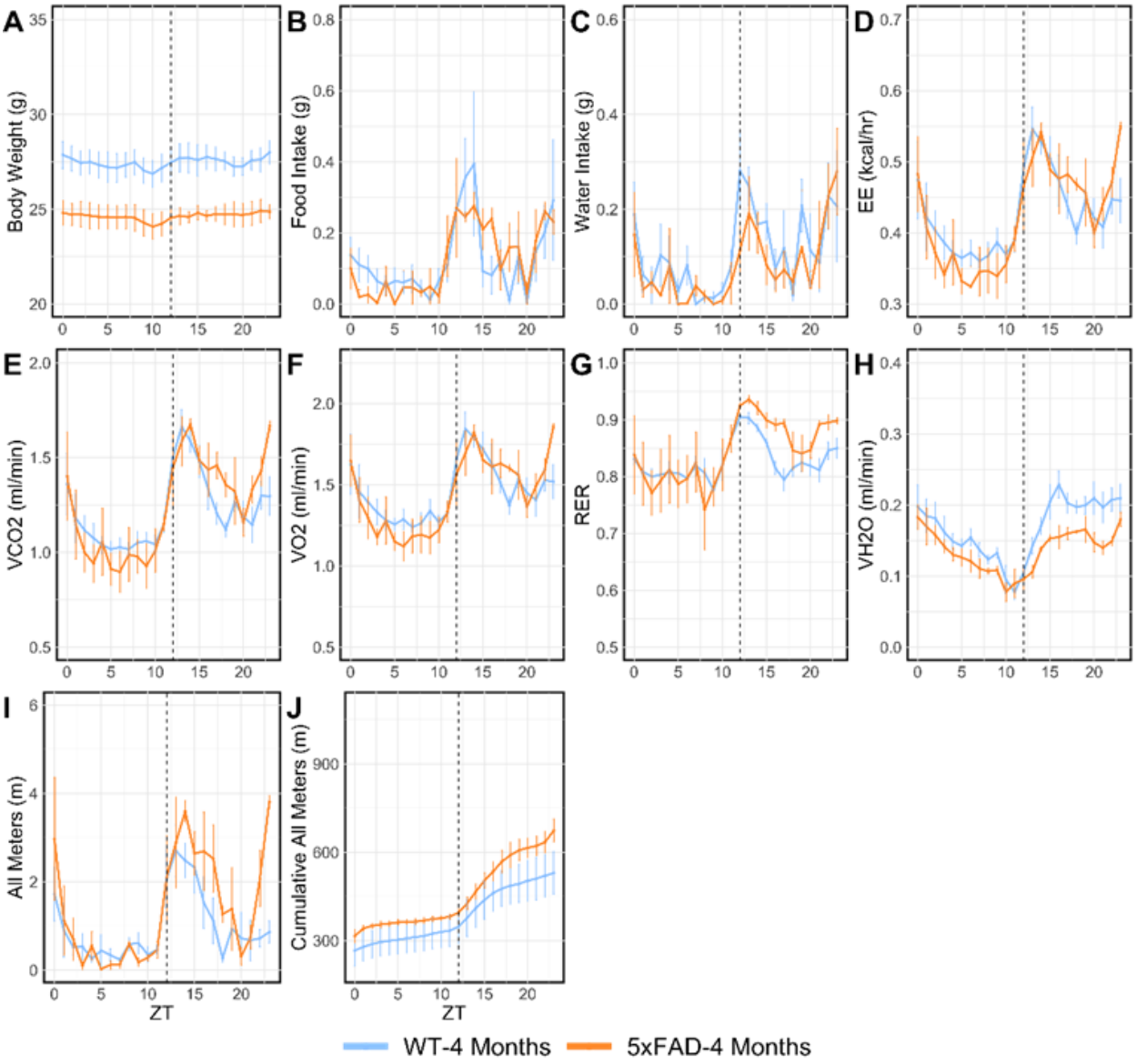

Figure 2.6. 4. Disease effect on metabolic phenotypic parameters in 4 months old WT and 5xFAD. Our data indicate a lower body weight exhibited in the 5xFAD group. Also, the 5xFAD group shows a significantly higher respiratory index (G) by increasing movement distances which correlated to the anxiety levels (I, and J). Interestingly, EE between the WT and 5xFAD was not significantly different from each other. Therefore, our data indicate that AD induces the anxiety that alters metabolic parameters

Table 2.3. 4. Statistical significance of 4 months WT vs. 5XFAD in Fig 2.6. 3.

ZT	0	1	2	3	4	5	6	7	8	9	10	11	12	13	14	15	16	17	18	19	20	21	22	23
Body Weight	*	*	*	*	*			*	*	*	*	*	*	*	*	*	*	*	**	*	*	*	*	*
Food Intake																			*					
Water Intake																	*		*				*	
EE																			*					*
VCO2																		*	*					*
VO2																			*					
RER													*		*	*	**	*				*		
VH2O																	*		*				*	
All Meters																								
Cumulative All Meters																			**				*	***

p<0.05 =*, p<0.01=**, p<0.001=***

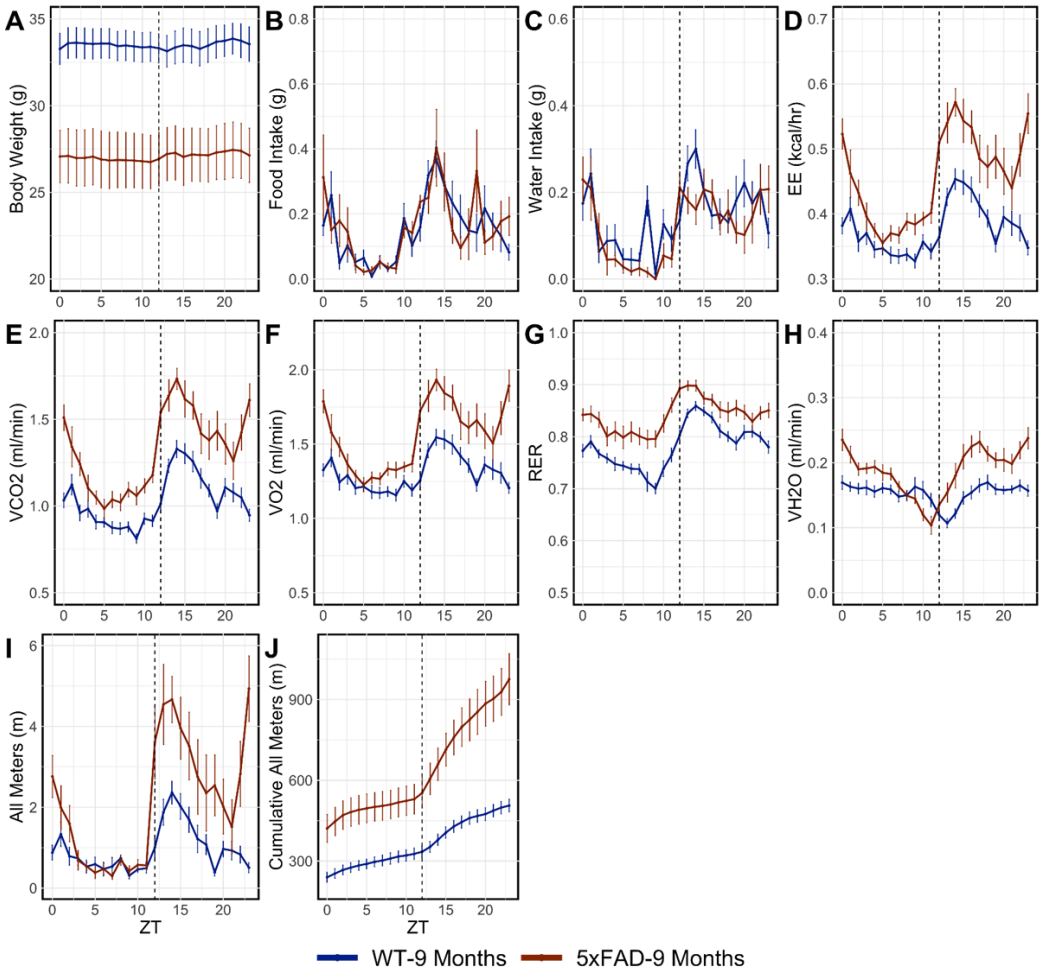

Figure 2.6. 5. Disease effect on metabolic phenotypic parameters in 9 months old WT and 5xFAD. Our data indicate significant difference between the WT and 5xFAD except for food (B) and water intake (B). Compared to the WT, the 5xFAD group shows significantly higher movement distances (I and J) reflect in significantly higher EE (D), respiratory index (E, F, and G), and dehydration rate (H). Compared to the data from Fig. 2.6. 3., 9 months groups of the WT and 5xFAD demonstrate distinguishable results that AD induces a higher metabolic rate in mice by inducing higher activity that may reflect an anxiety level as a neuropsychiatric symptom (I, J, K and L). Therefore, our data demonstrate that AD induces the anxiety in the 9 months old 5xFAD mice model.

Table 2.3. 5. Statistical significance of 9 months WT vs. 5xFAD in Fig 2.6. 4.

ZT	0	1	2	3	4	5	6	7	8	9	10	11	12	13	14	15	16	17	18	19	20	21	22	23
Body Weight	**	***	***	***	***	***	***	***	***	***	***	***	***	**	**	**	**	**	**	**	**	**	**	**
Food Intake																								
Water Intake									**						*									
EE	***		**						**	**	*	**	***	***	***	*	**		*	***			**	***
VCO2	***		**		*		*	*	***	***	**	***	***	***	***	**	**	*	**	***	*		**	***
VO2	***		*						*	*		*	***	**	***	*	**		*	***			**	***
RER	**	*	***	*	**	*	**	**	**	***	**	***	***	***	*		*		*	**			**	***
VH2O	**	**	*		*		*					*		**	**	**	***	**	*	**	**	**	**	***
All Meters	***	***	***	***	***	***	***	***	***	***	***	***	***	***	***	***	***	***	***	***	***	***	***	***
Cumulative All Meters	***												**	**	***	*	*			**			**	***

p<0.05 =*, p<0.01=**, p<0.001=***

2.4. 3. Effect of age and pathology on sleep pattern in WT and 5xFAD

As showed in Figure. 2.6. 3., mice sleeping time during the daytime is longer than the nighttime in both mice models. Sleeping behavior was also influenced by age and pathology. At day and night times, 9 months old WT and 5xFAD mice demonstrated a significantly lower sleeping time by ~ 30 and 40%, respectively, compared to the 4 months mice. For the effect of pathology on sleeping behavior, during the daytime, at the age of 4 months, there was no significant difference between the 2 mice models; during the nighttime, 5xFAD mice slept about 25% fewer hours than the WT mice, but this reduction was not significant ($p=0.12$). For older mice, although the effect didn't reach statistical significance ($p=0.06$), the pathology mildly impacted the sleep behavior during the daytime with 5xFAD mice sleeping 10% fewer hours compared to the WT mice; however, at nighttime, it was significantly reduced by 40% compared to the WT mice ($p=0.0016$).

2.4. 4. Effect of age and pathology on BBB function

In AD mice models, extravasation of large molecular size proteins, such as IgG, is commonly observed (96, 144). Thus, IgG extravasation into mice brains was assessed by immunohistochemistry to evaluate the effect of age and pathology on BBB function. As showed in Figure 2.6. 6., IgG extravasation was observed in the 5xFAD-4 months and the WT-9 and 5xFAD-9 months. For the effect of age, at 9 months of age, WT mice demonstrated a significant 5-6% increase in IgG extravasation in the mice hippocampus and the cortexes compared to the 4 months WT mice. In 9-month 5xFAD mice, significantly higher IgG extravasation in the both hippocampus and the cortex was observed by 5- and 8-fold, respectively, compared to 4-month 5xFAD mice. For the effect of pathology, compared to the WT mice, 5xFAD mice demonstrated

a significant increase in IgG extravasation by 3- to 5-fold at both ages in both regions (Figure 2.6. 6).

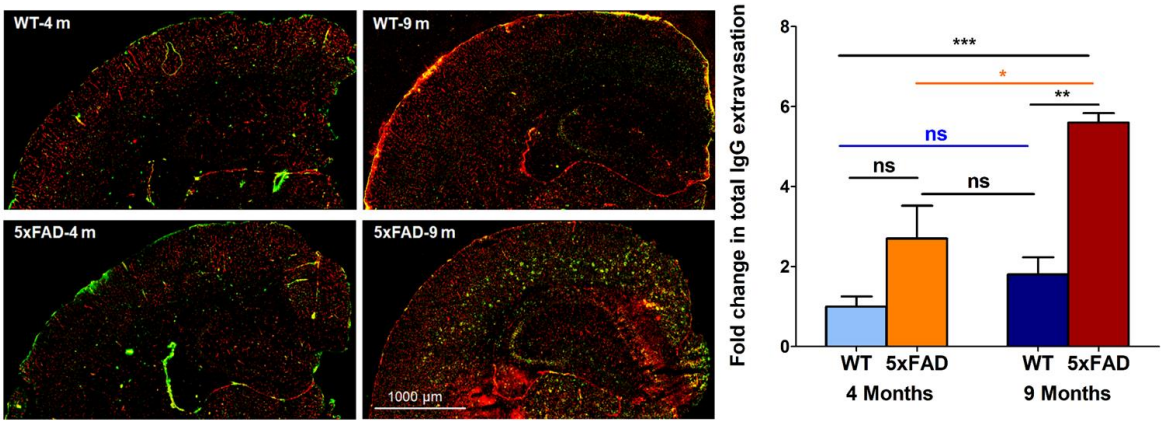

Figure 2.6. 6. IgG extravasation rate was significantly higher in 9 months old 5xFAD mice group. The IgG extravasation rate in 4 months old WT and 5xFAD showed no significant difference; however, 9 months of 5xFAD showed a higher IgG extravasation level compared to 9 months WT. Data are presented as mean ± SEM for n = 10 mice per group with * $p < 0.05$, ** $p < 0.01$,*** $p < 0.001$.

2.4. 5. Effect of age and pathology on plasma and brain Aβ levels in WT and 5xFAD mice

Plasma and brain $A\beta_{40}$ and $A\beta_{42}$ levels were analyzed by ELISA. As showed in Figure 2.6.7 for $A\beta_{40}$, while there was a trend of increased plasma levels in the 9-month compared to 4-months WT mice, this increase was not significant. On the other hand, for plasma $A\beta_{42}$, 9-months WT demonstrated 2-fold higher levels than the 4-month mice. Interestingly, in 5xFAD mice, 9 months mice showed a significant reduction by 3.5- and 2.5-fold in $A\beta_{40}$ and $A\beta_{42}$ plasma levels, respectively, in comparison to the 5xFAD-4 months. For the effect of pathology, at 4 months of age, the plasma levels of $A\beta_{40}$ and $A\beta_{42}$ in 5xFAD mice are 3- and 2.1-fold higher than the WT-4-

month mice; however, as the mice aged, the plasma levels of $A\beta_{40}$ and $A\beta_{42}$ in 5xFAD-9 months mice were significantly lower compared to the WT-9 months mice by 36% and 47%, respectively.

In the brain, as showed in Figure 8, $A\beta_{40}$ and $A\beta_{42}$ levels in the 9-month 5xFAD were significantly higher than 4-month 5xFAD by 4.4- and 3.3-fold, respectively; at both ages, brain $A\beta_{40}$ and $A\beta_{42}$ levels in 5xFAD mice were significantly higher than the WT mice, which showed negligible levels of $A\beta_{40}$ and $A\beta_{42}$ (Figure 2.6. 8.).

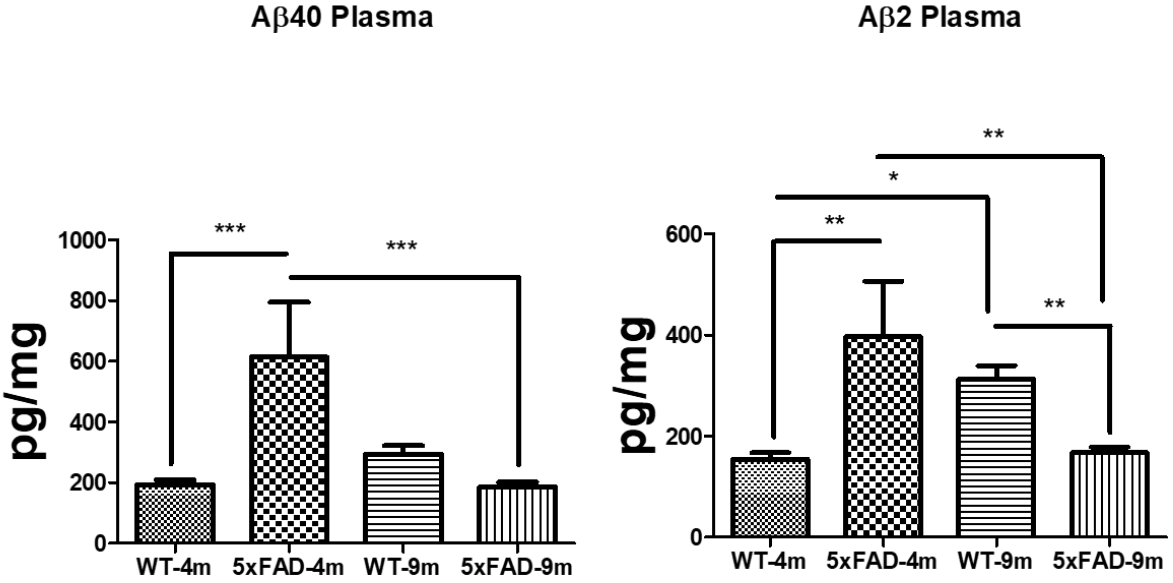

Figure 2.6.7. ELISA shows a significantly higher level of $A\beta_{40}$ and $A\beta_{42}$ in the plasma of 4 months of the 5xFAD mice group, but 9 months show higher $A\beta_{40}$ and $A\beta_{42}$ in the plasma of the WT mice group. Our data indicate a higher level of $A\beta_{40}$ and $A\beta_{42}$ in the plasm of 4 months of 5xFAD compared with 4 months WT. This indicates that 4 months old WT mice produce less level of Aβ in the brain, therefore Aβ excretion from the brain to blood level is lower than 4 months old 5xFAD. However, 9 months old 5xFAD shows a significantly lower level of $A\beta_{40}$ and $A\beta_{42}$ than 9 months of the WT. Related to the data of Fig. 2.6. 6., 9 months old 5xFAD shows higher IgG extravasation level in the brain microvessels, which indicates disruption of

BBB. In addition, 4 months old 5xFAD mice show no significant difference in the IgG extravasation compared to the WT. Therefore, our data indicate that lower level of plasma $A\beta_{40}$ and $A\beta_{42}$ in the 9 month 5xFAD is induced by disruption of BBB.

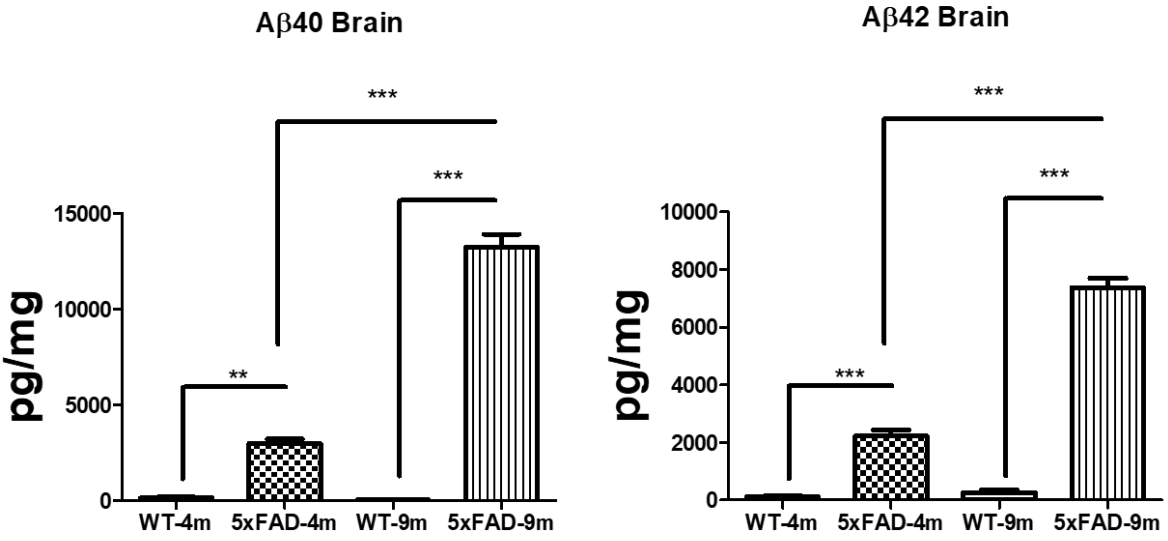

Figure 2.6.8. ELISA shows a significantly higher level of $A\beta_{40}$ and $A\beta_{42}$ in the brain of 4 and 9 months of the 5xFAD mice group. Our data indicate higher levels of brain $A\beta_{40}$ and $A\beta_{42}$ in both age groups of the 5xFAD mice group. Therefore, our data demonstrate that Aβ levels in the brain will worsen with aging in the 5xFAD mice group.

2.4. 6. Soluble Aβ, IgG extravasation, and sleep correlation

We performed correlation analysis to clarify the relationship between brain soluble Aβ, IgG extravasation and total sleep hours. As showed in Figure 2.6. 9., a positive correlation (R^2 = 0.5518) between levels of brain soluble Aβ levels and IgG extravasation was observed, suggesting, and as expected, soluble Aβ contribution to BBB breakdown. In addition, an inverse correlation

between total sleep time and IgG extravasation was also observed (R^2 = 0.6372); interestingly; however the correlation between brain soluble Aβ and sleep time was weak with R^2 = 0.2002.

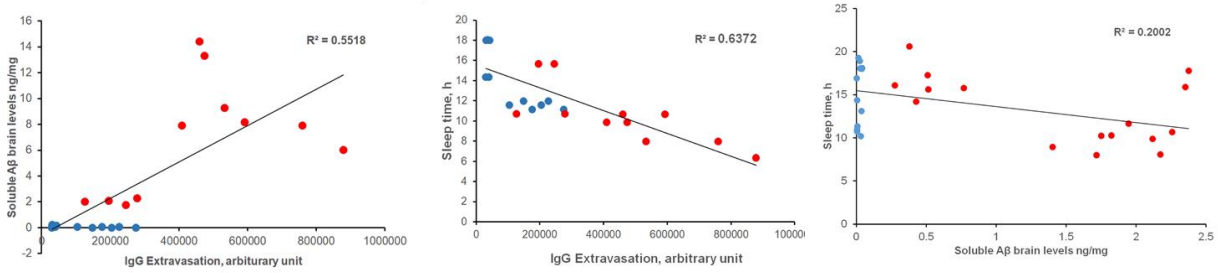

Figure 2.6. 9. Soluble Aβ contributes to BBB breakdown, and total sleep time is affected by IgG extravasation. Our data indicate a positive correlation (R^2 = 0.5518) between levels of brain soluble Aβ levels and IgG extravasation. In addition, an inverse correlation between total sleep time and IgG extravasation was also observed (R^2 = 0.6372). However, the correlation between brain soluble Aβ and sleep time was weak with R^2 = 0.2002.

2.5. Discussion

Aging is one of the factors that alter body metabolism. Aging induces changes in appetite and activity (145, 146). In addition, the elderly experience sleep disturbance and depression (147-149). The objective of this work was to assess changes in metabolic and behavior phenotypic parameters as a function of age and AD pathology. In addition, we aimed to associate such changes with BBB dysfunction and Aβ plasma and brain levels. Our findings demonstrated metabolic and behavioral alterations in the WT and 5xFAD mice models with age and pathology. Furthermore, our findings demonstrated an association between brain soluble Aβ levels, BBB leakage, and total sleep time.

Wang and colleagues reported that AD patients have lower body weight compared to cognitively normal individuals of the same age due to changes in appetite and metabolic state in AD patients (150). Similarly, we observed a lower body weight and higher energy expenditure levels in 5xFAD than the WT at 4 and 9 months. The authors stated that the existence of AD and poor appetite were the main risk factors of weight loss (150). While our findings didn't identify a significant difference in food intake between the same age groups, the increased movement and reduced sleep hours could contribute to the reduced body weight of 5xFAD mice.

Dehydration in the elderly is associated with poor health outcomes (151), which increases mortality risk (152). Dehydration is one of the symptoms induced in AD patients (153). Our data demonstrated a higher dehydrating rate (represented by the VH2O parameter and water intake) in 5xFAD mice compared to the WT mice, which could also be explained by the increased activity as determined by the increased energy expenditure and movement. Besides, memory loss should not be excluded as a contributing factor to the decreased water intake.

The elderly people are experience sleep-wake disorders that induced by physical changes or due to the presence of disease condition (154). For example, it has been showed that the elderly tend

to have more frequency to take light sleep than the deep sleep stages suggesting a less efficient circadian behavior in the elderly (154). In addition, a linkage between the elderly and sleep disorder due to diseases mediated by chronic pain or due to chronic disease such as hypertension and diabetes mellitus (155-157). In our study, with normal aging, 9 months WT mice demonstrated reduced sleep time compared to 4 months of young mice group. Our findings are consistent with those reported by Soltani and colleagues who assessed the effect of aging on sleep-wake cycle and concluded induced sleep disorder in C57BL/6 mice 12 months compared to 3 months old mice (158).

In AD, the progressive neuropathological alteration and Aβ burden have also been associated with sleep dysregulation, which impacts the sleep-wake activity (159-161). In AD, sleep disturbance is considered one of the well-known behavioral phenotypes of AD (162), which worsen with disease progression (121, 161). When tested in mice, the cerebral injection of Aβ25-35 significantly reduced non-rapid eye movement sleep, while it increased wakefulness in the WT mice (163, 164), suggesting the role of Aβ in sleep disturbances. Similar to the other studies, our study shows that sleep patterns of 5xFAD mice is influenced by both aging and AD pathology. Especially, where at 9 months of age, the AD mice model demonstrated a significantly reduced sleeping time compared to the WT mice of the same age.

Furthermore, AD patients are also characterized by the anxiety with a reported prevalence of about 40% (165, 166). Besides sleeping disturbances, the anxiety symptoms include increased heart rate, and rapid breathing. Thus, in this study, to monitor the anxiety in mice as a function of age and pathology, we assessed a few metabolic phenotypes that could relate to the anxiety symptoms, including movement distance (all meters and cumulative all meters parameters), energy expenditure, rate of oxygen consumption, rate of carbon dioxide emission, respiratory quotient,

and water vapor loss. Besides sleep disturbances, we observed higher activity and greater movement (i.e., less time spent at a specific space in the cage) with age and pathology in 5xFAD mice; however, WT mice demonstrated a decreased activity, metabolism and movement with age, suggesting Aβ pathology in 5xFAD is further contributing to the observed increase in metabolic and behavior parameters, and thus to the anxiety-like behavior. In comparison with other studies, Jawhar and colleagues monitored the anxiety in 5xFAD mice at 3, 6, 9, and 12 months of age using the elevated plus-maze test that was compared to the WT mice (167). The authors reported that 5xFAD mice with age $\geq$ 6 months demonstrate reduced the anxiety as monitored by the longer time spent in the open arms of the elevated plus maze when compared to the WT mice.

Previous assessments of the anxiety-like behavior in mice models of AD demonstrated inconsistent and contradictory results. For example, in some studies, 5xFAD and APP/PS1 mice exhibited decreased or equivalent the anxiety-like behavior in the open field or elevated plus maze relative to the WT mice (167-169). By contrast, increased the anxiety-like behavior has also been reported in 5xFAD mice and other AD mice models (170-172). Such inconsistencies in the results of the anxiety-like behaviors indicate the need for additional tests to model the anxiety-like behaviors in AD mice models. Compared to the elevated plus-maze tests to assess mice the anxiety by locating them at a specific height, which introduces a fear factor by exposing them to the open and height, the phenotypic behavior monitored in this work is fear-free and measures the mice the anxiety level under normal conditions similar to those showed in humans.

To associate changes in metabolic and behavioral phenotypes with Aβ, and related pathology as a function of age and pathology, we assessed plasma and brain Aβ levels, and the BBB function. As expected, as the disease progressed, 5xFAD mice brains demonstrated a significant increase in brain Aβ with age. In plasma, while the low Aβ levels were not altered in the WT mice with age,

in 5xFAD mice, the plasma levels of Aβ were significantly higher in 4 months compared to 9 months mice. Neurotoxic agents, such as Aβ, that induce neurodegeneration are cleared from the brain to the blood across the BBB (173). At 4 months of age, 5xFAD showed higher levels of plasma Aβ than the WT, which could be due to the increased production of brain Aβ that gets cleared to the blood across the BBB (174). As the disease progress, 9 months 5xFAD mice show reduced plasma levels of Aβ relative to the 5xFAD-4 months and the WT-9 months, which could be related to reduced Aβ degradation and clearance across the BBB. In AD and as the disease progress, the expression of Aβ degradation enzymes and key Aβ transport proteins expressed on BBB-endothelial cells are downregulated, leading to increased brain Aβ levels.

In AD mice models, increased brain Aβ is also associated with BBB breakdown supported by the increased IgG extravasation, which significantly increased as the disease progressed. Our correlation studies showed a positive correlation between brain Aβ and IgG extravasation. Our findings also demonstrated BBB breakdown in the WT mice as they age; however, to a much lower extent than the 5xFAD at the same age. Furthermore, we demonstrated a positive correlation between total sleep hours and IgG extravasation, which suggests the association of BBB breakdown with reduced sleep time, and effect that could be mediated by Aβ; however, the correlation between soluble Aβ and sleep hours was not strong. Additional studies are required to explain this finding; however, the correlation was made between soluble Aβ rather than total brain Aβ.

During aging there are major alterations in human sleep. Sleep plays a key role in multiple cognitive functions and sleep pattern changes with aging. Human studies revealed that aging decreases sleep efficiency and reduces the total sleep time (175).

In conclusion, we observed metabolic phenotypes alteration in aged WT and the 5xFAD mice model by compared with 4 months and 9 months WT, which demonstrates higher movement distance, higher kilocalories consumption, less time spent sleeping, loss of body weight, and higher dehydration rate. In addition, the parameter difference showed to be more distinguishable in the 9 months than the 4 months. Therefore, AD alters metabolic parameters in the 5xFAD mice model.

3. Oleocanthal rectifies metabolic and behavioral phenotypes and blood-brain barrier function in 5xFAD mice

3.1. Abstract

Transient receptor potential ankyrin 1 (TRPA1) is a cation channel receptor that regulates calcium homeostasis among other cations. Calcium dyshomeostasis is known to disrupt the blood-brain barrier (BBB). Besides its expression in neurons and astrocytes, TRPA1 is expressed in the endothelial cells of the BBB, which upregulated in Alzheimer's disease. Previous studies from our laboratory demonstrated that the protective effect of oleocanthal (OC) against Aβ and related pathology, enhanced the BBB function, and downregulated total TRPA1. The objective of this work is to investigate the effect of OC (1 and 10 mg/kg) treatment on metabolic and behavioral parameters, endothelium-TRPA1 expression and BBB function in 5XFAD mice. In addition, we performed in vitro studies to study the effect of OC on the expression of TRPA1, intracellular calcium and a cell-based BBB model. Our findings demonstrated that 10 mg/kg OC restored the metabolic and behavioral phenotypic parameters, enhanced BBB function, at least in part, by endothelium-TRPA1 downregulation and reduced brain Aβ levels. Findings from the in vitro studies showed a concentration dependent effect of OC on TRPA1 expression and intracellular calcium, which significantly reduced and improved the cell-based BBB model function

In conclusion, our data indicate the downregulation of endothelium-TRPA1 could enhance BBB function and that OC restored the BBB function and effect that was associated with restored metabolic and behavioral parameters.

3.2 Introduction

Alzheimer's disease (AD) is a progressive neurodegenerative disorder that causes dementia (Jones, 2022). AD is characterized by amyloid-β (Aβ) plaques in the brain, which is believed to promote the formation of neurofibrillary tangles (NFTs), thus inducing neurotoxicity, neuroinflammation, and neurodegeneration (176-178).

The blood-brain barrier (BBB) is a physical barrier, which regulates the passage of substances between the brain and the blood to maintain brain homeostasis. BBB consists of endothelial cells, basement membrane, pericytes, and astrocytes (179). The BBB-endothelium is sealed by a cell-to-cell junction maintained by tight junction proteins (66). The BBB protects neurons from the invasion of peripheral neurotoxins by selectively filtering out unwanted molecules and neurotoxins. The BBB function is required for proper synaptic and neuronal functioning (180). In AD, several studies have reported a dysfunctional BBB characterized by increased permeability of blood-derived debris, cells, and microbial pathogens into the brain and reduced clearance of toxic products such as Aβ (180-182). BBB dysfunction is associated with inflammatory and immune responses, which could cause neurodegeneration (180).

In humans, several studies have demonstrated BBB leakage in the hippocampi of individuals with mild cognitive impairment (MCI) using dynamic contrast enhanced (DCE) MRI (69, 183). In addition, other studies have reported an improvement in cognition ability following restoring the BBB function in AD disease mice models (88, 96, 184).

Endothelial cells are the most important cells in the BBB structure, presenting the actual barrier of BBB filtration and clearance due to the tight junctions (180). Examples of tight junction proteins include zona occluden-1 (ZO1), occludin, and claudin-5 (53). In humans, BBB breakdown is an early event in the aging brain that begins in the hippocampus and may contribute to cognitive

impairment (69, 185). In addition, AD mice models exhibit BBB disruption (186, 187). Therefore, maintaining BBB endothelial healthiness might be a potential treatment target in AD patients.

Transient receptor potential ankyrin 1 (TRPA1) is a calcium-permeable non-selective cation channel that is widely expressed in sensory neurons and in non-neuronal cells (92). TRPA1 is involved in calcium ion homeostatic functions in different organs (93). TRPA1 is activated by cold, and heat senses such as pain response (94). TRPA1 is known to be activated by spices and herbs such as capsaicin and mustard oil, which could induce the opening of these channels indirectly interacting with the gustatory system (188, 189). Recently, it has been reported that in AD mice models, the levels of brain TRPA1 mainly in the astrocytes, are upregulated (190), and that the blockade of Aβ-induced TRPA1 in astrocytes (191), and TRPA1 downregulation by supplementing the diet with extra-virgin olive oil (EVOO) (96) reduced Aβ-related pathology as well as TRPA1 expression.

Oleocanthal (OC) is one of the phenolic components of EVOO. OC has anti-inflammatory characteristics like those of ibuprofen (110, 112). OC is known as a TRPA1 activator when used in acute treatment studies (102). However, findings from our recent studies demonstrated the downregulation of brain TRPA1 following 3 months of treatment with EVOO suggesting the long-term treatment of OC downregulates TRPA1 expression (96).

In this work, we aimed first to evaluate the effect of OC (1 and 10 mg/kg) on metabolic and behavioral phenotypes, then to compare total and endothelium-TRPA1 levels between wild-type (WT) and5xFAD mice (an AD mice model), and finally to assess the in vitro effect of OC on the expression and function of endothelium-TRPA1 and on the function of cell-based BBB model.

3.3. Method and materials

3.3.1. Animals

Male wild type (WT) C57BL/6J and 5xFAD mice models at the ages of 6 months were used in the studies. The transgenic 5xFAD mice model expresses human amyloid precursor protein (APP) with the mutations APP KM670/671NL (Swedish), APP I716V (Florida), APP V717I (London), and PSEN1 M146L and PSEN1 L286V, leading to early and aggressive Aβ accumulation. Aβ accumulation is associated with progressive gliosis, synapse degeneration, neuronal loss, and deficits in spatial learning (Oakley, 2006). In 5xFAD, extracellular Aβ plaque deposition starts at 2 months of age with gliosis, which induces synaptic loss that results in cognitive impairment at the age of 4 months. The WT and 5xFAD mice were purchased from Jackson Laboratory (Bar Harbor, ME) and housed for breeding in plastic containers under the conditions of 12 h light/dark cycle, 22°C, 35% relative humidity, and ad libitum access to water and food. All animal experiments and procedures were approved by the Institutional Animal Care and Use Committee of Auburn University and according to the National Institutes of Health guidelines Principles of laboratory animal care.

For 5xFAD mice treatment, OC was dissolved in saline for the oral gavage. Administered volume was 150µl/30 g bodyweight to deliver a dose of 0 (saline as vehicle), 1 and 10 mg/kg OC (n=10 mice/group). We selected these doses to evaluate the effect at low dose OC (1 mg/kg) and high dose OC (10 mg/kg). Previously, we demonstrated the beneficial effect 10 mg/kg on BBB function (Abuznait et al., 2013). In the studies, we included WT mice as a control group that are cognitively normal (n=10 mice). Mice were treated with OC starting at the age of 6 months until 9 months old (i.e. treatment for 3 months). We selected this age based on the findings from Chapter 2 findings

demonstrating significant alteration in metabolic and behavioral parameters and BBB dysfunction in 5xFAD.

3.3.2. Metabolic and behavior phenotypes assessment

Promethion Metabolic Mouse Cages (Sable Systems, Las Vegas, NV) were used to house animals for metabolic screening and phenotyping. At the end of treatment (9 months old), animals were transferred from their home cages and singly housed in the metabolic cages for 3 consecutive days, with the first day stated for the cage environment adaptation, and the second and third days were for data collection. Animal activity was measured by Promethion XYZ Beambreak Activity Monitor. Food and water intake was measured as a mean mass consumed during an intake event in grams (g). Bodyweight was measured as the mean body mass of the animal, in grams. Movement distance was measured as the sum of all distances traveled within the beam break system in meters (m). This includes fine movement (such as grooming and scratching) as well as direct locomotion. Sleeping time was measured as the sum of the animal's sleep, in hours. The animal is considered sleeping when the animal has been "quiet" for more than 40 seconds. Animal's "quiet" time is defined as the time in which the animal is not engaged in eating, drinking, grooming, or locomotion. The volume of O2 was measured as the rate of oxygen consumption (VO2), in milliliters per minute. CO2 consumption was measured as the rate of carbon dioxide emission (VCO2), in milliliters per minute. Energy expenditure (EE) was measured in kilocalorie per hour (kcal/hr). RER was measured as mean respiratory quotient, VCO2/VO2 (unit-less). All the parameters were measured by Promethion precision MM-1 Load Cell sensors. The time for metabolic parameters measurement is defined as 12h:12h light:dark cycle with zeitgeber time (ZT) 0 representing lights on and ZT12 representing lights off. The amount of food and water withdrawn from the container was measured and analyzed. Water vapor, CO2, and O2 levels were analyzed

by the Promethion GA-3 gas analyzer to provide detailed respirometry data. Energy expenditure (EE) was calculated in kilocalories (kcal) by utilizing the Weir equation: 60*(0.003941*VO2 (n) +0.001106*VCO2 (n)) in which VO2 is the oxygen uptake and VCO2 is the carbon dioxide output, both of which are measured in ml/min. The respiratory exchange ratio (RER) was determined by measuring gas exchange within the metabolic cages to identify the substrate being primarily utilized for energy within the body. Specifically, RER is the ratio of CO2 produced to the volume of O2 consumed (RER = VCO2/VO2). All metabolic phenotyping data were analyzed using ExpeData software (version 1.8.2; Sable Systems) with Universal Macro Collection (version 10.1.3; Sable Systems).

3.3.3. Tissue collection and preparation

All animals were anesthetized with an intraperitoneal injection of xylazine and ketamine (20 and 125 mg/kg, respectively), followed by decapitation. The mice brains were extracted, and the two hemispheres of each brain were separated and used for analysis; blood samples were also collected for plasma Aβ quantification. All samples were stored at −80 °C until analysis.

3.3.4. Western blotting

The total protein concentration for each sample of brain homogenate and cell lysate was determined using the BCA protein assay. Protein samples (15μg) were loaded and resolved on 12% SDS-polyacrylamide gel, then transferred electrophoretically onto PVDF membranes. Membranes were incubated in 3% non-fat dried milk-blocking solution followed by overnight incubation at 4 °C with primary antibodies (Table 3.3.4). The analyzed proteins were TRPA1, anti-mouse claudin-5, and β-actin. Membranes were then incubated with anti-rabbit or anti-mouse secondary antibodies (Abcam, Cambridge, United Kingdom) for 1 h at room temperature after

washing with PBS x3 times. Protein blots were developed using a chemiluminescence detection kit (Thermo Fisher Scientific). Bands were visualized using ChemiDoc imaging system (Bio Rad; Hercules, CA, USA) and analyzed by Image Lab software v 6.0 (Bio-Rad).

Table. 3.3. 4. Table of primary antibodies used for Western blot and immunostaining

Primary antibody	Dilution	Company
Anti-rabbit TRPA1	1-1000	Abclonal (Woburn, Massachusetts)
Anti-mouse cloudin-5	1-100	Abcam (Cambridge, United Kingdom)
β-actin	1-1000	Santa Cruz Biotechnology, Inc, Dallas, TX
Alexa Fluor® 488 anti-β-amyloid (6E10)	1-1000	Biolegend
Anti-collagen Type IV	1-1000	Millipore Sigma

3.3.5. Immunohistochemistry

All cryostat brain slices (15 μm) were 4% paraformaldehyde-fixed and then blocked for 60 min with the blocking buffer TrueBlack background suppressor purchased from Biotum (Fremont, CA). To assess IgG extravasation from brain microvessels, brain sections were fixed and blocked, as described above, then probed by dual immunohistochemical staining for collagen-IV and mouse IgG extravasation using rabbit anti-collagen-IV and fluorescein-conjugated donkey anti-IgG (Santa Cruz Biotechnology Dallas, TX), respectively, both at 1:1000 dilution.

To assess the expression of vascular TRPA1, brain sections were fixed and blocked, as described above, then probed by anti-rabbit TRPA1 and anti-mouse IgG 488 tagged claudin-5 (Abcam, Cambridge, United Kingdom), both at 1:1000 dilution. The detection was followed by IgG-CFL 594 conjugated donkey anti-rabbit (Santa Cruz Biotechnology).

To assess the deposition of Aβ plaques in the brain, 15 μm brain sections were fixed and blocked. The blocked sections were then stained with 0.04% of Thioflavin-S (ThioS) in 70% ethanol solution for 60 mins at room temperature. All stained sections were then washed with PBS x3 times, each incubated for 5 min. For total Aβ staining, Alexa Fluor 488 tagged-amyloid β recombinant monoclonal antibody (6E10) was used (BioLegend, San Diego, CA).

For the in vitro studies, 80-95% of confluent cells were fixed and blocked, as described above. To stain TRPA1, cells were probed by dual immunohistochemical staining for TRPA1 and claudin-5 both at 1:1000 dilution. The detection was followed by IgG-CFL 594 conjugated donkey anti-rabbit (Santa Cruz Biotechnology) and 488 conjugated donkey anti-mouse as a secondary antibody (Abcam, Cambridge, United Kingdom).

Images were captured and adjusted to the lowest background signal using Nikon Eclipse Ti-S inverted fluorescence microscope (Melville, NY, USA). For quantification of total Aβ plaques and IgG extravasation, sections were normalized to the same background for the hippocampus and the cortex regions. Images were analyzed by Image J software (National Institutes of Health, Bethesda, MD, USA) that was set for mean value, minimum value, maximum value, and limit to the threshold followed by analysis.

3.3.6. Enzyme-Linked Immunosorbent Assay (ELISA)

To quantitatively analyze $A\beta_{40}$ and $A\beta_{42}$ levels in the WT and the 5xFAD mice brain homogenate and plasma, we used commercially available ELISA kits and were used according to the manufacturer's instructions (R&D Systems, Minneapolis, MN). All samples were run at least in duplicate.

3.3.7. Aβ monomers and $A\beta_{42}$ oligomers preparation

Synthetic $A\beta_{42}$ and $A\beta_{40}$ (AnaSpec, Inc, CA) were received as vials with powder. Solutions of synthetic Aβ monomers were prepared by suspending in 1, 1, 1, 3, 3, 3-hexafluoro-2-propanol (HFIP) (Sigma-Aldrich, MO) at a concentration of 1 mM and incubated for 1 h at room temperature for complete solubilization. Aβ solutions were aliquoted, followed by HFIP evaporation overnight at room temperature. Vials were then stored at −80°C as an HFIP film. For cells treatment, the HFIP film was mixed in media to reach 100 μM, which immediately used in the studies. For $A\beta_{42}$ oligomers preparation, the HFIP-film was suspended in anhydrous DMSO to a final concentration of 5 mM. DMSO solution of $A\beta_{42}$ was diluted with phenol red-free F-12 cell culture media (Gibco, NY) to a concentration of 100 μM, vortexed for 1 min and incubated at 4°C for 24 h. At the end of the incubation period, $A\beta_{42}$ oligomers solution was centrifuged at 14,000 rpm, 4°C for 10 min, aliquoted and stored at −80°C for the experiments. This oligomer was used in *in-vitro* BBB transport experiment.

3.3.8. Cell culture and treatments

The immortalized mouse brain endothelial cell line, bEnd3 was obtained from ATCC (Manassas, VA) . bEnd3 cells, passage 26–35, were cultured in DMEM supplemented with 10% fetal bovine serum (FBS), and penicillin G (100 IU/ml). Cultures were maintained in a humidified atmosphere (5%CO2/95% air) at 37°C and media was changed every 3 days.

To evaluate the effect of OC on TRPA1 expression, cells were treated with OC (dissolved in media) in the concentration range of 0.5-20 μM for 72 h. For Aβ treatment, cells were treated with $A\beta_{42}$ monomers (0.5 μM) for 72 h. At the end of treatments, cells were collected and lysed for Western blotting analysis.

3.3.9. Calcium assay

To confirm TRPA1 function in bEnd3 cells, we measured intracellular calcium as follows. Cells were treated for 1 h with $A\beta_{42}$ monomers (1 μM), or with the TRPA1 antagonist A-967079 (Tocris Bioscience, Bristol, United Kingdom) dissolved in DMSO as a stock solution of 10 mM, or the TRPA1 agonist allyl isothiocyanate (AITC; Alfa, Haverhill, MA), dissolved in DMSO as a stock solution of 10 mM. DMSO was added to the cells as a vehicle and didn't exceed 0.1%. To evaluate the effect of chronic OC treatment on TRPA1 expression, bEnd3 cells were seeded at 50,000 cells/cm^2 per well in a 96-well plate to be used the next day at 50% confluence. The plate was treated with OC (1-20 μM) as described above for 72 h followed by calcium assay. The Fluo-4 Calcium Assay Kit purchased from Invitrogen (Waltham, MA) was used following the manufacturer's instructions. After completion of the assay, plates were read using Cytation5 plate reader.

3.3.10. MTT assay

To confirm the toxicity effect of of OC and $A\beta_{42}$ monomers in bEnd3 cells, we performed MTT assay (Cat: V13154). bEnd3 cells were seeded in 96 well plate for 50,000 cells/cm^2. The concentration rage of OC were from 0-40 μM, and $A\beta_{42}$ monomers was 0-5 μM for 72hrs. The experiment procedure was followed as per the instruction manual supplied with the test kit (Thermo Fisher Scientific, Waltham, MA).

3.3.11. BBB Permeability and Aβ transport assays across the cell-based BBB model

bEnd3 cells at 50,000 cells/cm^2 were seeded onto a transwell 96-well plate with polycarbonate membrane inserts, 4.26 mm diameter with 3 μm pores size. Inserts were coated with fibronectin

(30 μg/ml) as a basement membrane substitute to achieve optimal barrier integrity of bEnd3 cells (192). Fibronectin diluted in sterile PBS was added to the apical side of each transwell filter. The transwell plate was incubated in a 37°C, 5% CO2/95% air incubator for 2 h to form a coat. bEnd3 cells were seeded after 150 μl of fresh media were added to the apical side of each transwell, then the total volume of fibronectin and media was removed by aspiration. For cell seeding, 50 μl of cell suspension was added to the apical side of each transwell, and 200 μl of fresh media was added to the basolateral side. Cells were incubated at 37°C, 5% CO2/95% air for 5 days. For the treatment, 10 μM of OC (apical), or 150 nM of $A\beta_{42}$ oligomers (basolateral) or OC and $A\beta_{42}$ oligomers were added for 72 h on the 3rd day following seeding. On the 6th day, the monolayer permeability and $A\beta_{40}$ transport were assessed by the addition of 0.05 mM ^{14}C-inulin (as a permeability marker) and 0.1 nM ^{125}I-$A\beta_{40}$, respectively, to the basolateral compartment (Qosa, 2014). To monitor molecules transport from basolateral to apical compartments, at the end of 60 min incubation, media in both compartments and cells were separately collected for ^{125}I-$A\beta_{40}$ analysis and inulin measurement to calculate their permeation coefficient (Pc) as follows:

$$Pc\ (cm/sec) = \frac{Va\ \times Ca}{Cb\ \times A\ \times T}$$

Where, V_a is the volume of the basolateral side (200 μl), C_a is the total ^{125}I-$A\beta_{40}$ cpm or total ^{14}C-inulin dpm in the basolateral compartment, C_b is the total ^{125}I-$A\beta_{40}$ cpm or total ^{14}C-inulin dpm in apical compartment, A is the membrane area (0.143 cm^2), and T is the time of transport (3600 sec).

All measurements were performed using the Luminescence counter 1450 Microbeta WALLAC Trilux from PerkinElmer.

3.3.12. Statistics

All metabolic and behavioral parameters were analyzed using R program by the unpaired student's t-test between 2 groups for the 24-hour circadian data. Multiple linear regression analysis (ANCOVA) was applied to assess the impact of AD pathology and OC treatment on metabolic cage parameters. For the day and nighttime data, a one-way ANOVA with *Tukey* post-hoc test in Graphpad Prism (San Diego, CA) was used. All biochemical analyses were analyzed using one-way ANOVA with *Tukey* post-hoc test. Significance for all measures was determined at $p < 0.05$, and all data are presented as Mean ± SEM or SD.

3.4. Results

3.4.1 OC prevents phenotypic parameters alteration in 5xFAD

The metabolic phenotype parameters were measured from 6 am to the next day at 6 am (24 h). To assess the effect of OC on metabolic and behavioral changes of 5xFAD, we measured body weight, activity rate, anxiety-like behavior and sleep pattern. As showed in Fig 3.6.1, mice treated with 10mg/kg OC received mice showed a similar trend of metabolic parameters to the WT in EE, VCO2, VO2, RER, All meters, and Cumulative all meters. However, 1mg/kg OC received mice showed no effect of treatment as much as 1mg/kg.

To observe behavioral changes by time, we divided the collected measurements on the parameters at day (summation of 0-11 h) and night (12-23 h) times. By dividing behavioral changes in day and nighttime, we observed a more distinguished behavioral alteration between the mice groups than 24 hours circadian figure. The body weight was 5g higher in the WT than the 5xFAD mice, respectively, suggesting a lower body weight gain in 5xFAD mice. However, we found 2g increasing of body weight of 1 and 10mg/kg OC received mice groups compare to 5xFAD mice. In the day and nighttime, 5xFAD mice shows higher EE, VCO_2, VO_2, RER and cumulative all meters compared to the WT mice. Our day and night data (Fig 3.6.2) indicates that 10 mg/kg OC received 5xFAD has showed WT like metabolic phenotypic parameters levels in EE, VCO_2, VO_2, RER and cumulative all meters compared to 5xFAD mice. However, 1mg/kg OC received 5xFAD has showed no significant difference from saline received 5xFAD. Therefore, our data indicates that 10 mg/kg OC restored the metabolic parameters to the WT levels.

Sleeping behavior was also influenced by pathology. In the nighttime, 5xFAD mice showed less time spending on sleeping than the WT. in addition, 1 and 10mg/kg OC received mice showed a higher time spending on sleeping than 5xFAD mice.

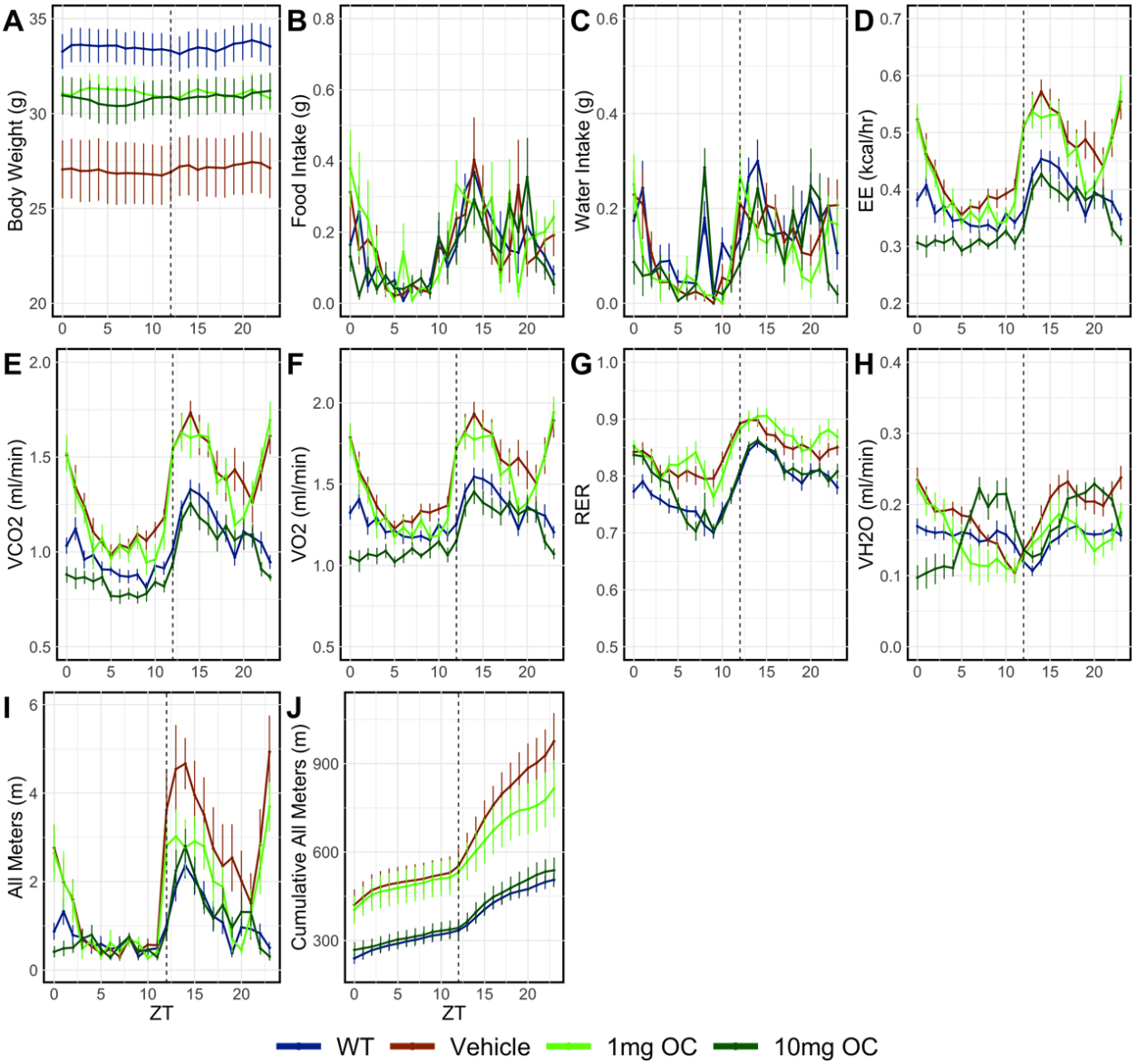

Figure 3.6 .1. 10mg/kg OC treatment prevents metabolic parameters alteration in 5xFAD.

We performed to 24hrs measure of metabolic phenotypic parameters as behavioral experiment. Our data indicate that 10mg/kg OC treatment prevents metabolic parameters alteration in 5xFAD. However, 1mg/kg OC treatment showed no significant difference with saline received 5xFAD.

Table. 3.4.5. 1. Statistical significance of body weight

Body Weight

ZT	**0**	**1**	**2**	**3**	**4**	**5**	**6**	**7**	**8**	**9**	**10**	**11**	**12**	**13**	**14**	**15**	**16**	**17**	**18**	**19**	**20**	**21**	**22**	**23**
WT-Vehicle	***	***	***	***	***	***	***	***	***	***	***	***	***	**	**	***	***	**	***	***	***	***	***	***
WT- 1mg OC																								
WT- 10mg OC																								
Vehicle - 1mg OC						*	*	*	*															
Vehicle- 10mg OC												*												

One-way ANOVA
$p<0.05$ =*, $p<0.01$=**, $p<0.001$=***

Table. 3.4.5. 2. Statistical significance of food intake

Food Intake																							
ZT	**0**	**1**	**2**	**3**	**4**	**5**	**6**	**7**	**8**	**9**	**10**	**11**	**12**	**13**	**14**	**15**	**16**	**17**	**18**	**19**	**20**	**21**	**22**	**23**
WT-Vehicle																								
WT- 1mg OC																								*
WT- 10mg OC																								
Vehicle - 1mg OC																				*				
Vehicle- 10mg OC																								
														One-way ANOVA										
														p<0.05 =*, p<0.01=**, p<0.001=***										

Table. 3.4.5. 3. Statistical significance of water intake

Water Intake

ZT	**0**	**1**	**2**	**3**	**4**	**5**	**6**	**7**	**8**	**9**	**10**	**11**	**12**	**13**	**14**	**15**	**16**	**17**	**18**	**19**	**20**	**21**	**22**	**23**
WT-Vehicle									**															
WT- 1mg OC									**		**				*									
WT- 10mg OC											*													
Vehicle - 1mg OC																								
Vehicle- 10mg OC									***															*

One-way ANOVA

$p<0.05$ =*, $p<0.01$=**, $p<0.001$=***

Table. 3.4.5. 4. Statistical significance of energy expenditure

EE																							
ZT	**0**	**1**	**2**	**3**	**4**	**5**	**6**	**7**	**8**	**9**	**10**	**11**	**12**	**13**	**14**	**15**	**16**	**17**	**18**	**19**	**20**	**21**	**22**	**23**
WT-Vehicle	***		*						*	*			***	**	**	*	*			***			**	***
WT- 1mg OC	***		*										***	**			*						**	***
WT- 10mg OC	*	*				**																		
Vehicle - 1mg OC																				*				
Vehicle- 10mg OC	***	***	***	*		**	*	*	***	*	*	**	***	***	***	**	***	*		**			***	***

One-way ANOVA

$p<0.05$ =*, $p<0.01$=**, $p<0.001$=***

Table. 3.4.5. 5. Statistical significance of CO_2

VCO2

ZT	0	1	2	3	4	5	6	7	8	9	10	11	12	13	14	15	16	17	18	19	20	21	22	23
WT-Vehicle	***		**					*	**	**	*	**	***	***	***	*	**		*	***			**	***
WT- 1mg OC	***		**						**			*	***	***	*	*	**		*				***	***
WT- 10mg OC						*																		
Vehicle - 1mg OC																				*				
Vehicle- 10mg OC	***	**	***	*		**	**	**	***	***	**	***	***	***	***	**	***	*		**			***	***

One-way ANOVA

$p<0.05$ =*, $p<0.01$=**, $p<0.001$=***

Table. 3.4.5. 6. Statistical significance of O_2

VO2																							
ZT	**0**	**1**	**2**	**3**	**4**	**5**	**6**	**7**	**8**	**9**	**10**	**11**	**12**	**13**	**14**	**15**	**16**	**17**	**18**	**19**	**20**	**21**	**22**	**23**
WT-Vehicle	***		*						*				***	**	**	*	*			***			**	***
WT- 1mg OC	***												***	**			*						**	***
WT- 10mg OC	*	*				**														*				
Vehicle - 1mg OC																								
Vehicle- 10mg OC	***	***	***	*		**	*		***	*	*	**	***	**	**	**	***	*		**			***	***

One-way ANOVA

$p<0.05$ =*, $p<0.01$=**, $p<0.001$=***

Table. 3.4.5. 7. Statistical significance of RER

RER																							
ZT	**0**	**1**	**2**	**3**	**4**	**5**	**6**	**7**	**8**	**9**	**10**	**11**	**12**	**13**	**14**	**15**	**16**	**17**	**18**	**19**	**20**	**21**	**22**	**23**
WT-Vehicle	**	*	**		*	*	**	*		***	**	***	***	*	*				*	*			*	**
WT- 1mg OC	***		**		**	**	***	***	*			**	***	*	*	***	*	**	**	*		**	***	***
WT- 10mg OC	**																							
Vehicle - 1mg OC																								
Vehicle- 10mg OC							**	***		***	**	***	**	*									*	

One-way ANOVA

p<0.05 =*, p<0.01=**, p<0.001=***

Table. 3.4.5. 8. Statistical significance of VH2O

VH2O

ZT	**0**	**1**	**2**	**3**	**4**	**5**	**6**	**7**	**8**	**9**	**10**	**11**	**12**	**13**	**14**	**15**	**16**	**17**	**18**	**19**	**20**	**21**	**22**	**23**
WT-Vehicle	**													*	*	*	*	*			*		**	***
WT- 1mg OC	*																							
WT- 10mg OC	**	*						**												*	***	**	*	
Vehicle - 1mg OC							*														**	*	**	*
Vehicle- 10mg OC	***	***	**	**	**					*	**	*												***

One-way ANOVA

$p<0.05$ =*, $p<0.01$=**, $p<0.001$=***

Table. 3.4.5. 9. Statistical significance of all meters

All Meters

ZT	**0**	**1**	**2**	**3**	**4**	**5**	**6**	**7**	**8**	**9**	**10**	**11**	**12**	**13**	**14**	**15**	**16**	**17**	**18**	**19**	**20**	**21**	**22**	**23**
WT-Vehicle	**												**	**	**	*	*			***			*	***
WT- 1mg OC	**																							***
WT- 10mg OC																								
Vehicle - 1mg OC															*					**	*			
Vehicle- 10mg OC	***												**		*		*			*			**	***

One-way ANOVA

$p<0.05$ =*, $p<0.01$=**, $p<0.001$=***

Table. 3.4.5. 10. Statistical significance cumulative all meters

Cumulative All Meters

ZT	**0**	**1**	**2**	**3**	**4**	**5**	**6**	**7**	**8**	**9**	**10**	**11**	**12**	**13**	**14**	**15**	**16**	**17**	**18**	**19**	**20**	**21**	**22**	**23**
WT-Vehicle	**	**	**	**	**	**	**	**	**	**	**	**	**	***	***	***	***	***	***	***	***	***	***	***
WT- 1mg OC	**	**	**	**	**	**	**	**	**	**	**	**	**	**	**	**	**	**	**	**	**	**	**	**
WT- 10mg OC																								
Vehicle - 1mg OC																								
Vehicle- 10mg OC	*	**	**	**	**	**	**	**	**	*	*	*	**	**	**	***	***	***	***	***	***	***	***	***

One-way ANOVA
p<0.05 =*, p<0.01=**, p<0.001=***

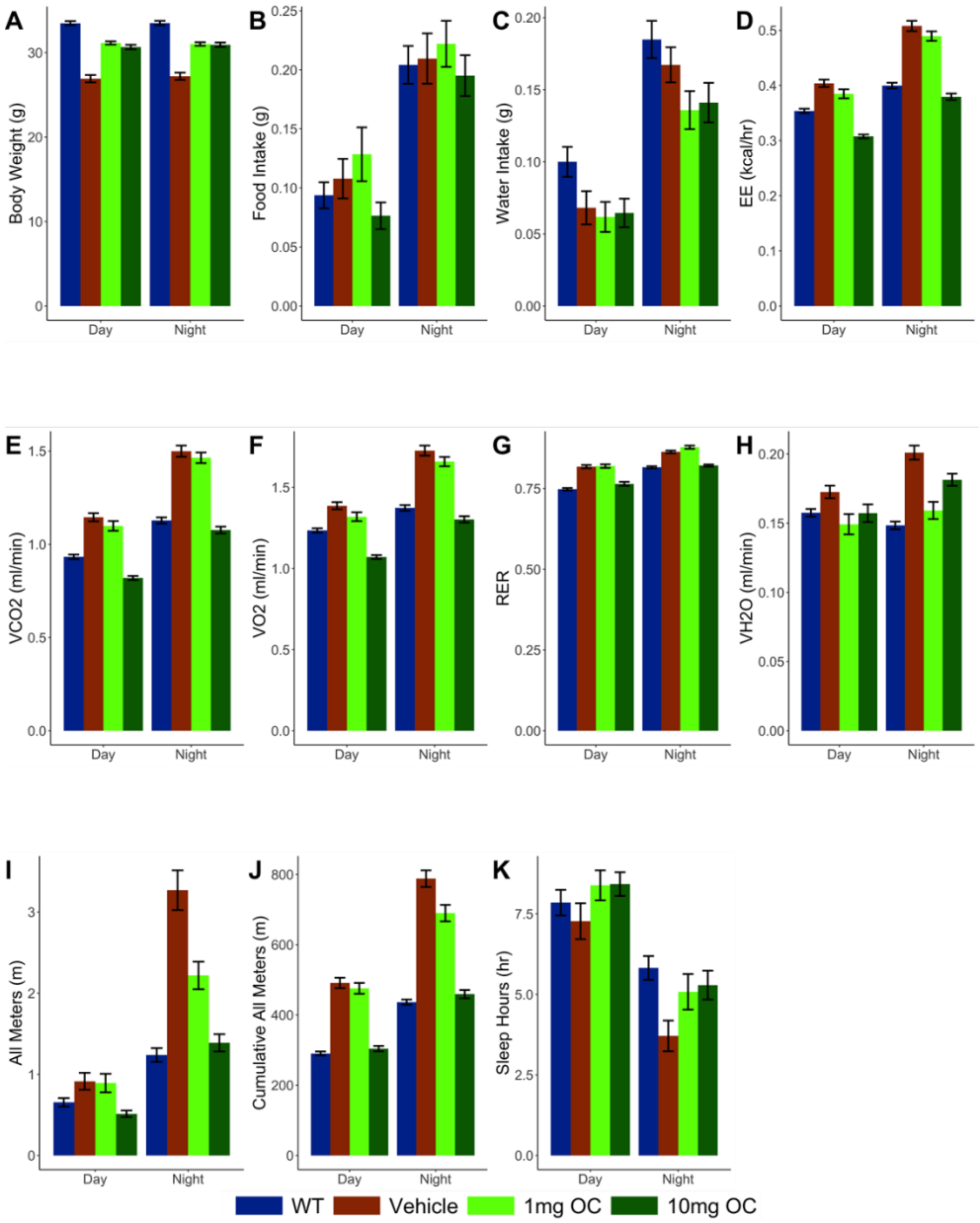

Figure 3.6. 2. 10mg/kg OC treatment prevents metabolic parameters alteration in 5xFAD. We performed to measure in day and night time of metabolic phenotypic parameters as a behavioral experiment. Our data indicates that 10mg/kg OC treatment prevents metabolic parameters alteration in 5xFAD. However, 1mg/kg OC treatment showed no significant difference with saline received 5xFAD.

Table. 3.4.5. 11. Statistical significance day and nighttime

Day Only

	Body weight	Food intake	Water Intake	EE	VCO2	VO2	RER	VH2O	All Meters	Cumulative All Meters	Sleep Hours
WT-Veh (5xFAD)	***			***	***	***	***			***	
WT-1mg OC	***			***	***	**	***			***	
WT-10mg OC	***			***	***	***					
Veh-1mg OC	***							*			
Veh -10mg OC	***			***	***	***	***			***	

Night Only

	Body weight	Food intake	Water Intake	EE	VCO2	VO2	RER	VH2O	All Meters	Cumulative All Meters	Sleep Hours
WT-Veh (5xFAD)	***			***	***	***	***	***	***	***	*
WT-1mg OC	***			***	***	***	***		***	***	
WT-10mg OC	***							***			
Veh-1mg OC	***							***	***	***	
Veh -10mg OC	***			***	***	***	***	*	***	***	

p<0.05 =*, p<0.01=**, p<0.001=***

Increased-Red (WT lower, Veh higher, or OC Treatment higher), Decreased Blue (WT higher, Veh lower, or OC Treatment Lower)

3.4. 2. OC reduced TRPA1 expression in 5xFAD mouse brain

The expression of TRPA1 in brain homogenate was analyzed by Western blotting. As showed in Figure 3.6.3, TRPA1 expression in 5xFAD mice brains is significantly higher than the WT by 84% (p<0.001). In addition, Figure. 3.6.1 shows that mice treated with 10 mg/kg OC significantly reduced TRPA1 levels by 77% (p<0.01) compared to vehicle-treated 5xFAD mice. However, the 1 mg/kg OC dose has no effect on TRPA1 expression.

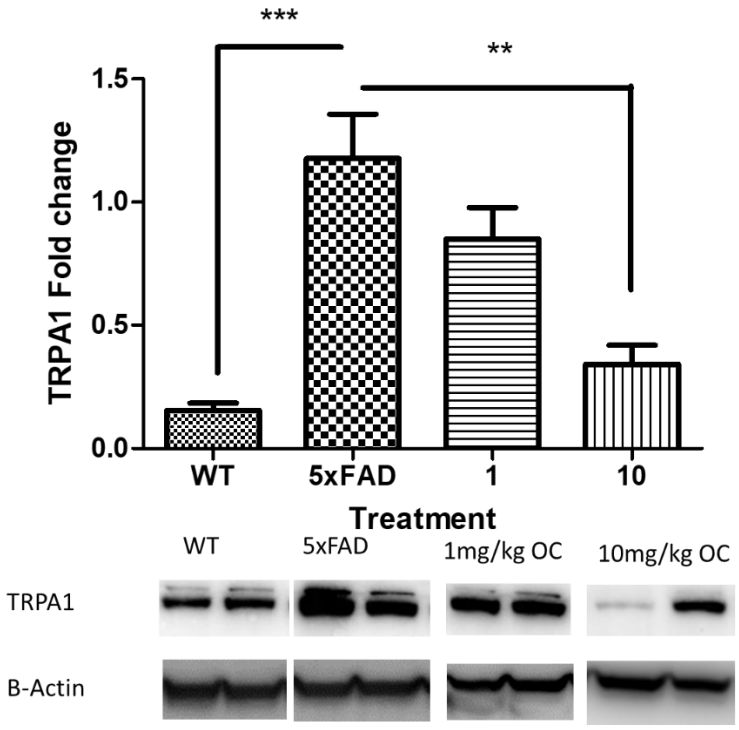

Figure 3.6. 3. Effect of OC on the expression of TRPA1 in the 5xFAD and WT mice. This figure demonstrate that higher expression of TRPA1 was observed in the brain of 5xFAD AD mice group. 10mg/kg OC received 5xFAD shows a reduction of TRPA1 expression in the brain of 5xFAD mice group. Data are presented as mean ± SEM for n = 10 mice per group with * $p < 0.05$, ** $p < 0.01$,*** $p < 0.001$.

3.4.3 OC reduced expression of BBB-endothelial TRPA1 in 5xFAD mice

Immunofluorescence (IF) of TRPA1 and claudin-5 (as a marker for endothelial cells) in the WT, 5xFAD and OC treated 5xFAD mice was performed. IF images were taken in the area of the hippocampus (Fig 3.6. 4. A) and the cortex (Fig 3.6. 4. B), and the quantification analysis was performed by using ImageJ (NIH). All images demonstrate the co-expression of TRPA1 with claudin-5, which indicates that TRPA1 is expressed in vascular endothelial cells. We also observed a significantly higher TRPA1 expression by 51% ($p<0.001$) in the hippocampus (Fig 3.6. 4.A) and 89% ($p<0.001$) in the cortex (Fig 3.6. 4.B) than in the WT mice. While 1 mg/kg OC didn't alter TRPA1 expression, 10 mg/kg OC significantly reduced TRPA1 expression by 74% in the hippocampus (Fig 3.6. 4.A) and 85% in the cortex (Fig 3.6. 4.B). These results indicate that TRPA1 is expressed in the vascular endothelial cells, and 10 mg/kg OC reduces endothelial TRPA1 expression in 5xFAD mice.

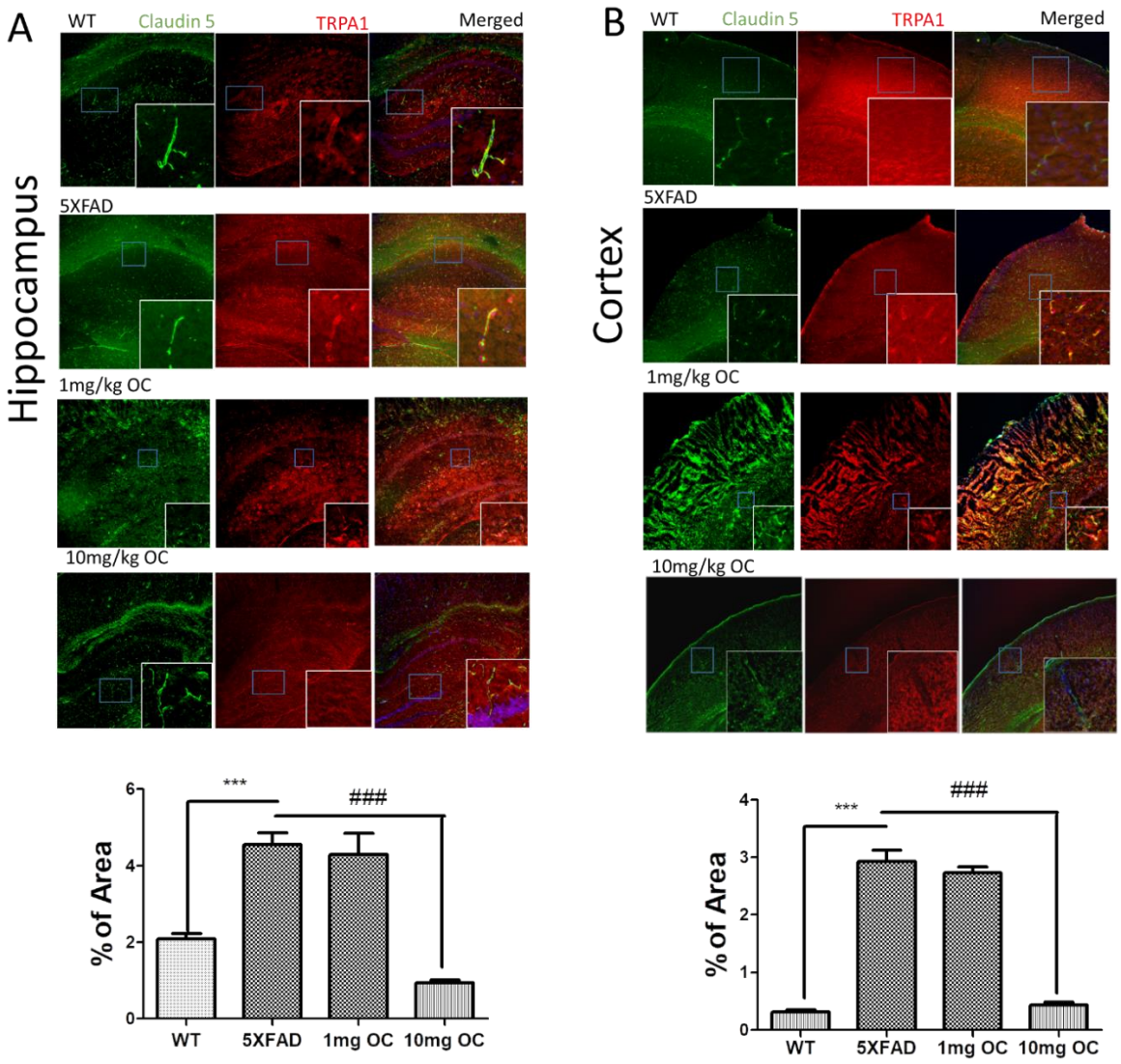

Figure 3.6. 4. BBB endothelial TRPA1 expression was reduced by OC treatment in 5xFAD AD mice brain hippocampus and cortex. This figure demonstrates BBB endothelial TRPA1, and it's expression level was higher in the 5xFAD hippocampus (A) and the cortex (B). 10mg/kg OC received 5xFAD shows a reduction of BBB endothelial TRPA1 expression in the brain of 5xFAD hippocampus (A) and the cortex (B). 1mg/kg OC did not reduce TRPA1 expression in the cortex and the hippocampus. Data are presented as mean ± SEM for n = 10 mice per group with * $p < 0.05$, ** $p < 0.01$,*** $p < 0.001$.

3.4.4. OC reduced IgG extravasation

The effect of OC on BBB leakiness was evaluated by IF of IgG extravasation, which used as an endogenous BBB permeability marker. IF was performed by using collagen IV (brain microvessels), and IgG primary antibody to detect IgG extravasation. Our data (Fig 3.6. 5) indicate a significantly higher IgG extravasation in the 5xFAD hippocampus by 2.5-fold (Fig 3.6. 3A) and the cortex by 3.4-fold (Fig 3.6. 5B) compared to the WT mice. 5xFAD mice received 10 mg/kg OC demonstrated a significant reduction in IgG extravasation by 50-60% in the hippocampus and the cortex (p<0.001) compared to vehicle-treated 5xFAD mice. On the other hand, 1mg/kg OC shows no significant difference in IgG extravasation compared to vehicle-treated 5xFAD mice. Therefore, our data indicate that 10 mg/kg OC rectified the BBB function in 5xFAD mice.

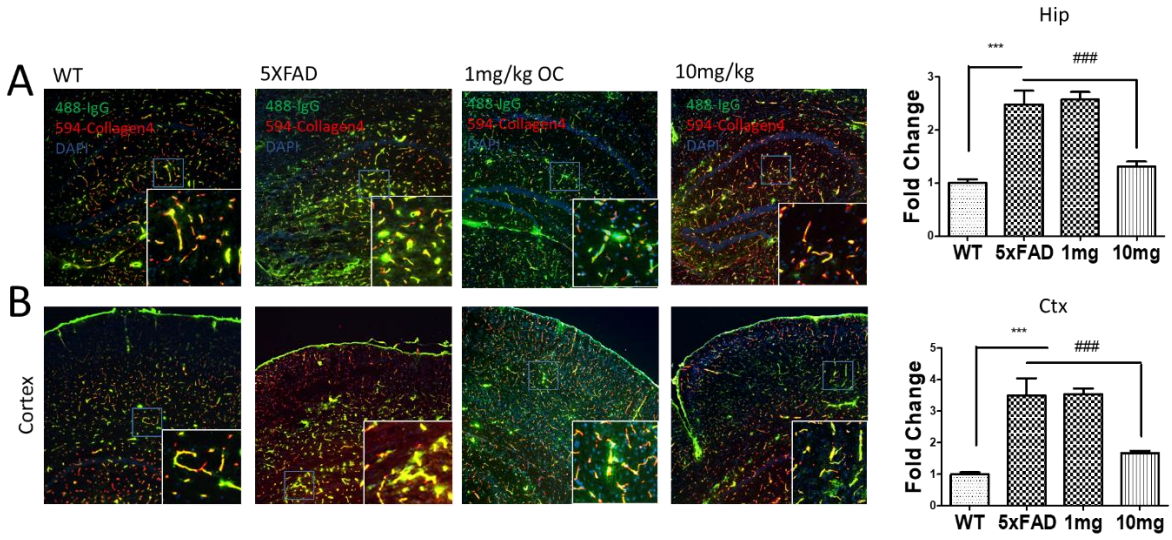

Figure 3.6. 5. IgG extravasation rate was reduced by OC treatment on 5xFAD AD mice brain hippocampus and cortex. This figure demonstrates IgG extravasation in the hippocampus (A) and the cortex (B). Our data indicate that 10mg/kg OC reduced the extravasation rate in the hippocampus and the cortex of 5xFAD. Data are presented as mean ± SEM for n = 10 mice per group with * p < 0.05, ** p < 0.01,*** p < 0.001.

3.4.5. OC reduced Aβ burden in 5xFAD mice brains and increased plasma Aβ

We used ThioS to stain Aβ deposits in mice brain (Fig 3.6.6). Compared to vehicle-treated 5xFAD mice, only 10 mg/kg OC significantly reduced Aβ burden in mice brain by about 50% (Fig. 3.6.6). We also measured total brain Aβ using 6E10 antibody, and the results demonstrated a significant reduction by ~70% compared to vehicle-treated mice (Fig 3.6. 7). While the 1 mg/kg OC reduced total Aβ, the effect was not significantly different. Soluble Aβ isoforms 40 and 42 were monitored by ELISA. As showed in Fig. Fig 3.6. 8A &B, the data demonstrate mice treatment with 10 mg/kg OC significantly reduced $A\beta_{40}$ levels by 58% ($p<0.001$; Fig 3.6. 8 A) and $A\beta_{42}$ levels by 43% (Fig 3.6. 8 B) compared to vehicle-treated mice. While there was a trend of reduction, the 1mg/kg OC didn't produce a significant effect compared to vehicle-treated mice.

In the plasma (Fig 3.6. 8 C&D), compared to the WT mice, 5xFAD mice showed a significantly lower $A\beta_{40}$ and $A\beta_{42}$ levels, which significantly increased to the WT levels in 10 mg/kg OC treated mice but not with the 1 mg/kg dose.

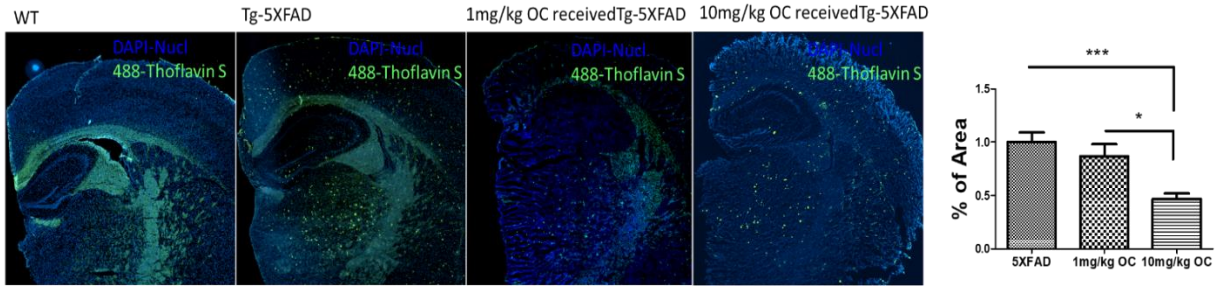

Figure 3.6. 6. Aβ plaque deposition was reduced by OC treatment on 5xFAD AD mice brain. ThioS staining was performed to detect Aβ plaque deposition in the brain. Our data indicates that 10mg/kg OC reduced Aβ plaque deposition in the 5xFAD brain. Data are presented as mean ± SEM for n = 10 mice per group with * $p < 0.05$, ** $p < 0.01$,*** $p < 0.001$.

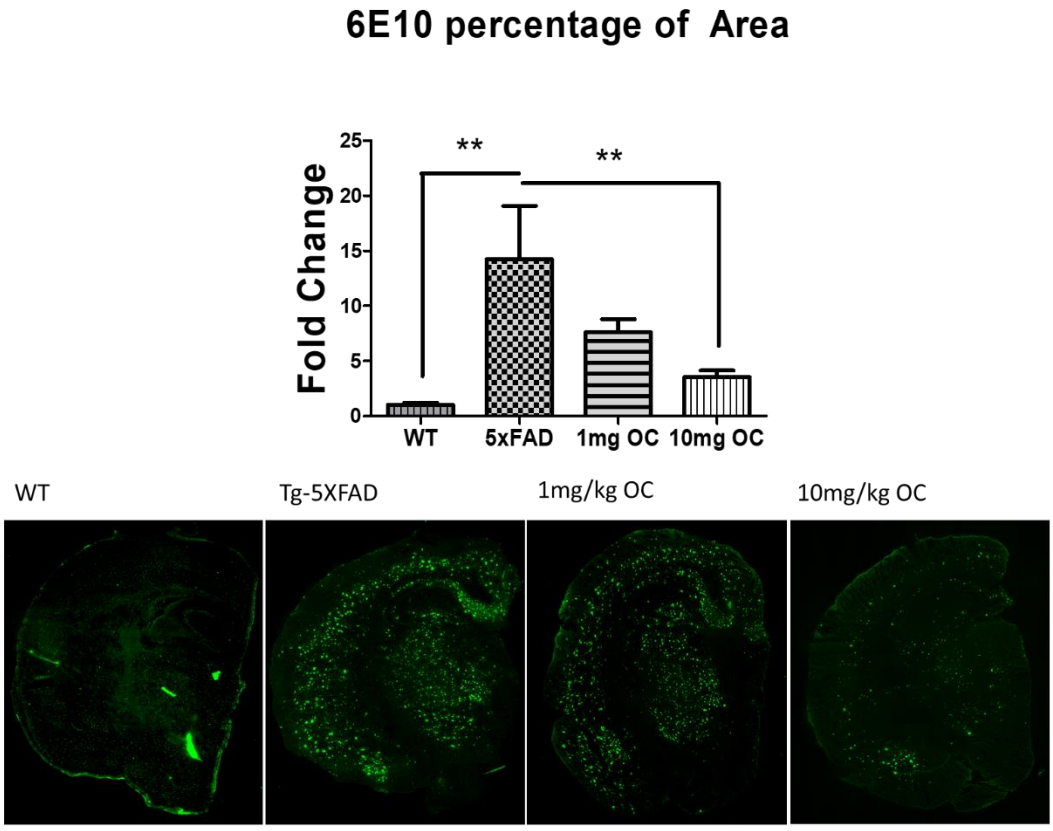

Figure 3.6. 7. Aβ 1-16, or APP (6E10) was reduced by OC treatment on 5xFAD AD mice brain hippocampus and cortex. We performed 6E10 staining to detect APP and Aβ 1-16 in the brain. Our data indicate that 10mg/kg OC reduced Aβ plaque deposition in the 5xFAD brain. Data are presented as mean ± SEM for n = 10 mice per group with * $p < 0.05$, ** $p < 0.01$,*** $p < 0.001$.

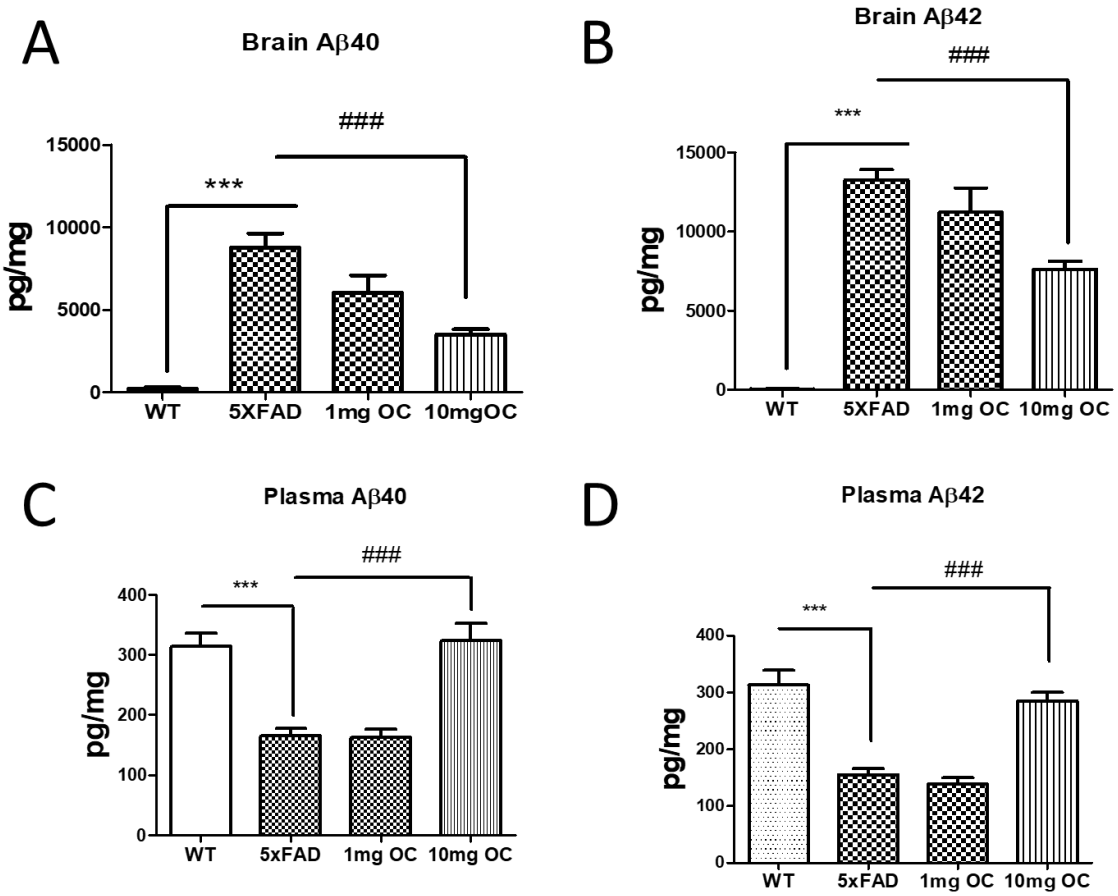

Figure 3.6. 8. OC treatment reduced Aβ 40 and Aβ 42 in the brain of 5xFAD, but in the plasma of 5xFAD. We performed ELISA quantification of $A\beta_{40}$ and $A\beta_{42}$. Our data indicates thatOC reduced Aβ burden in the brain by 42% in $A\beta_{40}$ (A) and 57% in $A\beta_{42}$ (B). In the plasma, our data indicates higher $A\beta_{40}$ (C) and $A\beta_{42}$ (D) in the WT and 5xFAD. Data are presented as mean ± SEM for n = 10 mice per group with * $p < 0.05$, ** $p < 0.01$,*** $p < 0.001$.

3.4.6. TRAP1 is expressed in bEnd3 cells

To confirm the expression of TRPA1 in bEnd3 cells, we performed immunocytochemistry to detect TRPA1. As showed in Figure 3.6.9, TRPA1 is expressed in bEnd3 cells and most notably on the plasma membrane of the cells.

To assess the TRPA1 function in bEnd3 cells, we used AITC and A967079 as TRPA1 modulators. As showed in Figure 3.6. 10, the data support functional TRPA1 where the agonist AITC significantly increased iCa^{2+} by 52%, and the antagonist A967079 significantly reduced iCa^{2+} by 27%. In addition, 1μM $A\beta_{42}$ monomer increased iCa^{2+} by 33% ($p<0.05$).

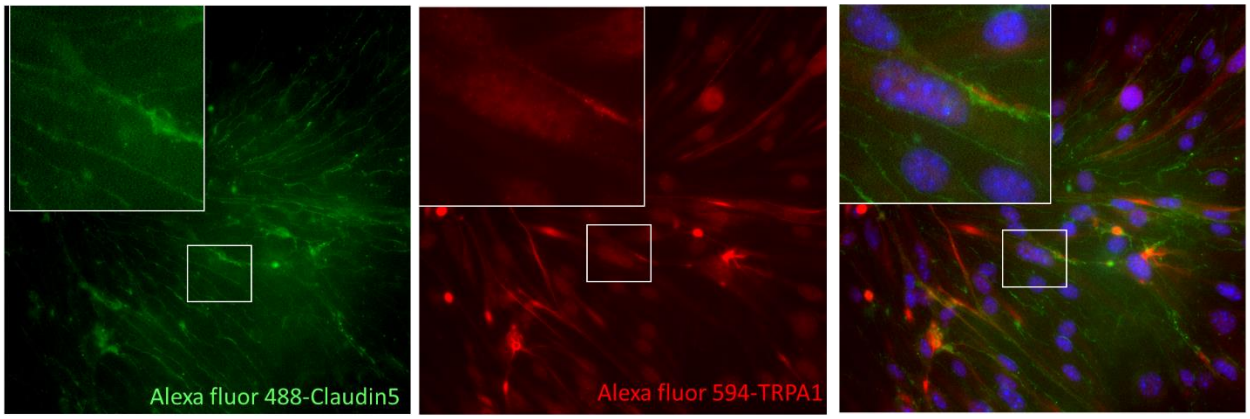

Figure 3.6. 9. Co-immunofluorescence shows that TRPA1 is expressed in bEnd3 cells. Co-immunofluorescence was performed to confirm TRPA1 expression in bEnd3 cells. Our data indicates that TRPA1 is expressed in bEnd3 cells.

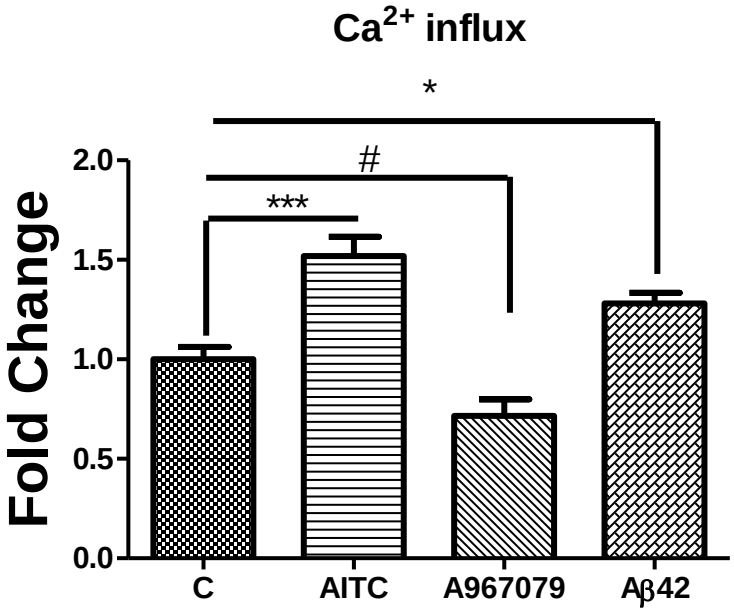

Figure 3.6. 10. TRPA1 modulators are effect on iCa^{2+} influx rate pf bEnd3 cells. We treated bEnd3 cells with AITC (10μM), A967079 (10μM) and $A\beta_{42}$ (1μM) for 72hrs to observe the iCa^{2+} influx rate difference. Our data indicate that AITC and Aβ 42 induced iCa^{2+} influx of bEnd3 cells. In addition to that, A967079 reduced iCa^{2+} influx of bEnd3 cells. Data are presented as mean ± SEM for n = 10 mice per group with * $p < 0.05$, ** $p < 0.01$,*** $p < 0.001$.

3.4.7. Aβ treatment increased TRPA1 levels in bEnd3 cells

Cultured bEnd3 cells were treated with 0.5 μM $A\beta_{42}$ monomers for 3 days. After treatment, cells were analyzed by Western blot. As showed in Figure 3.6.11, $A\beta_{42}$ treatment significantly increased the expression of TRPA1 by 55%. In addition, we performed an MTT assay to assess the effect of OC and Aβ treatment for 3 days on cells viability. In the concentration ranges of OC (0.5-40 μM), it was not toxic. For $A\beta_{42}$, at low concentration of 0.05 μM, it increased number of viable cells, but it was toxic at concentrations 2.5 and 5 μM (Fig 3.6.12).

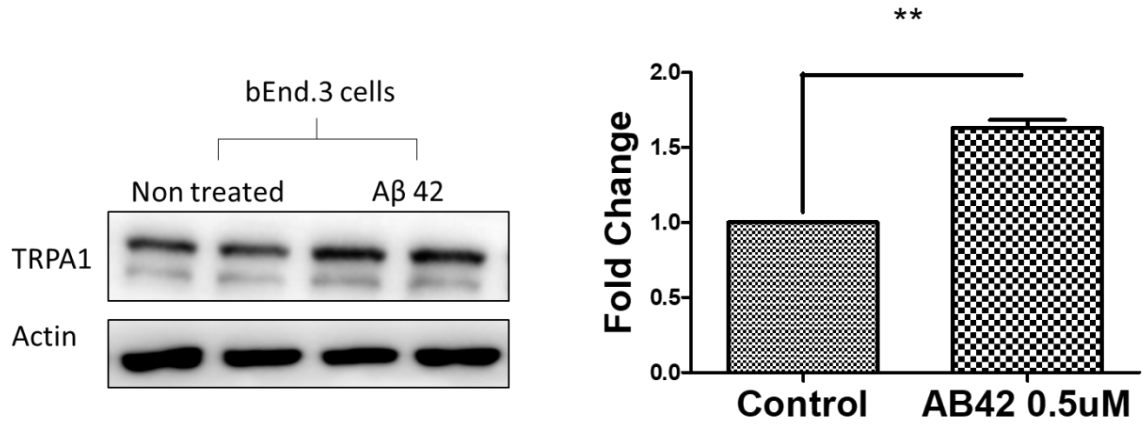

Figure 3.6. 11. Aβ induces TRPA1 expression in the bEnd3 cells. We performed 72hrsAβ treatment to the bEnd3 cells to confirm whether it effect on the TRPA1 expression levels. Our data indicates that $A\beta_{42}$ treatment induces TRPA1 expression in the bEnd3 cells. Data are presented as mean ± SEM for n = 10 mice per group with * $p < 0.05$, ** $p < 0.01$,*** $p < 0.001$.

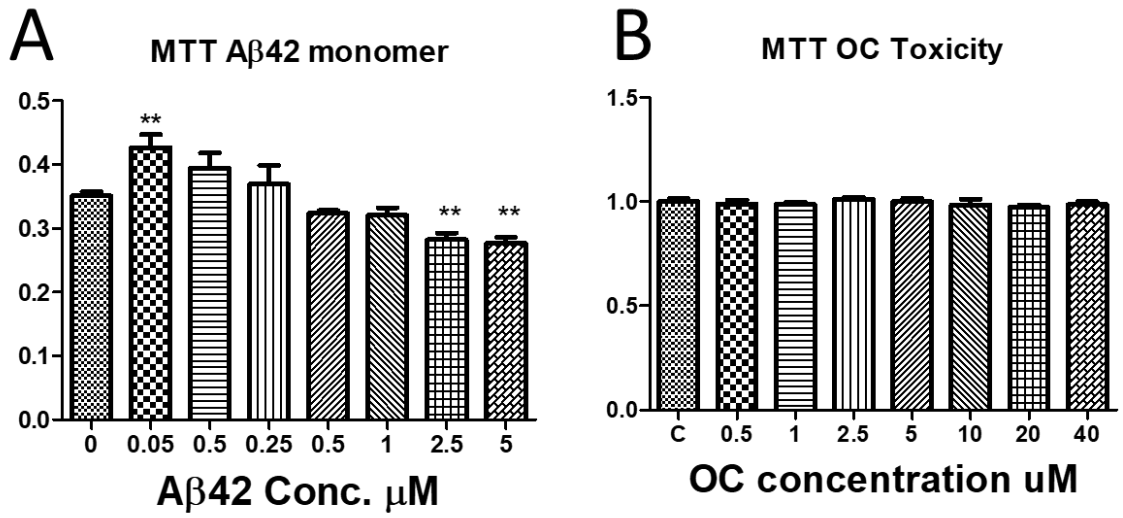

Figure 3.6. 12. MTT assay shows the non-toxicity effect of OC, and shows the toxicity effect of Aβ42. bEnd3 cells were treated with $A\beta_{42}$ and OC for 72 hrs. our data indicates non toxicity effect of OC, and 72hrs Aβ42 treatment shows a toxicity effect in higher than 2.5μM. Data are presented as mean ± SEM for n = 10 mice per group with * $p < 0.05$, ** $p < 0.01$,*** $p < 0.001$.

3.4.8. OC reduced TRPA1 levels and Ca^{2+} influx in bEnd3 cells

bEnd3 cells were treated daily with different concentrations of OC (1-20 μM) for three days. Treated cells were collected for Western blot analysis. As showed in Figure 3.6.13, the data indicate a significant reduction in TRPA1 levels in the range 5-20 μM by 48-65% (p<0.001). In addition, 3 days of treatment with OC (1-20 μM) significantly reduced intracellular calcium (iCa^{2+}) in a concentration-dependent manner (Figure 3.6.14). Therefore, our data indicate OC reduced iCa^{2+} levels, an effect that could be mediated, at least in part by reduced TRPA1 expression.

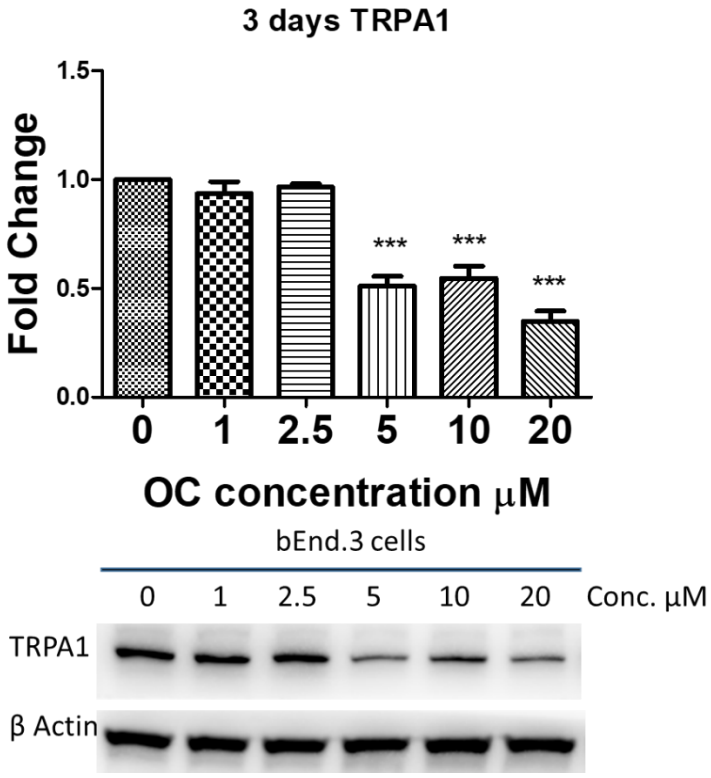

Figure 3.6. 13. OC reduces TRPA1 expression level in bEnd3 cells. We performed western blot to observe TRPA1 expression level by adding OC treatment for 72hrs. Our data indicates that higher than 5μM OC treatment reduces TRPA1 expression in the bEnd3 cells. Data are presented as mean ± SEM for n = 10 mice per group with * $p < 0.05$, ** $p < 0.01$,*** $p < 0.001$.

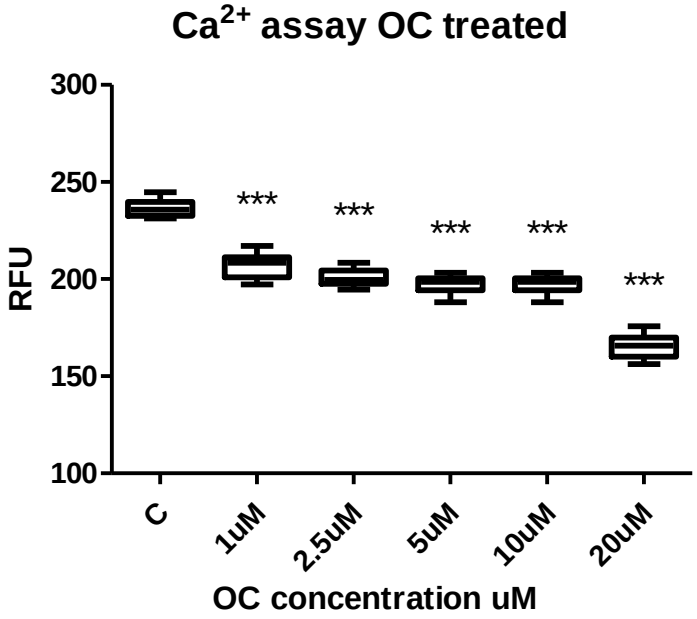

Figure 3.6. 14. OC reduces iCa^{2+} rate of bEnd3 cells. We performed Ca^{2+} assay to observe the effect of OC to the iCa^{2+} influx rate in bEnd3 cells. Our data indicates that 72 hours of OC treatment between 1-20μM reduced the iCa^{2+} influx rate of bEnd3 cells. Data are presented as mean ± SEM for n = 10 mice per group with * $p < 0.05$, ** $p < 0.01$,*** $p < 0.001$.

3.4.9. OC reduced inulin permeability and enhanced Aβ transport across the in vitro BBB model

Cultured bEnd3 cells in the transwell inserts were treated with 10 μM of OC or 150 nM of $A\beta_{42}$ oligomers or their combination for 72 h as we previously reported (192). As showed in Figure 3.6.15, $A\beta_{42}$ oligomers significantly increased inulin permeability across the monolayer by 18% ($p<0.05$), suggesting monolayer disruption, while reduced ^{125}I-$A\beta_{40}$ by 13%. OC, on the other hand, while it showed a trend for decrease and increase, respectively, the effect was not significant. The combined treatment of 10 μM OC and 150 nM of $A\beta_{42}$ oligomers demonstrated OC rectified the leaky effect of Aβ oligomers, reduced inulin permeability by 22% ($p<0.05$) and increased ^{125}I-$A\beta_{40}$ transport by 10% when compared to $A\beta_{42}$ oligomers alone. Therefore, the data demonstrate that OC prevents the monolayer BBB disruption, an effect that could be mediated, at least in part, by TRPA1 downregulation.

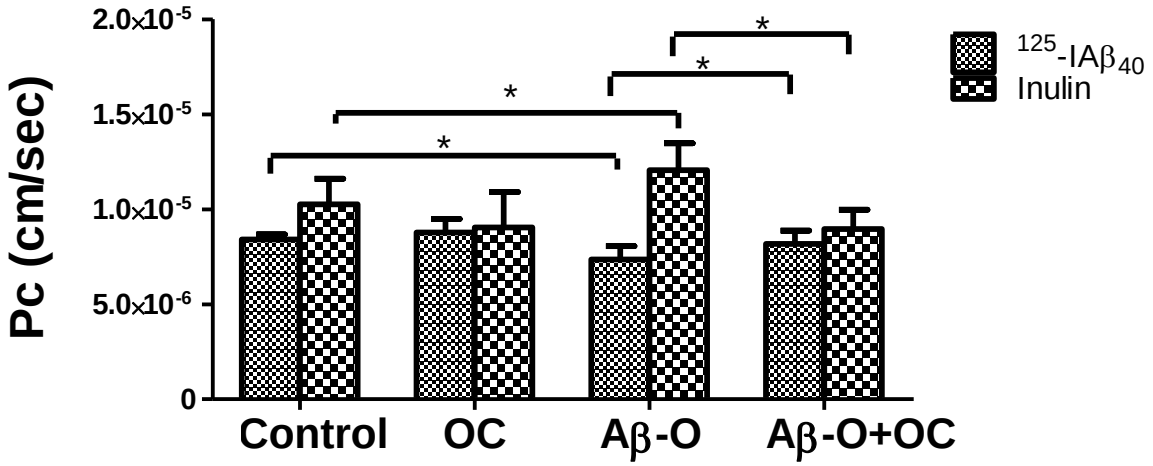

Figure 3.6. 15. OC treatment reduces permeability of Aβ oligomer *in-vitro* BBB model. We performed permeability assay of bEnd3 cells-based BBB model. Our data indicates that higher permeability of inulin was observed in 72hrs 150nM Aβ oligomer treated cells. In addition to that, we observed low permeability of inulin when it received OC (10μM) and OC+ Aβ oligomer (150nM) for 72 hrs. For the ^{125}-IAβ_{40} transport, we observed higher ^{125}-IAβ_{40} transport in OC treatment received cells. However, 150nM Aβ oligomer treated cells showed reduced ^{125}-IAβ_{40} transport. Data are presented as mean ± SEM for n = 10 mice per group with * $p < 0.05$, ** $p < 0.01$,*** $p < 0.001$.

3.5. Discussion

AD is a progressive neurodegenerative disorder (193). AD mice models with APP mutations demonstrate the deposition of brain Aβ plaque (194), which caused by the increased production and reduced clearance of Aβ (195). Aβ accumulation is also associated with BBB dysfunction (196). BBB is a tight physical barrier between the brain and the peripheral system (197). Therefore, protecting and restoring the BBB function could be a therapeutic approach to preventing or treating AD. Our previous data demonstrate that restoring the BBB function in AD mice models would reduce brain Aβ deposition that improve memory ability in EVOO (OC rich) treated 5xFAD mice by enhancing Aβ clearance and reducing production (96, 116). In addition, following mice treated with EVOO, a significant reduction in total brain TRPA1 of AD mice was observed (96). The purpose of this work was to evaluate the effect of OC on metabolic and behavioral phenotypes parameters, BBB function, and TRPA1 expression in vascular endothelial cells in 5xFAD mice model of AD.

Our data indicate higher expression of BBB-endothelium TRPA1 in 5xFAD mice brains compared to the WT. TRPA1 is a calcium-regulating cell membrane receptor (198) that is also expressed in the throat that detects OC pungent taste (199). The activation of TRPA1 induces Ca^{2+} influx to the cell (200), and it is induced by temperature mainly as a cold sensor (201). In human and rodents, TRPA1 is known as a pain sensor (202-204). Therefore, TRPA1 in the mice model is expected to have similar functions and properties as human TRPA1. Recently, we showed reduced levels of TRPA1 in AD mice brains that received OC treatment (96).

Our findings demonstrate that TRPA1 is expressed in endothelial cells and that it is upregulated by Aβ. OC treatment significantly reduced brain Aβ levels in 5xFAD, an effect that was associated with endothelium-TRPA1 downregulation, which could play a role in rectifying the function.

An acute (short-term) exposure to OC in in-vitro models demonstrated that OC is a TRPA1 agonist that induces iCa^{2+}influx into TRPA1 transfected HEK293 cells (102). However, relevant to our previous study, it demonstrates a reduced TRPA1 expression in the AD mice brain with long-term OC-rich EVOO treated (96), which is similar to our data. Therefore, our data indicate long-term OC treatment downregulates TRPA1 expression.

Not only BBB endothelial cells but also astrocytes express TRPA1 (101, 190). An application of soluble Aβ oligomers (Aβo) induced fast and widespread Ca^{2+} hyperactivity in the astrocytic population, and astrocyte hyperactivity is independent of neuronal activity and is repaired by TRPA1 channels blockade (190). Similarly, our data indicate higher Ca^{2+} influx in the BBB endothelial cells with Aβ treatment, and blockage of TRPA1 by 3 days of treatment of OC was observed. Therefore, reduced expression of TRPA1 could be a therapeutic target to maintain the BBB function.

Measurement of plasma protein level is one of the preclinical approaches of AD that helps to predict cerebral amyloidosis (205). However, there is no established correlation between BBB dysfunction and plasma Aβ levels. Our data suggested that AD-induced BBB dysfunction in the 5xFAD mice shows less $Aβ_{40}$ and $Aβ_{42}$ levels in plasma compared to the WT mice. Interestingly, OC treatment showed higher plasma $Aβ_{40}$ and $Aβ_{42}$ levels approaching their levels in the WT mice. Some of the studies are show the important role of BBB in Aβ clearance from the brain to peripheral system and that the dysfunction of BBB reduced Aβ clearance from the brain (166, 206). Our data indicate that the WT mice without BBB disruption shows higher plasma $Aβ_{40}$ and $Aβ_{42}$ levels than 5xFAD. Therefore, we found that lower plasma $Aβ_{40}$ and $Aβ_{42}$ could be related to BBB dysfunction in the 5xFAD mice.

AD patients are experiencing neuropsychiatric symptoms such as loss of appetite, low activity rate, anxiety, and sleep disorder (207, 208). Here, to evaluate the effect of OC on these metabolic and behavioral parameters, we monitored the effect of OC on body weight, activity rate, anxiety-like behavior, and sleep time. Our data demonstrated that 10 mg/kg OC almost restored these parameters to their levels in the WT mice. Therefore, our data indicate that AD induces a significant metabolic parameters alteration, and this alteration could be rectified by 10 mg/kg OC treatment in 5xFAD mice.

Benzodiazepines and barbiturates are medicines currently used for the treatment of insomnia. However, the long-term treatment with these drugs has been associated with cognitive impairment (209). Here we observed the effect of OC on AD-induced sleep disturbances, where 10 mg/kg OC increased the sleep duration in 5xFAD mice without side effects. These results suggest the potential use of OC for the treatment of insomnia. However, additional studies are required to clarify the mechanism. In addition to that, we observed 10mg/kg OC ameliorate the integrity of the BBB that help to enhance cognitive function in AD. Therefore, OC rectifies sleep disturbances without cognitive impairment as an adverse effect.

In conclusion, we observed that higher BBB endothelial TRPA1 expression might involve in BBB disruption in AD; however, OC treatment reduced BBB endothelial TRPA1 expression, which helps to enhance the Aβ clearance rate to reduces Aβ deposition in the brain. In addition, OC treatment improved the metabolic and phenotypic behaviors in 5xFAD mice suggesting OC could improve metabolic and neuropsychiatric symptoms in AD patients.

4. Summary and conclusion

Alzheimer's disease (AD) patients are experiencing cognitive impairment, which induced by brain amyloid-β (Aβ) deposition induced neurodegeneration. In addition, AD patients experience blood-brain barrier (BBB) dysfunction that is related to Aβ deposition in the brain of AD patients. To better understand the relevance between BBB and Aβ deposition in AD, we selected oleocanthal (OC) as a treatment that help to maintain hthe ealthiness of BBB. However, how the effect of OC that enhances BBB function and healthiness has not been investigated. Based on the literature of our previous study, we observed a reduction of TRPA1 in the AD mice model with OC treated. However, the role of TRPA1 in the BBB function and behavioral alteration have not been investigated yet. To fill the gap in the literature, we selected the 5xFAD AD mice model as a vehicle, and measured metabolic parameters to observe behavioral alteration. In addition, we selected bEnd3 cells to confirm and observe the function and expression of TRPA1 in the BBB endothelial cells. The objective of the first project is to observe the effect of aging and AD pathology on the alteration of metabolic parameters. We successfully observed that aging induces metabolic parameters alteration. However, we found worsened metabolic parameter changes in AD mice model with Aβ deposition in the brain. In the second project, we observed higher expression of TRPA1 with worse BBB disruption and higher Aβ deposition in the AD mice brain compared to the WT. However, we observed that OC rectifies the function of BBB and reduces TRPA1 expression in the BBB. We also observed that OC restored the metabolic parameters of 5xFAD mice groups as much as the WT. Especially, we observed that OC reduced sleep disturbance and increased sleep duration in 5xFAD. Next, we selected bEnd3 cells to specify and observe TRPA1 in end BBB endothelial cells. We observed that Aβ treatment induces higher

expression of TRPA1 with higher Ca^{2+} influx (iCa^{2+}) in the bEnd3 cells; however, OC prevents Ca^{2+} influx (iCa^{2+}) and reduces the levels of TRPA1 in the bEnd3 cells. In addition to that, we observed OC treatment induces clearance of Aβ in the BBB transport model that OC enhances BBB function and enhances Aβ clearance from that brain.

In conclusion, we observed a altered metabolic parameters in 5xFAD mice compared to WT, specially at the order 9 months age mice. Beside of the effect of pathology, aging altered the parameters. In addition, we found TRPA1 is expressed in the BBB endothelial cells with a significantly increased levels in 5xfad mice compared to WT mice. Finally, we also found that 10mg/kg OC was able to ameliorate the metabolic parameters in the 5xFAD mice, rectified the BBB integrity, reduced the brain Aβ levels, and downregulated TRPA1 levels in the BBB endothelial cells. These result suggest monitoring metabolic behavioral phenotypes as assessment tool for AD diagnosis and therapeutic effect could be beneficial to assess AD. In addition, suppressing TRPA1 could provide therapeutic approach against AD.

4.1. Future directions

Based on my observations from this study, I suggest the following studies as future directions:

1. The role of TRPA1 in the BBB has not been well established. Therefore, to better understand and investigate the role of TRPA1 against AD, an establishment of signal pathway between TRPA1 and AD-induced BBB pathology is necessary.
2. I was unable to succeed in the transfection of bEnd3 cells to perform knockout/-in of TRPA1. Therefore, transfection of TRPA1 in bEnd3 cells is necessary to specify the effect of TRPA1.

3. This study does not include female mice subjects. Therefore, including female subject might help to better understand the function of TRPA1 in the BBB.

5. References

1. Serrano-Pozo A, Frosch MP, Masliah E, Hyman BT. Neuropathological alterations in Alzheimer disease. Cold Spring Harb Perspect Med. 2011;1(1):a006189.

2. Gomez-Isla T, Hollister R, West H, Mui S, Growdon JH, Petersen RC, et al. Neuronal loss correlates with but exceeds neurofibrillary tangles in Alzheimer's disease. Ann Neurol. 1997;41(1):17-24.

3. Daulatzai MA. Cerebral hypoperfusion and glucose hypometabolism: Key pathophysiological modulators promote neurodegeneration, cognitive impairment, and Alzheimer's disease. J Neurosci Res. 2017;95(4):943-72.

4. Silverberg NB, Ryan LM, Carrillo MC, Sperling R, Petersen RC, Posner HB, et al. Assessment of cognition in early dementia. Alzheimers Dement. 2011;7(3):e60-e76.

5. Chantanachai T, Taylor ME, Lord SR, Menant J, Delbaere K, Sachdev PS, et al. Risk factors for falls in community-dwelling older people with mild cognitive impairment: a prospective one-year study. PeerJ. 2022;10:e13484.

6. Petersen RC, Caracciolo B, Brayne C, Gauthier S, Jelic V, Fratiglioni L. Mild cognitive impairment: a concept in evolution. J Intern Med. 2014;275(3):214-28.

7. Petersen RC. Mild cognitive impairment as a diagnostic entity. J Intern Med. 2004;256(3):183-94.

8. Ferman TJ, Smith GE, Kantarci K, Boeve BF, Pankratz VS, Dickson DW, et al. Nonamnestic mild cognitive impairment progresses to dementia with Lewy bodies. Neurology. 2013;81(23):2032-8.

9. Baumgart M, Snyder HM, Carrillo MC, Fazio S, Kim H, Johns H. Summary of the evidence on modifiable risk factors for cognitive decline and dementia: A population-based perspective. Alzheimers Dement. 2015;11(6):718-26.

10. Yaffe K, Vittinghoff E, Pletcher MJ, Hoang TD, Launer LJ, Whitmer R, et al. Early adult to midlife cardiovascular risk factors and cognitive function. Circulation. 2014;129(15):1560-7.

11. Virta JJ, Heikkila K, Perola M, Koskenvuo M, Raiha I, Rinne JO, et al. Midlife cardiovascular risk factors and late cognitive impairment. Eur J Epidemiol. 2013;28(5):405-16.

12. Chen GF, Xu TH, Yan Y, Zhou YR, Jiang Y, Melcher K, et al. Amyloid beta: structure, biology and structure-based therapeutic development. Acta Pharmacol Sin. 2017;38(9):1205-35.

13. Kumar-Singh S, Theuns J, Van Broeck B, Pirici D, Vennekens K, Corsmit E, et al. Mean age-of-onset of familial alzheimer disease caused by presenilin mutations correlates with both increased Abeta42 and decreased Abeta40. Hum Mutat. 2006;27(7):686-95.

14. Yin YI, Bassit B, Zhu L, Yang X, Wang C, Li YM. {gamma}-Secretase Substrate Concentration Modulates the Abeta42/Abeta40 Ratio: IMPLICATIONS FOR ALZHEIMER DISEASE. J Biol Chem. 2007;282(32):23639-44.

15. Buee L, Bussiere T, Buee-Scherrer V, Delacourte A, Hof PR. Tau protein isoforms, phosphorylation and role in neurodegenerative disorders. Brain Res Brain Res Rev. 2000;33(1):95-130.

16. Guo JL, Lee VM. Neurofibrillary tangle-like tau pathology induced by synthetic tau fibrils in primary neurons over-expressing mutant tau. FEBS Lett. 2013;587(6):717-23.

17. Kahlson MA, Colodner KJ. Glial Tau Pathology in Tauopathies: Functional Consequences. J Exp Neurosci. 2015;9(Suppl 2):43-50.

18. Salim S. Oxidative Stress and the Central Nervous System. J Pharmacol Exp Ther. 2017;360(1):201-5.

19. Hulbert AJ, Pamplona R, Buffenstein R, Buttemer WA. Life and death: metabolic rate, membrane composition, and life span of animals. Physiol Rev. 2007;87(4):1175-213.

20. Hensley K, Hall N, Subramaniam R, Cole P, Harris M, Aksenov M, et al. Brain regional correspondence between Alzheimer's disease histopathology and biomarkers of protein oxidation. J Neurochem. 1995;65(5):2146-56.

21. Di Domenico F, Pupo G, Giraldo E, Badia MC, Monllor P, Lloret A, et al. Oxidative signature of cerebrospinal fluid from mild cognitive impairment and Alzheimer disease patients. Free Radic Biol Med. 2016;91:1-9.

22. Butterfield DA, Poon HF, St Clair D, Keller JN, Pierce WM, Klein JB, et al. Redox proteomics identification of oxidatively modified hippocampal proteins in mild cognitive impairment: insights into the development of Alzheimer's disease. Neurobiol Dis. 2006;22(2):223-32.

23. Butterfield DA, Boyd-Kimball D. Oxidative Stress, Amyloid-beta Peptide, and Altered Key Molecular Pathways in the Pathogenesis and Progression of Alzheimer's Disease. J Alzheimers Dis. 2018;62(3):1345-67.

24. Patel NS, Paris D, Mathura V, Quadros AN, Crawford FC, Mullan MJ. Inflammatory cytokine levels correlate with amyloid load in transgenic mouse models of Alzheimer's disease. J Neuroinflammation. 2005;2(1):9.

25. Bermejo P, Martin-Aragon S, Benedi J, Susin C, Felici E, Gil P, et al. Differences of peripheral inflammatory markers between mild cognitive impairment and Alzheimer's disease. Immunol Lett. 2008;117(2):198-202.

26. Laske C, Stransky E, Hoffmann N, Maetzler W, Straten G, Eschweiler GW, et al. Macrophage colony-stimulating factor (M-CSF) in plasma and CSF of patients with mild cognitive impairment and Alzheimer's disease. Curr Alzheimer Res. 2010;7(5):409-14.

27. Ivannikov MV, Sugimori M, Llinas RR. Calcium clearance and its energy requirements in cerebellar neurons. Cell Calcium. 2010;47(6):507-13.

28. Jadiya P, Kolmetzky DW, Tomar D, Di Meco A, Lombardi AA, Lambert JP, et al. Impaired mitochondrial calcium efflux contributes to disease progression in models of Alzheimer's disease. Nat Commun. 2019;10(1):3885.

29. Calvo-Rodriguez M, Bacskai BJ. Mitochondria and Calcium in Alzheimer's Disease: From Cell Signaling to Neuronal Cell Death. Trends Neurosci. 2021;44(2):136-51.

30. Boyman L, Karbowski M, Lederer WJ. Regulation of Mitochondrial ATP Production: Ca(2+) Signaling and Quality Control. Trends Mol Med. 2020;26(1):21-39.

31. Esteras N, Abramov AY. Mitochondrial Calcium Deregulation in the Mechanism of Beta-Amyloid and Tau Pathology. Cells. 2020;9(9).

32. Gualtieri R, Kalthur G, Barbato V, Di Nardo M, Adiga SK, Talevi R. Mitochondrial Dysfunction and Oxidative Stress Caused by Cryopreservation in Reproductive Cells. Antioxidants (Basel). 2021;10(3).

33. Arundine M, Tymianski M. Molecular mechanisms of calcium-dependent neurodegeneration in excitotoxicity. Cell Calcium. 2003;34(4-5):325-37.

34. Verma M, Lizama BN, Chu CT. Excitotoxicity, calcium and mitochondria: a triad in synaptic neurodegeneration. Transl Neurodegener. 2022;11(1):3.

35. Okubo Y, Sekiya H, Namiki S, Sakamoto H, Iinuma S, Yamasaki M, et al. Imaging extrasynaptic glutamate dynamics in the brain. Proc Natl Acad Sci U S A. 2010;107(14):6526-31.

36. Tymianski M, Charlton MP, Carlen PL, Tator CH. Source specificity of early calcium neurotoxicity in cultured embryonic spinal neurons. J Neurosci. 1993;13(5):2085-104.

37. Choi DW. Excitotoxicity: Still Hammering the Ischemic Brain in 2020. Front Neurosci. 2020;14:579953.

38. Erdo F, Denes L, de Lange E. Age-associated physiological and pathological changes at the blood-brain barrier: A review. J Cereb Blood Flow Metab. 2017;37(1):4-24.

39. Knox EG, Aburto MR, Clarke G, Cryan JF, O'Driscoll CM. The blood-brain barrier in aging and neurodegeneration. Mol Psychiatry. 2022;27(6):2659-73.

40. Wen J, Ding Y, Wang L, Xiao Y. Gut microbiome improves postoperative cognitive function by decreasing permeability of the blood-brain barrier in aged mice. Brain Res Bull. 2020;164:249-56.

41. Banks WA, Reed MJ, Logsdon AF, Rhea EM, Erickson MA. Healthy aging and the blood-brain barrier. Nat Aging. 2021;1(3):243-54.

42. Coomber BL, Stewart PA. Morphometric analysis of CNS microvascular endothelium. Microvasc Res. 1985;30(1):99-115.

43. Tietz S, Engelhardt B. Brain barriers: Crosstalk between complex tight junctions and adherens junctions. J Cell Biol. 2015;209(4):493-506.

44. Reese TS, Karnovsky MJ. Fine structural localization of a blood-brain barrier to exogenous peroxidase. J Cell Biol. 1967;34(1):207-17.

45. Stamatovic SM, Keep RF, Andjelkovic AV. Brain endothelial cell-cell junctions: how to "open" the blood brain barrier. Curr Neuropharmacol. 2008;6(3):179-92.

46. Daneman R, Prat A. The blood-brain barrier. Cold Spring Harb Perspect Biol. 2015;7(1):a020412.

47. Loscher W, Potschka H. Blood-brain barrier active efflux transporters: ATP-binding cassette gene family. NeuroRx. 2005;2(1):86-98.

48. Mittapalli RK, Manda VK, Adkins CE, Geldenhuys WJ, Lockman PR. Exploiting nutrient transporters at the blood-brain barrier to improve brain distribution of small molecules. Ther Deliv. 2010;1(6):775-84.

49. Daneman R, Zhou L, Agalliu D, Cahoy JD, Kaushal A, Barres BA. The mouse blood-brain barrier transcriptome: a new resource for understanding the development and function of brain endothelial cells. PLoS One. 2010;5(10):e13741.

50. Aird WC. Phenotypic heterogeneity of the endothelium: II. Representative vascular beds. Circ Res. 2007;100(2):174-90.

51. Henninger DD, Panes J, Eppihimer M, Russell J, Gerritsen M, Anderson DC, et al. Cytokine-induced VCAM-1 and ICAM-1 expression in different organs of the mouse. J Immunol. 1997;158(4):1825-32.

52. Cong X, Kong W. Endothelial tight junctions and their regulatory signaling pathways in vascular homeostasis and disease. Cell Signal. 2020;66:109485.

53. Zihni C, Mills C, Matter K, Balda MS. Tight junctions: from simple barriers to multifunctional molecular gates. Nat Rev Mol Cell Biol. 2016;17(9):564-80.

54. Shin K, Fogg VC, Margolis B. Tight junctions and cell polarity. Annu Rev Cell Dev Biol. 2006;22:207-35.

55. Jiao H, Wang Z, Liu Y, Wang P, Xue Y. Specific role of tight junction proteins claudin-5, occludin, and ZO-1 of the blood-brain barrier in a focal cerebral ischemic insult. J Mol Neurosci. 2011;44(2):130-9.

56. Sandoval KE, Witt KA. Blood-brain barrier tight junction permeability and ischemic stroke. Neurobiol Dis. 2008;32(2):200-19.

57. Nitta T, Hata M, Gotoh S, Seo Y, Sasaki H, Hashimoto N, et al. Size-selective loosening of the blood-brain barrier in claudin-5-deficient mice. J Cell Biol. 2003;161(3):653-60.

58. Heiskala M, Peterson PA, Yang Y. The roles of claudin superfamily proteins in paracellular transport. Traffic. 2001;2(2):93-8.

59. Bonvento G, Bolanos JP. Astrocyte-neuron metabolic cooperation shapes brain activity. Cell Metab. 2021;33(8):1546-64.

60. Sofroniew MV. Astrocyte Reactivity: Subtypes, States, and Functions in CNS Innate Immunity. Trends Immunol. 2020;41(9):758-70.

61. Matejuk A, Ransohoff RM. Crosstalk Between Astrocytes and Microglia: An Overview. Front Immunol. 2020;11:1416.

62. Jensen CJ, Massie A, De Keyser J. Immune players in the CNS: the astrocyte. J Neuroimmune Pharmacol. 2013;8(4):824-39.

63. Michinaga S, Koyama Y. Dual Roles of Astrocyte-Derived Factors in Regulation of Blood-Brain Barrier Function after Brain Damage. Int J Mol Sci. 2019;20(3).

64. Alvarez JI, Katayama T, Prat A. Glial influence on the blood brain barrier. Glia. 2013;61(12):1939-58.

65. Wosik K, Cayrol R, Dodelet-Devillers A, Berthelet F, Bernard M, Moumdjian R, et al. Angiotensin II controls occludin function and is required for blood brain barrier maintenance: relevance to multiple sclerosis. J Neurosci. 2007;27(34):9032-42.

66. Abbott NJ, Ronnback L, Hansson E. Astrocyte-endothelial interactions at the blood-brain barrier. Nat Rev Neurosci. 2006;7(1):41-53.

67. Rhea EM, Banks WA. Role of the Blood-Brain Barrier in Central Nervous System Insulin Resistance. Front Neurosci. 2019;13:521.

68. Armulik A, Genove G, Mae M, Nisancioglu MH, Wallgard E, Niaudet C, et al. Pericytes regulate the blood-brain barrier. Nature. 2010;468(7323):557-61.

69. Montagne A, Barnes SR, Sweeney MD, Halliday MR, Sagare AP, Zhao Z, et al. Blood-brain barrier breakdown in the aging human hippocampus. Neuron. 2015;85(2):296-302.

70. Montagne A, Huuskonen MT, Rajagopal G, Sweeney MD, Nation DA, Sepehrband F, et al. Undetectable gadolinium brain retention in individuals with an age-dependent blood-brain barrier breakdown in the hippocampus and mild cognitive impairment. Alzheimers Dement. 2019;15(12):1568-75.

71. Verheggen ICM, de Jong JJA, van Boxtel MPJ, Gronenschild E, Palm WM, Postma AA, et al. Increase in blood-brain barrier leakage in healthy, older adults. Geroscience. 2020;42(4):1183-93.

72. Shams S, Wahlund LO. Cerebral microbleeds as a biomarker in Alzheimer's disease? A review in the field. Biomark Med. 2016;10(1):9-18.

73. Poliakova T, Levin O, Arablinskiy A, Vasenina E, Zerr I. Cerebral microbleeds in early Alzheimer's disease. J Neurol. 2016;263(10):1961-8.

74. Shams S, Martola J, Granberg T, Li X, Shams M, Fereshtehnejad SM, et al. Cerebral microbleeds: different prevalence, topography, and risk factors depending on dementia diagnosis-the Karolinska Imaging Dementia Study. AJNR Am J Neuroradiol. 2015;36(4):661-6.

75. Yates PA, Villemagne VL, Ellis KA, Desmond PM, Masters CL, Rowe CC. Cerebral microbleeds: a review of clinical, genetic, and neuroimaging associations. Front Neurol. 2014;4:205.

76. Heringa SM, Reijmer YD, Leemans A, Koek HL, Kappelle LJ, Biessels GJ, et al. Multiple microbleeds are related to cerebral network disruptions in patients with early Alzheimer's disease. J Alzheimers Dis. 2014;38(1):211-21.

77. Brundel M, Heringa SM, de Bresser J, Koek HL, Zwanenburg JJ, Jaap Kappelle L, et al. High prevalence of cerebral microbleeds at 7Tesla MRI in patients with early Alzheimer's disease. J Alzheimers Dis. 2012;31(2):259-63.

78. Nelson AR, Sweeney MD, Sagare AP, Zlokovic BV. Neurovascular dysfunction and neurodegeneration in dementia and Alzheimer's disease. Biochim Biophys Acta. 2016;1862(5):887-900.

79. Hachinski V. Correction. World Stroke Organization. Stroke and potentially preventable dementias proclamation: updated World Stroke Day proclamation. Stroke. 2016;47(2):e37.

80. Snyder HM, Corriveau RA, Craft S, Faber JE, Greenberg SM, Knopman D, et al. Vascular contributions to cognitive impairment and dementia including Alzheimer's disease. Alzheimers Dement. 2015;11(6):710-7.

81. Wardlaw JM, Smith EE, Biessels GJ, Cordonnier C, Fazekas F, Frayne R, et al. Neuroimaging standards for research into small vessel disease and its contribution to ageing and neurodegeneration. Lancet Neurol. 2013;12(8):822-38.

82. Faraco G, Park L, Zhou P, Luo W, Paul SM, Anrather J, et al. Hypertension enhances Abeta-induced neurovascular dysfunction, promotes beta-secretase activity, and leads to amyloidogenic processing of APP. J Cereb Blood Flow Metab. 2016;36(1):241-52.

83. Iadecola C. The pathobiology of vascular dementia. Neuron. 2013;80(4):844-66.

84. Iturria-Medina Y, Sotero RC, Toussaint PJ, Mateos-Perez JM, Evans AC, Alzheimer's Disease Neuroimaging I. Early role of vascular dysregulation on late-onset Alzheimer's disease based on multifactorial data-driven analysis. Nat Commun. 2016;7:11934.

85. Arvanitakis Z, Capuano AW, Leurgans SE, Bennett DA, Schneider JA. Relation of cerebral vessel disease to Alzheimer's disease dementia and cognitive function in elderly people: a cross-sectional study. Lancet Neurol. 2016;15(9):934-43.

86. Toledo JB, Cairns NJ, Da X, Chen K, Carter D, Fleisher A, et al. Clinical and multimodal biomarker correlates of ADNI neuropathological findings. Acta Neuropathol Commun. 2013;1:65.

87. Kook SY, Hong HS, Moon M, Ha CM, Chang S, Mook-Jung I. Abeta(1)(-)(4)(2)-RAGE interaction disrupts tight junctions of the blood-brain barrier via Ca(2)(+)-calcineurin signaling. J Neurosci. 2012;32(26):8845-54.

88. Abdallah IM, Al-Shami KM, Yang E, Kaddoumi A. Blood-Brain Barrier Disruption Increases Amyloid-Related Pathology in TgSwDI Mice. Int J Mol Sci. 2021;22(3).

89. Nilius B, Owsianik G. The transient receptor potential family of ion channels. Genome Biol. 2011;12(3):218.

90. Nilius B, Owsianik G. Transient receptor potential channelopathies. Pflugers Arch. 2010;460(2):437-50.

91. Nilius B, Owsianik G, Voets T, Peters JA. Transient receptor potential cation channels in disease. Physiol Rev. 2007;87(1):165-217.

92. Hu F, Song X, Long D. Transient receptor potential ankyrin 1 and calcium: Interactions and association with disease (Review). Exp Ther Med. 2021;22(6):1462.

93. Thakore P, Alvarado MG, Ali S, Mughal A, Pires PW, Yamasaki E, et al. Brain endothelial cell TRPA1 channels initiate neurovascular coupling. Elife. 2021;10.

94. Earley S. TRPA1 channels in the vasculature. Br J Pharmacol. 2012;167(1):13-22.

95. Rhyu MR, Kim Y, Lyall V. Interactions between Chemesthesis and Taste: Role of TRPA1 and TRPV1. Int J Mol Sci. 2021;22(7).

96. Al Rihani SB, Darakjian LI, Kaddoumi A. Oleocanthal-Rich Extra-Virgin Olive Oil Restores the Blood-Brain Barrier Function through NLRP3 Inflammasome Inhibition Simultaneously with Autophagy Induction in TgSwDI Mice. ACS Chem Neurosci. 2019;10(8):3543-54.

97. Kremeyer B, Lopera F, Cox JJ, Momin A, Rugiero F, Marsh S, et al. A gain-of-function mutation in TRPA1 causes familial episodic pain syndrome. Neuron. 2010;66(5):671-80.

98. Zhu MX. Multiple roles of calmodulin and other Ca(2+)-binding proteins in the functional regulation of TRP channels. Pflugers Arch. 2005;451(1):105-15.

99. Hasan R, Leeson-Payne AT, Jaggar JH, Zhang X. Calmodulin is responsible for Ca(2+)-dependent regulation of TRPA1 Channels. Sci Rep. 2017;7:45098.

100. Shigetomi E, Tong X, Kwan KY, Corey DP, Khakh BS. TRPA1 channels regulate astrocyte resting calcium and inhibitory synapse efficacy through GAT-3. Nat Neurosci. 2011;15(1):70-80.

101. Shigetomi E, Jackson-Weaver O, Huckstepp RT, O'Dell TJ, Khakh BS. TRPA1 channels are regulators of astrocyte basal calcium levels and long-term potentiation via constitutive D-serine release. J Neurosci. 2013;33(24):10143-53.

102. Peyrot des Gachons C, Uchida K, Bryant B, Shima A, Sperry JB, Dankulich-Nagrudny L, et al. Unusual pungency from extra-virgin olive oil is attributable to restricted spatial expression of the receptor of oleocanthal. J Neurosci. 2011;31(3):999-1009.

103. Kameda T, Zvick J, Vuk M, Sadowska A, Tam WK, Leung VY, et al. Expression and Activity of TRPA1 and TRPV1 in the Intervertebral Disc: Association with Inflammation and Matrix Remodeling. Int J Mol Sci. 2019;20(7).

104. Abuznait AH, Qosa H, Busnena BA, El Sayed KA, Kaddoumi A. Olive-oil-derived oleocanthal enhances beta-amyloid clearance as a potential neuroprotective mechanism against Alzheimer's disease: in vitro and in vivo studies. ACS Chem Neurosci. 2013;4(6):973-82.

105. Corona G, Spencer JP, Dessi MA. Extra virgin olive oil phenolics: absorption, metabolism, and biological activities in the GI tract. Toxicol Ind Health. 2009;25(4-5):285-93.

106. Aguilera CM, Mesa MD, Ramirez-Tortosa MC, Nestares MT, Ros E, Gil A. Sunflower oil does not protect against LDL oxidation as virgin olive oil does in patients with peripheral vascular disease. Clin Nutr. 2004;23(4):673-81.

107. Harper CR, Edwards MC, Jacobson TA. Flaxseed oil supplementation does not affect plasma lipoprotein concentration or particle size in human subjects. J Nutr. 2006;136(11):2844-8.

108. Lopez-Miranda J, Perez-Jimenez F, Ros E, De Caterina R, Badimon L, Covas MI, et al. Olive oil and health: summary of the II international conference on olive oil and health consensus report, Jaen and Cordoba (Spain) 2008. Nutr Metab Cardiovasc Dis. 2010;20(4):284-94.

109. Cicerale S, Lucas L, Keast R. Biological activities of phenolic compounds present in virgin olive oil. Int J Mol Sci. 2010;11(2):458-79.

110. Beauchamp GK, Keast RS, Morel D, Lin J, Pika J, Han Q, et al. Phytochemistry: ibuprofen-like activity in extra-virgin olive oil. Nature. 2005;437(7055):45-6.

111. Van Dam D, Coen K, De Deyn PP. Ibuprofen modifies cognitive disease progression in an Alzheimer's mouse model. J Psychopharmacol. 2010;24(3):383-8.

112. Parkinson L, Keast R. Oleocanthal, a phenolic derived from virgin olive oil: a review of the beneficial effects on inflammatory disease. Int J Mol Sci. 2014;15(7):12323-34.

113. Darakjian LI, Rigakou A, Brannen A, Qusa MH, Tasiakou N, Diamantakos P, et al. Spontaneous In Vitro and In Vivo Interaction of (-)-Oleocanthal with Glycine in Biological Fluids: Novel Pharmacokinetic Markers. ACS Pharmacol Transl Sci. 2021;4(1):179-92.

114. Kaddoumi A, Sayed KE. Comment on Lopez-Yerena et al. "Absorption and Intestinal Metabolic Profile of Oleocanthal in Rats" Pharmaceutics 2020, 12, 134. Pharmaceutics. 2020;12(8).

115. Qosa H, Mohamed LA, Batarseh YS, Alqahtani S, Ibrahim B, LeVine H, 3rd, et al. Extra-virgin olive oil attenuates amyloid-beta and tau pathologies in the brains of TgSwDI mice. J Nutr Biochem. 2015;26(12):1479-90.

116. Batarseh YS, Kaddoumi A. Oleocanthal-rich extra-virgin olive oil enhances donepezil effect by reducing amyloid-beta load and related toxicity in a mouse model of Alzheimer's disease. J Nutr Biochem. 2018;55:113-23.

117. Holmes E, Loo RL, Stamler J, Bictash M, Yap IK, Chan Q, et al. Human metabolic phenotype diversity and its association with diet and blood pressure. Nature. 2008;453(7193):396-400.

118. Luo Y, Burrington CM, Graff EC, Zhang J, Judd RL, Suksaranjit P, et al. Metabolic phenotype and adipose and liver features in a high-fat Western diet-induced mouse model of obesity-linked NAFLD. Am J Physiol Endocrinol Metab. 2016;310(6):E418-39.

119. Woodie LN, Luo Y, Wayne MJ, Graff EC, Ahmed B, O'Neill AM, et al. Restricted feeding for 9h in the active period partially abrogates the detrimental metabolic effects of a Western diet with liquid sugar consumption in mice. Metabolism. 2018;82:1-13.

120. Patel H, Kerndt CC, Bhardwaj A. Physiology, Respiratory Quotient. StatPearls. Treasure Island (FL)2022.

121. Brzecka A, Leszek J, Ashraf GM, Ejma M, Avila-Rodriguez MF, Yarla NS, et al. Sleep Disorders Associated With Alzheimer's Disease: A Perspective. Front Neurosci. 2018;12:330.

122. Mendelsohn AR, Larrick JW. Sleep facilitates clearance of metabolites from the brain: glymphatic function in aging and neurodegenerative diseases. Rejuvenation Res. 2013;16(6):518-23.

123. Lee H, Xie L, Yu M, Kang H, Feng T, Deane R, et al. The Effect of Body Posture on Brain Glymphatic Transport. J Neurosci. 2015;35(31):11034-44.

124. O'Donnell J, Ding F, Nedergaard M. Distinct functional states of astrocytes during sleep and wakefulness: Is norepinephrine the master regulator? Curr Sleep Med Rep. 2015;1(1):1-8.

125. Krueger JM, Frank MG, Wisor JP, Roy S. Sleep function: Toward elucidating an enigma. Sleep Med Rev. 2016;28:46-54.

126. Xie L, Kang H, Xu Q, Chen MJ, Liao Y, Thiyagarajan M, et al. Sleep drives metabolite clearance from the adult brain. Science. 2013;342(6156):373-7.

127. Ju YE, McLeland JS, Toedebusch CD, Xiong C, Fagan AM, Duntley SP, et al. Sleep quality and preclinical Alzheimer disease. JAMA Neurol. 2013;70(5):587-93.

128. Patel P, Masurkar AV. The Relationship of Anxiety with Alzheimer's Disease: A Narrative Review. Curr Alzheimer Res. 2021;18(5):359-71.

129. Gimson A, Schlosser M, Huntley JD, Marchant NL. Support for midlife anxiety diagnosis as an independent risk factor for dementia: a systematic review. BMJ Open. 2018;8(4):e019399.

130. Pentkowski NS, Rogge-Obando KK, Donaldson TN, Bouquin SJ, Clark BJ. Anxiety and Alzheimer's disease: Behavioral analysis and neural basis in rodent models of Alzheimer's-related neuropathology. Neurosci Biobehav Rev. 2021;127:647-58.

131. Di Iulio F, Palmer K, Blundo C, Casini AR, Gianni W, Caltagirone C, et al. Occurrence of neuropsychiatric symptoms and psychiatric disorders in mild Alzheimer's disease and mild cognitive impairment subtypes. Int Psychogeriatr. 2010;22(4):629-40.

132. Grundman M, Corey-Bloom J, Jernigan T, Archibald S, Thal LJ. Low body weight in Alzheimer's disease is associated with mesial temporal cortex atrophy. Neurology. 1996;46(6):1585-91.

133. Oakley H, Cole SL, Logan S, Maus E, Shao P, Craft J, et al. Intraneuronal beta-amyloid aggregates, neurodegeneration, and neuron loss in transgenic mice with five familial Alzheimer's disease mutations: potential factors in amyloid plaque formation. J Neurosci. 2006;26(40):10129-40.

134. Youmans KL, Tai LM, Kanekiyo T, Stine WB, Jr., Michon SC, Nwabuisi-Heath E, et al. Intraneuronal Abeta detection in 5xFAD mice by a new Abeta-specific antibody. Mol Neurodegener. 2012;7:8.

135. Chu TH, Cummins K, Sparling JS, Tsutsui S, Brideau C, Nilsson KPR, et al. Axonal and myelinic pathology in 5xFAD Alzheimer's mouse spinal cord. PLoS One. 2017;12(11):e0188218.

136. Bhattacharya S, Haertel C, Maelicke A, Montag D. Galantamine slows down plaque formation and behavioral decline in the 5XFAD mouse model of Alzheimer's disease. PLoS One. 2014;9(2):e89454.

137. JafariNasabian P, Inglis JE, Reilly W, Kelly OJ, Ilich JZ. Aging human body: changes in bone, muscle and body fat with consequent changes in nutrient intake. J Endocrinol. 2017;234(1):R37-R51.

138. Fjell AM, Walhovd KB. Structural brain changes in aging: courses, causes and cognitive consequences. Rev Neurosci. 2010;21(3):187-221.

139. Carvalho DZ, St Louis EK, Knopman DS, Boeve BF, Lowe VJ, Roberts RO, et al. Association of Excessive Daytime Sleepiness With Longitudinal beta-Amyloid Accumulation in Elderly Persons Without Dementia. JAMA Neurol. 2018;75(6):672-80.

140. Suma S, Watanabe Y, Hirano H, Kimura A, Edahiro A, Awata S, et al. Factors affecting the appetites of persons with Alzheimer's disease and mild cognitive impairment. Geriatr Gerontol Int. 2018;18(8):1236-43.

141. Westerterp KR. Control of energy expenditure in humans. Eur J Clin Nutr. 2017;71(3):340-4.

142. Masule MV, Rathod S, Agrawal Y, Patil CR, Nakhate KT, Ojha S, et al. Ghrelin mediated regulation of neurosynaptic transmitters in depressive disorders. Curr Res Pharmacol Drug Discov. 2022;3:100113.

143. Yanai S, Endo S. Functional Aging in Male C57BL/6J Mice Across the Life-Span: A Systematic Behavioral Analysis of Motor, Emotional, and Memory Function to Define an Aging Phenotype. Front Aging Neurosci. 2021;13:697621.

144. Mehta RI, Carpenter JS, Mehta RI, Haut MW, Ranjan M, Najib U, et al. Blood-Brain Barrier Opening with MRI-guided Focused Ultrasound Elicits Meningeal Venous Permeability in Humans with Early Alzheimer Disease. Radiology. 2021;298(3):654-62.

145. Baum JI, Kim IY, Wolfe RR. Protein Consumption and the Elderly: What Is the Optimal Level of Intake? Nutrients. 2016;8(6).

146. Pilgrim AL, Robinson SM, Sayer AA, Roberts HC. An overview of appetite decline in older people. Nurs Older People. 2015;27(5):29-35.

147. Bombois S, Derambure P, Pasquier F, Monaca C. Sleep disorders in aging and dementia. J Nutr Health Aging. 2010;14(3):212-7.

148. De Sousa RAL, Rocha-Dias I, de Oliveira LRS, Improta-Caria AC, Monteiro-Junior RS, Cassilhas RC. Molecular mechanisms of physical exercise on depression in the elderly: a systematic review. Mol Biol Rep. 2021;48(4):3853-62.

149. Fernandez M, Gobartt AL, Balana M, Group CS. Behavioural symptoms in patients with Alzheimer's disease and their association with cognitive impairment. BMC Neurol. 2010;10:87.

150. Wang PN, Yang CL, Lin KN, Chen WT, Chwang LC, Liu HC. Weight loss, nutritional status and physical activity in patients with Alzheimer's disease. A controlled study. J Neurol. 2004;251(3):314-20.

151. Manz F. Hydration and disease. J Am Coll Nutr. 2007;26(5 Suppl):535S-41S.

152. Stookey JD, Purser JL, Pieper CF, Cohen HJ. Plasma hypertonicity: another marker of frailty? J Am Geriatr Soc. 2004;52(8):1313-20.

153. Albert SG, Nakra BR, Grossberg GT, Caminal ER. Vasopressin response to dehydration in Alzheimer's disease. J Am Geriatr Soc. 1989;37(9):843-7.

154. Gulia KK, Kumar VM. Sleep disorders in the elderly: a growing challenge. Psychogeriatrics. 2018;18(3):155-65.

155. Birhanu TT, Hassen Salih M, Abate HK. Sleep Quality and Associated Factors Among Diabetes Mellitus Patients in a Follow-Up Clinic at the University of Gondar Comprehensive

Specialized Hospital in Gondar, Northwest Ethiopia: A Cross-Sectional Study. Diabetes Metab Syndr Obes. 2020;13:4859-68.

156. Honda H, Ashizawa R, Kiriyama K, Take K, Hirase T, Arizono S, et al. Chronic pain in the frail elderly mediates sleep disorders and influences falls. Arch Gerontol Geriatr. 2022;99:104582.

157. Uchmanowicz I, Markiewicz K, Uchmanowicz B, Koltuniuk A, Rosinczuk J. The relationship between sleep disturbances and quality of life in elderly patients with hypertension. Clin Interv Aging. 2019;14:155-65.

158. Soltani S, Chauvette S, Bukhtiyarova O, Lina JM, Dube J, Seigneur J, et al. Sleep-Wake Cycle in Young and Older Mice. Front Syst Neurosci. 2019;13:51.

159. Brown BM, Rainey-Smith SR, Bucks RS, Weinborn M, Martins RN. Exploring the bi-directional relationship between sleep and beta-amyloid. Curr Opin Psychiatry. 2016;29(6):397-401.

160. Brown BM, Rainey-Smith SR, Villemagne VL, Weinborn M, Bucks RS, Sohrabi HR, et al. The Relationship between Sleep Quality and Brain Amyloid Burden. Sleep. 2016;39(5):1063-8.

161. Van Erum J, Van Dam D, De Deyn PP. Sleep and Alzheimer's disease: A pivotal role for the suprachiasmatic nucleus. Sleep Med Rev. 2018;40:17-27.

162. Bliwise DL. Sleep disorders in Alzheimer's disease and other dementias. Clin Cornerstone. 2004;6 Suppl 1A:S16-28.

163. Cordone S, Annarumma L, Rossini PM, De Gennaro L. Sleep and beta-Amyloid Deposition in Alzheimer Disease: Insights on Mechanisms and Possible Innovative Treatments. Front Pharmacol. 2019;10:695.

164. Liu Z, Wang F, Tang M, Zhao Y, Wang X. Amyloid beta and tau are involved in sleep disorder in Alzheimer's disease by orexin A and adenosine A(1) receptor. Int J Mol Med. 2019;43(1):435-42.

165. Mendez MF. The Relationship Between Anxiety and Alzheimer's Disease. J Alzheimers Dis Rep. 2021;5(1):171-7.

166. Zhang W, Wang X, Lu Y, Yu W. Relations of neuropsychiatric symptoms with disease stage, sex, and daily function in mild cognitive impairment and dementia due to Alzheimer's disease: A cross-sectional study. J Psychosom Res. 2022;161:110994.

167. Jawhar S, Trawicka A, Jenneckens C, Bayer TA, Wirths O. Motor deficits, neuron loss, and reduced anxiety coinciding with axonal degeneration and intraneuronal Abeta aggregation in the 5XFAD mouse model of Alzheimer's disease. Neurobiol Aging. 2012;33(1):196 e29-40.

168. Arendash GW, Gordon MN, Diamond DM, Austin LA, Hatcher JM, Jantzen P, et al. Behavioral assessment of Alzheimer's transgenic mice following long-term Abeta vaccination: task specificity and correlations between Abeta deposition and spatial memory. DNA Cell Biol. 2001;20(11):737-44.

169. Radde R, Bolmont T, Kaeser SA, Coomaraswamy J, Lindau D, Stoltze L, et al. Abeta42-driven cerebral amyloidosis in transgenic mice reveals early and robust pathology. EMBO Rep. 2006;7(9):940-6.

170. Flanigan TJ, Xue Y, Kishan Rao S, Dhanushkodi A, McDonald MP. Abnormal vibrissa-related behavior and loss of barrel field inhibitory neurons in 5xFAD transgenics. Genes Brain Behav. 2014;13(5):488-500.

171. Lippi SLP, Smith ML, Flinn JM. A Novel hAPP/htau Mouse Model of Alzheimer's Disease: Inclusion of APP With Tau Exacerbates Behavioral Deficits and Zinc Administration Heightens Tangle Pathology. Front Aging Neurosci. 2018;10:382.

172. Sterniczuk R, Antle MC, Laferla FM, Dyck RH. Characterization of the 3xTg-AD mouse model of Alzheimer's disease: part 2. Behavioral and cognitive changes. Brain Res. 2010;1348:149-55.

173. Lopez OL, Kuller LH, Mehta PD, Becker JT, Gach HM, Sweet RA, et al. Plasma amyloid levels and the risk of AD in normal subjects in the Cardiovascular Health Study. Neurology. 2008;70(19):1664-71.

174. Deane R, Bell RD, Sagare A, Zlokovic BV. Clearance of amyloid-beta peptide across the blood-brain barrier: implication for therapies in Alzheimer's disease. CNS Neurol Disord Drug Targets. 2009;8(1):16-30.

175. Mander BA, Winer JR, Walker MP. Sleep and Human Aging. Neuron. 2017;94(1):19-36.

176. Hampel H, Hardy J, Blennow K, Chen C, Perry G, Kim SH, et al. The Amyloid-beta Pathway in Alzheimer's Disease. Mol Psychiatry. 2021;26(10):5481-503.

177. Lee JH, Ahn NH, Choi SB, Kwon Y, Yang SH. Natural Products Targeting Amyloid Beta in Alzheimer's Disease. Int J Mol Sci. 2021;22(5).

178. Murphy MP, LeVine H, 3rd. Alzheimer's disease and the amyloid-beta peptide. J Alzheimers Dis. 2010;19(1):311-23.

179. Abbott NJ, Patabendige AA, Dolman DE, Yusof SR, Begley DJ. Structure and function of the blood-brain barrier. Neurobiol Dis. 2010;37(1):13-25.

180. Sweeney MD, Sagare AP, Zlokovic BV. Blood-brain barrier breakdown in Alzheimer disease and other neurodegenerative disorders. Nat Rev Neurol. 2018;14(3):133-50.

181. Barisano G, Montagne A, Kisler K, Schneider JA, Wardlaw JM, Zlokovic BV. Blood-brain barrier link to human cognitive impairment and Alzheimer's Disease. Nat Cardiovasc Res. 2022;1(2):108-15.

182. Zenaro E, Piacentino G, Constantin G. The blood-brain barrier in Alzheimer's disease. Neurobiol Dis. 2017;107:41-56.

183. Barnes SR, Ng TS, Montagne A, Law M, Zlokovic BV, Jacobs RE. Optimal acquisition and modeling parameters for accurate assessment of low Ktrans blood-brain barrier permeability using dynamic contrast-enhanced MRI. Magn Reson Med. 2016;75(5):1967-77.

184. Kamintsky L, Beyea SD, Fisk JD, Hashmi JA, Omisade A, Calkin C, et al. Blood-brain barrier leakage in systemic lupus erythematosus is associated with gray matter loss and cognitive impairment. Ann Rheum Dis. 2020;79(12):1580-7.

185. Senatorov VV, Jr., Friedman AR, Milikovsky DZ, Ofer J, Saar-Ashkenazy R, Charbash A, et al. Blood-brain barrier dysfunction in aging induces hyperactivation of TGFbeta signaling and chronic yet reversible neural dysfunction. Sci Transl Med. 2019;11(521).

186. Batarseh YS, Bharate SS, Kumar V, Kumar A, Vishwakarma RA, Bharate SB, et al. Crocus sativus Extract Tightens the Blood-Brain Barrier, Reduces Amyloid beta Load and Related Toxicity in 5XFAD Mice. ACS Chem Neurosci. 2017;8(8):1756-66.

187. Hussain B, Fang C, Chang J. Blood-Brain Barrier Breakdown: An Emerging Biomarker of Cognitive Impairment in Normal Aging and Dementia. Front Neurosci. 2021;15:688090.

188. Guimaraes MZP, Jordt SE. TRPA1 : A Sensory Channel of Many Talents. In: Liedtke WB, Heller S, editors. TRP Ion Channel Function in Sensory Transduction and Cellular Signaling Cascades. Frontiers in Neuroscience. Boca Raton (FL)2007.

189. Merrill AW, Cuellar JM, Judd JH, Carstens MI, Carstens E. Effects of TRPA1 agonists mustard oil and cinnamaldehyde on lumbar spinal wide-dynamic range neuronal responses to innocuous and noxious cutaneous stimuli in rats. J Neurophysiol. 2008;99(2):415-25.

190. Bosson A, Paumier A, Boisseau S, Jacquier-Sarlin M, Buisson A, Albrieux M. TRPA1 channels promote astrocytic Ca(2+) hyperactivity and synaptic dysfunction mediated by oligomeric forms of amyloid-beta peptide. Mol Neurodegener. 2017;12(1):53.

191. Paumier A, Boisseau S, Jacquier-Sarlin M, Pernet-Gallay K, Buisson A, Albrieux M. Astrocyte-neuron interplay is critical for Alzheimer's disease pathogenesis and is rescued by TRPA1 channel blockade. Brain. 2022;145(1):388-405.

192. Qosa H, Mohamed LA, Al Rihani SB, Batarseh YS, Duong QV, Keller JN, et al. High-Throughput Screening for Identification of Blood-Brain Barrier Integrity Enhancers: A Drug Repurposing Opportunity to Rectify Vascular Amyloid Toxicity. J Alzheimers Dis. 2016;53(4):1499-516.

193. Zott B, Busche MA, Sperling RA, Konnerth A. What Happens with the Circuit in Alzheimer's Disease in Mice and Humans? Annu Rev Neurosci. 2018;41:277-97.

194. Edwards FA. A Unifying Hypothesis for Alzheimer's Disease: From Plaques to Neurodegeneration. Trends Neurosci. 2019;42(5):310-22.

195. Xin SH, Tan L, Cao X, Yu JT, Tan L. Clearance of Amyloid Beta and Tau in Alzheimer's Disease: from Mechanisms to Therapy. Neurotox Res. 2018;34(3):733-48.

196. Yamazaki Y, Kanekiyo T. Blood-Brain Barrier Dysfunction and the Pathogenesis of Alzheimer's Disease. Int J Mol Sci. 2017;18(9).

197. Ma Q, Zhao Z, Sagare AP, Wu Y, Wang M, Owens NC, et al. Blood-brain barrier-associated pericytes internalize and clear aggregated amyloid-beta42 by LRP1-dependent apolipoprotein E isoform-specific mechanism. Mol Neurodegener. 2018;13(1):57.

198. Wang YY, Chang RB, Waters HN, McKemy DD, Liman ER. The nociceptor ion channel TRPA1 is potentiated and inactivated by permeating calcium ions. J Biol Chem. 2008;283(47):32691-703.

199. Hata T, Tazawa S, Ohta S, Rhyu MR, Misaka T, Ichihara K. Artepillin C, a major ingredient of Brazilian propolis, induces a pungent taste by activating TRPA1 channels. PLoS One. 2012;7(11):e48072.

200. McNamara CR, Mandel-Brehm J, Bautista DM, Siemens J, Deranian KL, Zhao M, et al. TRPA1 mediates formalin-induced pain. Proc Natl Acad Sci U S A. 2007;104(33):13525-30.

201. Laursen WJ, Anderson EO, Hoffstaetter LJ, Bagriantsev SN, Gracheva EO. Species-specific temperature sensitivity of TRPA1. Temperature (Austin). 2015;2(2):214-26.

202. Heber S, Gold-Binder M, Ciotu CI, Witek M, Ninidze N, Kress HG, et al. A Human TRPA1-Specific Pain Model. J Neurosci. 2019;39(20):3845-55.

203. Sinica V, Zimova L, Barvikova K, Macikova L, Barvik I, Vlachova V. Human and Mouse TRPA1 Are Heat and Cold Sensors Differentially Tuned by Voltage. Cells. 2019;9(1).

204. Suo Y, Wang Z, Zubcevic L, Hsu AL, He Q, Borgnia MJ, et al. Structural Insights into Electrophile Irritant Sensing by the Human TRPA1 Channel. Neuron. 2020;105(5):882-94 e5.

205. Vergallo A, Megret L, Lista S, Cavedo E, Zetterberg H, Blennow K, et al. Plasma amyloid beta 40/42 ratio predicts cerebral amyloidosis in cognitively normal individuals at risk for Alzheimer's disease. Alzheimers Dement. 2019;15(6):764-75.

206. Rosas-Hernandez H, Cuevas E, Raymick JB, Robinson BL, Sarkar S. Impaired Amyloid Beta Clearance and Brain Microvascular Dysfunction are Present in the Tg-SwDI Mouse Model of Alzheimer's Disease. Neuroscience. 2020;440:48-55.

207. Boutoleau-Bretonniere C, Pouclet-Courtemanche H, Gillet A, Bernard A, Deruet AL, Gouraud I, et al. The Effects of Confinement on Neuropsychiatric Symptoms in Alzheimer's Disease During the COVID-19 Crisis. J Alzheimers Dis. 2020;76(1):41-7.

208. Isik AT, Soysal P, Solmi M, Veronese N. Bidirectional relationship between caregiver burden and neuropsychiatric symptoms in patients with Alzheimer's disease: A narrative review. Int J Geriatr Psychiatry. 2019;34(9):1326-34.

209. Stewart SA. The effects of benzodiazepines on cognition. J Clin Psychiatry. 2005;66 Suppl 2:9-13.